**Effect of cellulose nanocrystals addition on electrospun silk fibroin composites for the valorization of sericulture production waste streams**

by

Simon Sanchez Diaz

A dissertation submitted to the Graduate Faculty of
Auburn University
in partial fulfillment of the
requirements for the Degree of
Master of Science

Auburn, Alabama
May 4, 2019

Keywords: Silk fibroin, cellulose nanocrystals, electrospinning, composites, reinforcement, bio-materials



Approved by

Dr. Maria Soledad Peresin, Chair, Assistant Professor, Forest biomaterials
Dr. Thomas Elder, Affiliate faculty, Research Scientist USDA forest service
Dr. Maria Lujan Auad, Professor, Director of the Center for Polymers and Advanced Composites
Dr. Brian K. Via, Regions Bank Professor, Director of the Forest Products Development Center

## Abstract

The accelerated development in sciences experienced during the last decades, along with the significant expansion of our knowledge about material synthesis and processing have produced relevant breakthroughs in several key disciplines and industries ultimately intended to improve personal and social welfare. Nevertheless, the continuous demand for sustainable solutions to address different problems has limited the use of traditional materials and has opened the door for the application of alternative approaches.

*Bombix mori* silk, the most commonly used type of silk worldwide, is a naturally occurring polymer primarily based on a fibrillar protein called fibroin (SF), and a globular protein known as sericine. Silk has been used by mankind for thousands of years, predominantly as a staple for textiles, and for wound dressing. With its inherent biological and mechanical properties, silk is a promising candidate for use in biomedical applications such as tissue engineering, drug delivery and cell culture. However, in most cases in order to process and take advantage of these properties, sericine must be removed and fibroin dissolved to produce a solution of regenerated SF, which can be processed into various shapes depending on the final application.

Electrospinning or electrostatic spinning, is a processing technique to generate ultra-thin polymer fibers, where a strong electrostatic field is generated in the space between a reservoir containing a polymer in solution, and a conductive surface used as collector. In the last few decades, the interest in this technique has increased by virtue of the fascinating set of properties of electrospun materials including high porosities and surface areas, and enhanced thermal resistance and surface energy.

Consequently, based on the properties of silk, electrospinning has been proposed as a potential processing technique, such that the production of SF electrospun nonwovens is expected to impact different areas like material science, nanotechnology, textiles, and biomedicine. Such applications have been hindered by reports regarding poor mechanical performance and degradation control for materials produced using regenerated SF.

To address this, studies have examined reinforcing SF electrospun mats by blending with other polymers, or adding fillers to regenerated SF solution before electrospinning. It has also been reported that cellulose nanocrystals (CNC), with, high aspect ratios, interfacial adhesion and surface activity can be used to reinforce different polymers, resulting in improved mechanical properties. Additionally, due to its renewability, biocompatibility, biodegradability and availability, CNC may be a replacement for non-renewable fillers. Hence, CNC might represent a new opportunity with potential revenues accruing to the forest products industry.

This project is concerned with blending regenerated SF with CNC at different ratios, followed by electrospinning to generate SF/CNC composites with enhanced properties. The reinforcing capacity of CNC was assessed through mechanical and thermal testing, whereas morphological, chemical and rheological variations generated by the addition of CNC into SF were observed in each sample.

## Acknowledgments

I want to dedicate this achievement to all the efforts, love, and help provided by my parents Beatriz Eugenia Díaz and Julio Cesar Sánchez, to my brothers Juan Manuel Sánchez and Julio Cesar Sánchez, and to all the members of my beautiful family, which I love so much. And to my girlfriend who has supported me during the most difficult times.

I would like to give a special recognition to all my team members, including the outstanding help provided by my advisor Dr. Maria Soledad Peresin, whose knowledge and expertise helped to grow as person and professional. And to my laboratory mates Diego Gomez, Marina Hornus, Celeste Iglesias, Alejandro Cardozo, Ossai Asafu-Adiaye, Charles Essien, Dr. George Cheng, Dr. Beatriz Vega, and all the other people who has expend part of their labor day with me.

I also want to thanks to the ones who have contributed in this project like Nima Alizadeh, Dr.Gabriela Chavez, Dr. Bart Prorok, Dr. Sarah Zohdy, Dr. Ilari Filpponen, Dr. Oladiran Fasina, and Dr. Sushil Adhikari. To the members of the committee Dr. Maria Auad, Dr. Thomas Elder, and Dr. Brian Via. And additionally to one of my mentors Dr. Adriana M. Restrepo-Osorio, and the members of my team back in Colombia Natalia Jaramillo, Ana María Gaviria, and Angel Daniel Ríos. And to every person I have met in this experience, thanks.

Finally, I want to acknowledge the opportunity to be here, to the USDA Forest service, which founded this work through the project numbered 203855-145001-2000, granted to Dr. Thomas Elder. Thanks to this agency and to Dr. Elder, this goal was possible.

To all of you thanks, this work would not be possible without your support.

Table of Contents

List of Tables

List of Illustrations

List of Abbreviations

| | |
|---|---|
| CNC | Cellulose nanocrystals |
| SF | Silk fibroin |
| RSF | Regenerated silk fibroin |
| ES | Electrospun |
| SEM | Scanning electron microscope |
| FTIR | Fourier-Transformed Infrared Spectroscopy |
| TGA | Thermogravimetric analysis |
| XRD | X-ray Diffraction |
| PEG | Polyethylene glycol |
| RSF/CNC | Composite of regenerated silk fibroin with cellulose nanocrystals |

## Rationale & Hypotheses

CNC would foster the production of thinner fibers and more homogeneous electrospun structures of silk

CNC would serve as nucleation agent for silk, leading to increased mechanical and thermal resistance

The formation of a continuous network of CNC in the structure of silk, and the interactions between both components would enhance the mechanical and thermal resistance of the electrospun silk nonwovens

## Objectives

### General

To evaluate the reinforcing capacity of cellulose nanocrystals on electrospun silk nonwovens, in terms of thermal and mechanical performance

### Specific

To assess the effects of the addition of CNC on the rheological behavior of silk in solution

To define the minimum concentration of CNC to produce a continuous network in silk solutions (percolation threshold)

To evaluate the consequences of changing CNC concentration on the viscosity, conductivity, and the spinability of silk/CNC solutions

# Chapter 1

# Background

## 1.1. Introduction

Natural polymers like polysaccharides and proteins are materials that have played key roles in human history, by use as textiles, food, medicines, construction, pulp and paper, and even military applications. As societal needs have changed, however, synthetic polymers with specific properties, have largely displaced natural polymers

Silkworm silk is a well-known, naturally occurring fibrous polymer whose glossiness, versatility for processing, physiological, and mechanical properties, have made it an ideal candidate for the production of fine textiles dating back to between five and five thousand years ago. [1]–[6], and its use as material for suturing wounds has been reported for centuries [7], [8]. The characteristics of silk are due to the two major components, sericine and fibroin; While sericine is a globular and hydrophilic protein which represents the majority of the amorphous structure, fibroin is a fibrillar and hydrophobic protein comprising most of the crystalline domains [8]–[11]. As a result of this blend, the chemical composition of silk is mainly based on the amino acid residues glycine, alanine and serine, and other minor residues such as tyrosine, valine and glutamic acid [12]. As a consequence silk is biocompatible, degradable, non-cytotoxic, can be chemically modified, and has the capacity for immobilization of macromolecules [2]. These characteristics in addition to the successful utilization of silk in wound healing have positioned

silk as a prospective source for biomedical applications, leading to the production of silk based biomaterials for use in tissue engineering, drug release systems, food packing, biosensing, and biotechnology [2], [13].

In order to utilize silkworm silk for biomedical or biotechnological applications, sericine is removed to reduce hypersensitive or allergic responses [14], [15]. The removal of sericine is achieved by boiling silkworm cocoons in a mild alkali solution for few minutes, which removes 25-30% of total silk mass [2] ,[15], [16]. The resulting product is known as degummed silk, which is subsequently isolated by dissolution in a solvent that disrupts the strong intermolecular hydrogen bonds between protein chains, producing a silk fibroin solution, referred to as regenerated silk, which can be processed in different shapes and/or blended with other compounds [17].

Among the different approaches for silk fibroin processing, electrospinning has been identified as a promising manufacturing techniques for the production of fibrous matrices for functionalized textiles and biomedical devices, due to its ability in processing different polymers using a comparatively inexpensive setup, and the inherent properties of the final product such as small fiber diameter ranging from micros to tens of nanometers, controllable porous structures, large surface area, high porosity and aspect ratio [17], [18]. Such characteristics allows the production of nonwoven fibrous structures that closely mimic the conditions of the extracellular matrix, which make electrospun materials ideal for applications in tissue engineering, cell culturing, production of manmade organs, fabrication of controlled drug releasing systems, support for enzyme immobilization, and wound dressings [9], [17], [18].

Electrospinning has been employed to study and modulate the natural spinning process of silk, and in several studies focused on the production of electrospun silk biomaterials or silk-composites [2], [14], [19]. Through various projects on the fabrication of electrospun silk fibroin non-wovens, materials have been produced that meet the chemical, morphological, and biological requirements for use in biomedicine, as well as enhanced thermal and electrical resistance [18], [20]–[22]; Isolated silks, however, exhibit poor degradation control and reduced mechanical properties compared to native silk fibroin, thus limiting their applications [5], [23], [24]. These drawbacks mainly arise from the regeneration or isolation process of silk fibroin, which disrupts most of the intermolecular hydrogen bonds that stabilize the antiparallel β-sheet arrangement of silk, leading to a predominantly silk I structure with lower crystalline domains, resulting in reduced mechanical properties and increased the brittleness of the material [2], [3], [20], [25].

Since biomaterials must be able to withstand varied stresses and loads, improvement of mechanical properties for electrospun silk non-wovens is indispensable. Therefore, blending silk fibroin with other polymers or fillers before electrospinning to produce silk fibroin composites has been proposed and studied by the use of minerals, synthetic polymers, polysaccharides, proteins, carbon nanotubes, carbon black, and cells, as reinforcement for silk fibroin [17], [20], [21], [26]. Diverse composites have shown superior mechanical performance, but problems regarding stability, dispersibility in regenerated silk solutions, aggregation, weak interfacial bounding, high energy and cost of production, biocompatibility, and degradability, have discouraged their implementation [2], [14], [17], [19], [20], [27]. Given their good compatibility with silk, polysaccharides such as alginate, chitin, chitosan, hyaluronic acid, and cellulose have been found to impart remarkable stability and enhanced mechanical properties of silk matrix. Furthermore, their application as reinforcement is enhanced by their abundance, availability and degradability [17], [23], [28] as well as their biocompatibility, hydrolytic stability, chelating capacity and mechanical properties, [20], [29].

Within the polysaccharides, cellulose nanocrystals (CNC) have been identified as a promising filler for polymers or matrix reinforcement, whose superior mechanical properties are attributed to their high aspect ratio, crystallinity and strong surface activity, yielding performances comparable to carbon nanotubes or fiberglass [3], [5], [20], [25], [29], [30]. CNC are typically produced through acid hydrolysis of cellulose pulp, where the disordered regions within fibers are cleaved, while crystalline structures are preserved, leading to rod-like cellulose nanostructures with a similar type of crystalline structure as the original fibres, but with higher crystallinity [31]. Depending on the cellulose source and parameters for the acid hydrolysis, assorted shapes and surface characteristics are obtained, leading to variations in mechanical performance and stability. For instance, CNC produced through acid hydrolysis with hydrochloric acid exhibits poor dispersability in water, whereas, hydrolysis with sulphuric acid induces higher dispersibility via charge repulsion from grafted sulphate ester groups, but with reduced CNC thermal stability [31]–[33]. Therefore, several strategies for achieving stability of CNC without compromising their potential reinforcing capabilities have been tested [32].

Studies on the blending silk fibroin with either cellulose nanocrystals or cellulose nanofibrils by varying the solvents, silk-cellulose ratios, and processing systems, have yielded composites with diverse morphologies, physicochemical, and mechanical properties. For instance,

Huang, *el al.* [20], successfully improved tensile strength and reduced fiber width of electrospun silk fibroin non-wovens by adding up to 4% w/w of cellulose nanocrystals to a solution of silk fibroin in formic acid. But, a reduction in the strain at breaking was observed as CNC content increased. Likewise, Park, *et al.* [5] dispersed bacterial cellulose nanocrystals (BCN) into a solution of silk fibroin in formic acid to produce silk fibroin/BCN electrospun composites with increased Young's modulus and tensile strengths until BCN levels increased up to 7%. Interestingly, the elongation at break was not affected by the addition of BCN. In addition, Lee, *et al.* [34], fabricated wet-spun fibers of silk fibroin/TEMPO-oxidized cellulose nanofibrils (TO-CNF), employing formic acid as solvent, and methanol as coagulating agent. It was found that TO-CNF decreased the drawing ratio of the fibers, and the crystalline index of the composite since TO-CNF might have restricted the crystallization of silk fibroin. Yao, *et al.* [35], blended cellulose pulp and silk fibroin in different ratios by dissolving the compounds into 1-Butyl-3-methylimidazolium chloride to produce microfibers via jet-dry wet spinning. The tensile strength, elastic modulus, crystallinity, and drawing ratio decreased as silk fibroin percentages increased, while all the fibers exhibited excellent mechanical performance. Liu and Yao [36], compared the mechanical and thermal performance of degummed silk and wet-spun regenerated silk fibroin, against wet-spun SF composites reinforced with CNC, produced by adding the crystals at different ratios into SF aqueous solutions before coagulating in a methanol bath. The wet-spun SF-CNC composites presented superior crystallinity, thermal resistance, Young's modulus, and tensile strength compared to the wet-spun regenerated silk fibroin and the degummed silk fibers. Shefa, *et al*. [37], developed SF:TO-CNC composites with wound healing capability by blending regenerated silk fibroin with TO-CNC at different ratios. The components were successfully linked by producing amide bonds between primary amides in silk fibroin with carboxylic groups on TO-CNC surface, using carbodiimide crosslinkers, and then freeze-dried. SF:TO-CNC composites exhibited biocompatibility as well as increased water uptake capacity and accelerated wound healing capacity (related to percentage of wound closure), compared to other wound dressing materials, although the mechanical performance of the composites was not tested.

It can be seen that in most of the aforementioned approaches, non-benign solvents like formic acid have been used for the production of silk fibroin-CNC composites. The use of harsh solvents may be deleterious for the fabrication of composites, whose applications involve handling, contact, or human health impacts. Therefore, in order to overcome this complication, in

the current project, silk fibroin-cellulose nanocrystals electrospun composites have been produced by blending a concentrated solution of regenerated silk fibroin in an aqueous solution with CNC dispersed in water. Cellulose nanocrystals produced via acid hydrolysis of regenerated wood pulp were used as the reinforcing agent for electrospun silk fibroin composites. The effects of adding CNC in different ratios were assessed through the determination of mechanical and thermal properties, and the morphology, crystallinity, and chemical characteristics of the fabricated materials. In addition, the properties of the solutions of silk fibroin and CNC were studied to evaluate their implications on the electrospinning process, and to determine the percolation threshold of the CNC in the solution of concentrated silk fibroin, in order to ensure that the system works under satisfactory conditions. To the best of our knowledge, no reports about the fabrication of electrospun SF-CNC composites employing water as solvent including an analysis of the percolation threshold for the reinforcing agent have been published.

## 1.2. Electrospinning

Electrospinning is a versatile processing technique in which different natural and synthetic polymers in a solution are used to produce of non-woven fibrous materials in a wide variety of shapes, with controlled structural properties and average diameter sizes ranging from microns to tens of nanometers. This technique relies on the application of an electrical field strong enough to overcome the surface tension and viscous forces within a polymer solution placed in between a conductive and charge dissipating surface. To produce the electrical field, the polymer solution is electrically charged generating a difference in the electrical potential between the conductive surface where the polymer is placed and the charge dissipating surface. When the electrical field exceeds the strength of viscous and surface forces in the polymer solution, a thin filament of polymer is ejected the in the direction of the field until it reaches the dissipating surface. During the time when the polymer solution is in the electrical field, the solvent is evaporated while the polymer undergoes stretching and repulsive forces, as well as bending and whipping movements allowing the elongation of the polymer until fine fibres in the submicron scale are produced [18], [26], [38], [39].

In spite of the fact that electrospinning has been studied and analysed for more than a hundred years, its implementation in fundamental and applied research had not received much

attention, until recent decades. As interest in nanotechnology increases and due the continuous demand for functionalized, ultra-light, and strong fibers, electrospinning has been examined as a relatively inexpensive, versatile, and easy to use technique for the fabrication of fibres with features otherwise unattainable through conventional spinning methods [26].

### 1.2.1. Electrospinning history

The first insights regarding the electrospinning process were reported given by Rayleigh, who evaluated the stability and effects of charge induction in water jets during the end of the 19$^{th}$ century [39]. However, the first official report of a recognized electrospinning process was described by J.F. Cooley in 1902, in the US patent titled "Apparatus for electrically dispersing fibres" in which a detailed method for generating yarns using high voltages, viscous polymer solutions, and volatile solvents was illustrated [40], [41]. In the same year, W. J. Morton was granted the US patent 705,691, entitled "Method of dispersing fluids", where a method for dispersing fluids mixed with volatile solvents into a non-volatile solvent using an electrical field was developed [42]. The following year, once again J. F. Cooley presented an improvement of his invention described in the US patent 745,276, entitled "Electrical method of dispersing fluids" [41]. Nevertheless, no substantial progress in electrospinning theory or setup was made until 1914 when Zeleny published his work regarding the behavior of fluid droplets suspended in the tip of metal capillaries under the influence of electrostatic forces, as well as a first description of the electrospraying process of solutions in the tip of a capillary [18], [43].

The aforementioned works served as a guide for Anton Formhals, who first successfully explained the electrospinning process and produced continuous filaments of artificial polymers. Between 1934 and 1944 Formhals patented a number of experimental setups for the production of filaments using electrostatic forces [44], [45], [46], [47], [48], [49], [50]. His first approaches did not result in many improvements in the technical aspects regarding filament drying and collection, because of the small distances between the nozzles and collector. Formhals overcame the drawbacks of his first apparatus by enabling interchangeable distances between the nozzles and collector, which provided longer drying times. Later on, Formhals proposed a mechanism for the fabrication of composite fiber-webs by electrospinning multiple polymers and composites onto

a moving substrate. Figure 1-1 shows one of the first electrospinning methods for the production of continuous artificial fibers proposed by Formhals in his patent US 2,187,306.

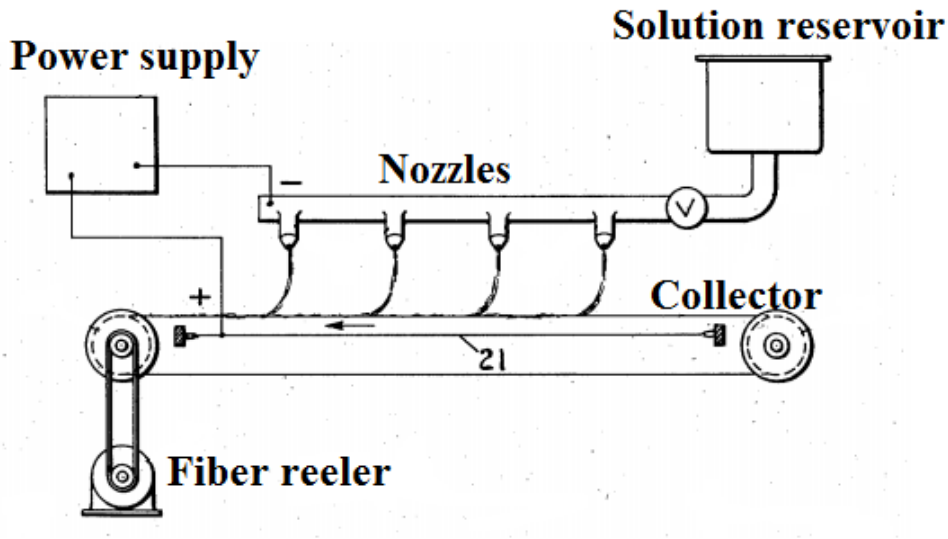


**FIGURE 1-1.** Diagrammatic view of the apparatus proposed by Anton Formhals for the production of continuous artificial threads or yarns. It Includes a storage reservoir containing a quantity of spinning solution. A storage reservoir is connected to a header conduit with multiple nozzles through which a stream of spinning solution is extruded. A base thread about two grooved pulleys (collector) may be rotated by means of a motor or any other desirable mechanism. Figure adapted from US Patent No. 2,187,306 (1940)., granted to Anton Formhals.

More recently, between 1964 and 1969, Sir Geoffrey Ingram Taylor postulated the theoretical underpinnings of electrospinning, by mathematically modelling the formation of the cone produced when a fluid droplet supported on the tip of a capillary is subjected to electrostatic forces. This phenomenon is known as the “Taylor cone”. Taylor observed that the shape of fluid droplet changes from rounded or spherical to tapered as the strength of the electrical field increases, until the electrical force is strong enough to overcome the surface and viscous forces that holds the droplet, producing jet ejection from the vertices of the cone [51]. In addition, his work with J. R. Melcher led to the development of the “leaky dielectric model” for conducting fluids [41], [52]–[54].

After the investigations of Formhals and Taylor, the main focus of research on electrospinning was concerned with understanding the relationships between electrospinning

parameters and the structural features of electrospun filaments. Only few decades ago, electrospinning was rediscovered as a potential technique for the production of nanofibers through a relatively inexpensive and simple process [39]. This upsurge in interest for electrospinning was inspired by the work of Reneker and Doshi [55], where filaments with diameters ranging from 5 μm to 50 nm were generated by varying the voltage and concentration of polyethylene oxide in solution. This approach served as evidence of the suitability of electrospinning for the production of nanoscale materials. Since then further theoretical and applied investigations have strengthened the fundamentals of this technique, leading to significant improvements in processing conditions, and the development of innovative systems [39], [41].

As evidence of the increasing interest in the electrospinning process, more than 200 institutions are currently using electrospinning for different purposes. Various private companies have invested in projects related to the production of nanocomposites through electrospinning, or are actually employing this technique [18]; Additionally, by conducting a search in the SciFinder database on the number of publications associated with the term “electrospinning” within the last 20 years, a significant increment in the number of publications in this field was observed until 2015, followed by an slight decrease in the last three years as summarized in the figure 1-2. It is important to point out that before the year 1995 the term “electrospinning”, referring to the electrostatic spinning process had not been coined, and was not completely standardized until 2000. Therefore, data before this date might be biased [41]. During the surveyed period more than 15,000 peer-reviewed articles were published and 290 US patents were granted.

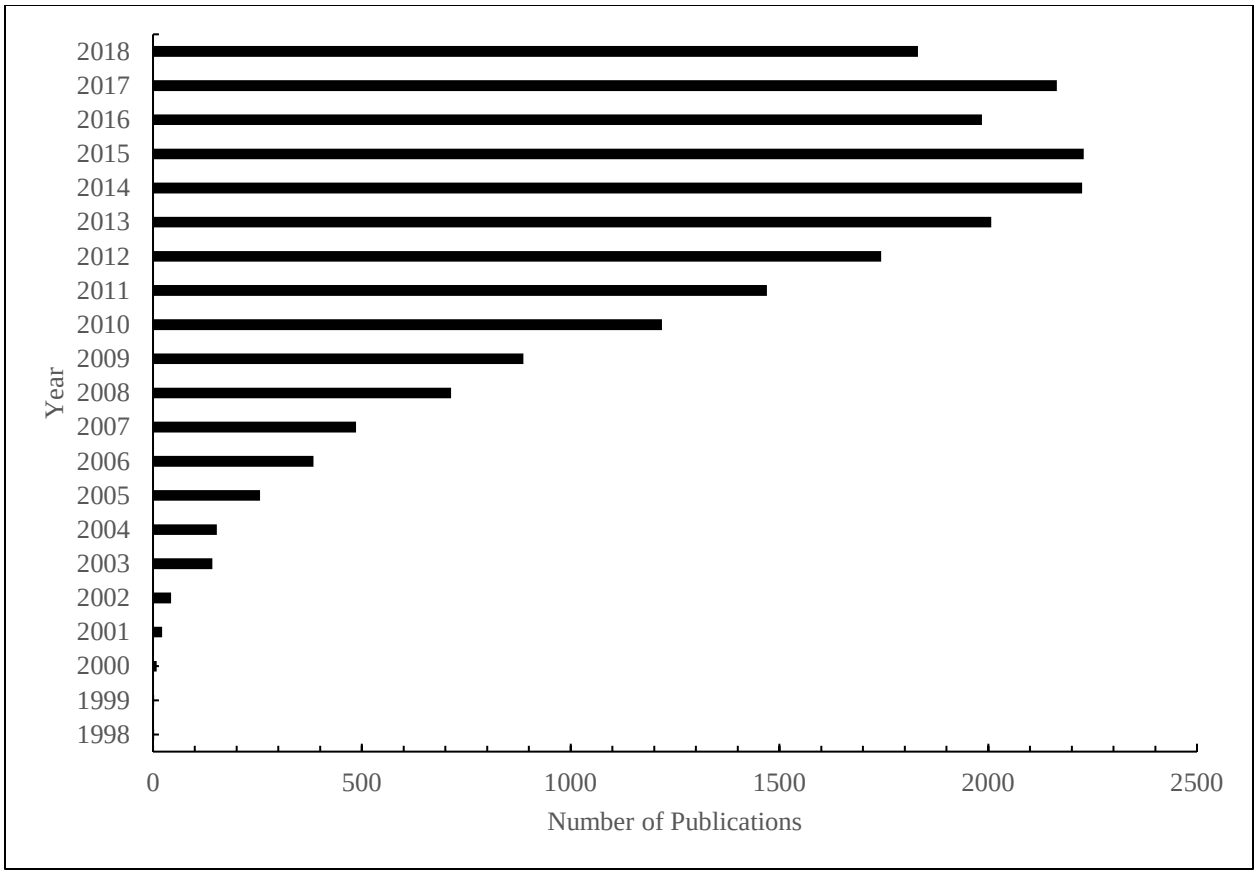


**FIGURE 1-2.** Number of peer reviewed articles associated with electrospinning, published during the last two decades (Data obtained from SciFinder, by searching under the keyword electrospinning, Data surveying on 10/08/2018).

### 1.2.2. Electrospinning technique

Electrospinning and electrospraying phenomena are governed by a delicate balance between viscous and surface forces which keep the fluid together in its minimum energy state, and an external electric field responsible of breaking these forces to produce a fluid jet. In both systems a polymer in solution or molten polymer is subjected to an electrical force that opposes the surface tension, producing charge induction on the polymer solution surface. When the electrostatic charge is increased to a critical value, the equilibrium between surface and electric forces is disturbed, leading to charge repulsion followed by the formation of electrical stresses on polymer surface [26]. As the electrostatic charge becomes stronger, the electrical stresses start to converge in a

specific point, leading to the extension of the polymer and to a change in shape from rounded to tapered [26], [41]. The resulting structure arising from this stretching is also named the "Taylor cone" in honour of the contributions and work performed by Sir Geoffrey Taylor in this field. The tip of the Taylor cone serves as junction for all the electrical stresses [54]. Figure 1-3 shows the evolution of the droplet up to the formation of Taylor cone, as electric force increases.

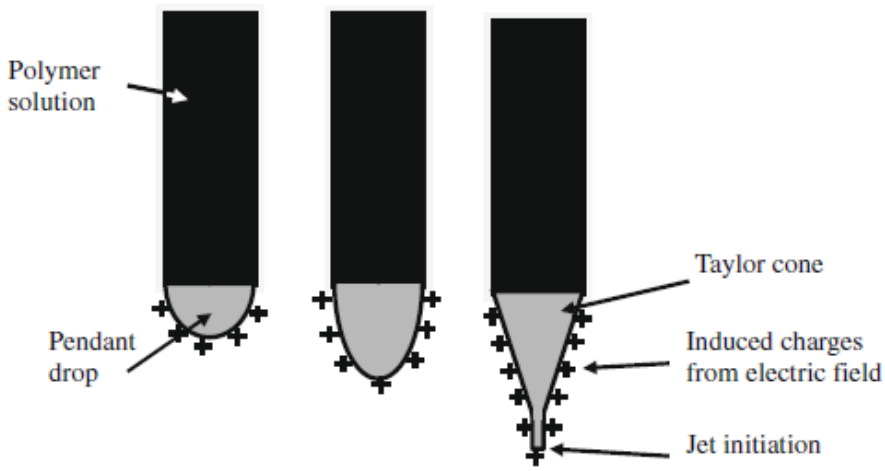


**FIGURE 1-3.** Schematic representation of the formation of the Taylor cone, as a consequence of the increment in electric force. Figure adapted from [26]. Copyright Elsevier 2010.

At low electrostatic forces, the dripping of the pendant drop at the top of Taylor's cone is restrained by the viscous forces, but as the electrostatic force is increased to a critical value it becomes strong enough to overcome the surface forces and produce a discrete or continuous ejection of polymer for electrospraying or electrospinning, respectively [18], [56], [57]. Once the polymer is ejected from the tip of the Taylor cone, as a consequence of the electrical charge brought by the polymer jet, it will be drawn in the direction of the electric field, and after a short time the polymer undergoes various instabilities which lead to stretching and continuous fiber formation. The principal instabilities of the polymer at this point are the axisymmetric Plateau-Raleigh, off-axis bending, and bending or whipping instability.

In the Plateau-Raleigh instability the surface tension turns the polymer jet into a shape with minimum surface area, leading to the jet breaking up into small droplets. This instability occurs when the applied electric force is not strong enough to overcome the surface forces, and generate a continuous jet. This instability is avoided in high electric fields and by increasing chain

entanglement of polymer in solution [26], [58]. The second type of instability occurs at strong electric forces, where electrical stresses on the jet surface produce perturbations, and consequently changes in the surface charge occur. As result, the perturbation is reinforced leading to the jet breaking up into droplets [58]. Finally, in the third instability, which also occurs at strong electric forces above a critical value, a continuous jet is generated and experiences a series of whipping movements leading to the formation of expanding loops which allow polymer stretching, until the material is finally deposited on the surface of a collector [59], [60]. As the polymer jet is stretched, its surface area is increased, facilitating the evaporation of solvent until a solid fiber is obtained [41].

### 1.2.3. Electrospinning apparatus

A basic electrospinning system is based on three main components, a capillary tube which holds the polymer in solution or molten state, a power supply to charge the polymer and provide the electric field, and a ground connected collector or dissipating surface to collect the produced filaments [51], [57], [61]. Figure 1-4 shows a typical arrangement for electrospinning, including a syringe pump for controlling the flow of polymer, a syringe with a needle used as capillary tube, a power supply, and a ground connected metallic plate employed to collect the fibers.

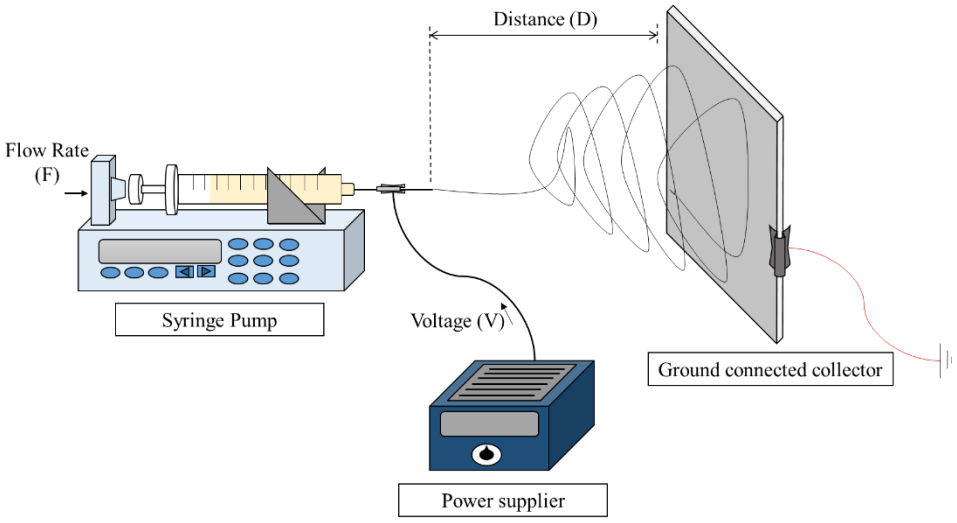


**FIGURE 1-4.** Typical setup employed for electrospinning process. Copyright Simon Sanchez Diaz

In this system, the syringe pump controls the ejection of material, while the needle of the syringe serves as capillary nozzle to extrude the polymer and electrode to connect one terminal of the power supply. The other terminal of the power supply is attached to the collector. The order in which the poles of the power supply are connected do not affect the resulting products. Finally, on the ground connected collector the produced fibers assemble to form a non-woven matrix, in a pattern and orientation defined by the type of collector. The most commonly used types of collector are the static metallic plate and rotating drum, however, other configurations like rotating disc or parallel drums are also available [18], [52].

As polymers can be considered dielectric materials [62], through the usage of this arrangement, once a strong electric field is generated between the nozzle and collector, the polymer molecules respond to the excitation by changing location within solution, which generates stresses on the liquid surface, followed by the jet ejection, and finally the production of the instabilities which result in stretching and solvent evaporation [39].

Electrospinning can be arranged horizontally (as highlighted in Figure 1-4) or vertically, although several shortcomings regarding solution dripping have been observed using the vertical arrangement, which affects the surface of the product. In contrast, gravitational forces are not as significant in the horizontal setup, making the electric field the main driving force for this process [18], [39]. In addition, with the increasing interest in electrospinning, many research groups and companies have developed and patented innovative systems to improve the conditions and efficiency of the electrospinning process [38], [63]–[67].

### 1.2.4. Parameters involved in electrospinning process

Electrospinning is governed by various parameters related to the properties of the polymer solution, processing variables, and ambient conditions. Within the parameters related to the polymer solutions, the most important factors are viscosity, concentration, molecular weight, surface tension, conductivity and the type of solvent. Among the process variables, voltage, flow rate, distance from capillary tip to collector, type of collector, and ejector diameter are the most important factors. Each of these can have single or multiple impacts on the morphology and final properties of the fibers, such that their control is essential for the formation of desirable products [18], [38], [39], [41], [52], [61], [68].

### i. Polymer solution factors affecting electrospinning:

***Concentration.***

As a measure of the amount of polymer in solution, the higher the concentration, the greater the chances for intermolecular interaction or entanglement in solution. Therefore, a critical value for this factor is required to lessen the instabilities and avoid the jet breaking up [41]. At low concentrations Plateau-Rayleigh instability dominates the process, and the formation of beads or droplet is preferred over continuous fibers. As the concentration is increased a combination of fibers and beads are observed until the concentration exceeds a critical value where only fibers are produced. Further increases in concentration above the critical value leads to fiber thickening [18].

***Molecular weight.***

Molecular weight reflects the number of monomer units within a macromolecule, quantifying the polymer length and level of entanglement, which directly affect the viscosity of the solution. It has been found that an increase in molecular weight contributes to continuous fiber formation, as well as larger fiber diameter. Interestingly, a high molecular weight allows a continuous polymer jet even at low polymer concentration, as long as the level of entanglement is large enough to hinder the jet from breaking up [69], [70]. Furthermore, molecular weight is associated with other properties such as surface tension, conductivity, and dielectric constant [18].

***Viscosity.***

This property results from the different interaction between polymer(s) and solvent(s), and it is correlated with concentration and molecular weight. At low viscosities the jet can break up easily due to poor polymer-polymer interactions, but by increasing the viscosity until reach a critical value, continues fibers of polymer are produce due to the raise in polymer-polymer interactions, which allows longer relaxation times for the polymer in solution, and helps the jet to withstand the first order instabilities (Plateau-Rayleigh). Further increments in viscosity above the critical value leads to the production of more uniform and thicker continuous fibers. However,

when the viscosity is too high, the electrospinning process is hindered by the strength of the viscous forces, even when employing strong electric fields [71], [72].

***Surface tension.***

Surface tension arises from the type of solvent and its interaction with the polymer. By working under ideal concentrations and viscosities, the reduction in surface tension enables electrospinning to proceed at lower electrostatic forces, and to generate continuous fibers by reducing the occurrence of first order instabilities [18], [58], [73], [74]. In addition, surfactants can help to reduce the surface tension [41].

**Conductivity.**

Conductivity, or the ability of the solution to carry a charge, depends on the type of solvent, and the composition and length of the polymer. It has been noticed that slight increments in conductivity lead to thinner and more uniform fibers, as a result of increases in the bending or whipping instabilities which helps to stretch the fibers [75]. At very low conductivity, the jet is unable to carry electrical charges and bead formation is preferred. But, once the conductivity is above a critical value, continuous fibers are generated, which can be made thinner by further increases of conductivity. If the conductivity is very high, however, an enhancement in whipping instabilities occurs, broadening the size distribution of fibers, and eventually resulting in the jet breaking up [18]. Conductivity can be easily modified by adding electrolytes or conductive fillers to the solution [41], [76].

**Type of solvent.**

The selection of an ideal solvent is vital for the electrospinning process due to its contributions to the final conductivity, surface tension, and viscosity of the solution [58]. In addition, the solvent plays an important role by facilitating polymer chain motion in solution and in the jet, allowing the subsequent stretching of the polymer fiber until the solvent is completely evaporated and the polymer crystallized. Consequently, when the solvent has low volatility wet

fibers are produced, leading to re-deposition of solvent in which the collected fibers may merge, collapse, or be re-dissolved. In contrast, very volatile solvents may lead to poor polymer stretching or the early solidification of polymer in the capillary, restricting the whole process [18], [77]. Moreover, increasing the dielectric properties of the solvent promotes the formation of defect-free fibers with thinner diameters [41], [78].

### ii. Processing variables:

#### Voltage.

As the main driving force for electrospinning, the voltage or applied electrostatic force is responsible for the creation of the electric field and for the induction of the necessary charge in the solution. Many effects on the fiber shape have been attributed to variation in voltage, however, there are still questions about this topic. Some investigations have found that increasing the applied voltage produces thicker fibers as the result of more polymer ejection [57], [79], [80], while other authors have stated that increasing the electrostatic potential results in thinner fibers due to stronger repulsive forces producing more stretching [18], [41], [72], [81]. Nevertheless, most reports agree with the second assumption, which also implies that faster evaporation of the solvent occurs as the surface area of the fiber is increased with thinner fibers.

#### Flow rate.

Flow rate defines the jet velocity and the amount of mass ejected from the capillary. It has been observed that increasing the flow rate leads to larger fiber diameters and pore sizes, as consequence of the extra mass ejected, as well as to bead formation caused by improper drying time [82], [83]. Nevertheless, a minimum polymer ejection rate must be kept in order to produce a stable Taylor cone and subsequent continuous polymer jet [68].

**Distance from capillary tip to collector.**

A minimum working distance is required to allow whipping instabilities and stretching of the fibers, as well as to provide enough flying time for the evaporation of the solvent. It has been noticed that distances that are either too small or too large lead to bead formation because of short flying time and the drop in the intensity of the electric field (which is inversely proportional to distance) [18], [39], [84], [85].

**Type of collector.**

` The collector serves as a conductive surface where the fibers dissipate their charges and are collected to form a non-woven matrix. It has been found that reducing the conducting area of the collector results in the formation of beaded structures instead of continuous fibers [86]. However, the main contribution of the collector resides in the type of orientation that it can provide to the structure of the produced material. Static metallic plates usually lead to unoriented fibrous structures, therefore anisotropic non-woven mats are generated. Whereas, the use of rotating drum collectors provides certain degree of alignment and stretching for the fibers, generating a better degree of isotropy for the nonwovens [87], [88]. Furthermore, the rotational speed affects the orientation of the polymer fiber by aligning the crystals in the direction of the rotating axis [89]. While the static metallic plate and rotating drum are the most typically used collectors for electrospinning, other types of collectors have emerged as alternatives to improve the final properties of the electrospun nonwovens. Some of these innovative approaches are variations of the rotating drum, including rotating discs, parallel electrodes, and gridded bars [52]. In addition, conductive paper, conductive cloth, wire meshes, and even coagulation baths have been employed for the deposition of the fibers [18], [86], [90]. Figure 1-5 displays different types of rotating collectors employed in the electrospinning process.

***FIGURE 1-5.*** Variations on the rotating collectors employed in electrospinning process. Reference: [52].

**Ejector diameter.**

The size of the orifice through which the solution flows, has a tremendous impact on the shear forces and deformation of the extruded polymer droplet. It has been found that large orifices result in thicker fibers. But, orifices that are too big hinder the formation of Taylor's cone restricting the electrospinning process [91]. Likewise, orifices that are too small reduce the amount of ejected material, causing fast evaporation of the solvent when the Taylor cone is produced [92]. Moreover, the ejector diameter might have some effect on the rheological behaviour of the solution, which might be due to shear thickening or shear thinning of the polymer, resulting in the aforementioned outcomes when the viscosity changes [41], [93].

**iii. Ambient conditions:**

Environmental parameters like humidity and temperature can produce significant changes in the morphology and properties of the final product. It has been found that high humidity can result in the occurrence of beads due to slow solvent volatility, therefore, reducing the elongation forces that stretch the jet [94]. In contrast, very low humidity may result in extremely fast solvent evaporation rates, such that the electrospinning process may proceed for only a short period of time before the polymer in the tip of the ejector solidifies and clogs the nozzle [18], [95], [96]. It has been suggested that humidity can promote the dissipation of charges along the polymer fiber

and the subsequent reduction in the third order instabilities, leading to thicker fibers [97], [98]. Other authors have reported the opposite effect of relative humidity on fiber diameter when hydrophilic polymers are employed [99], [100]. For hydrophobic polymers, water acts as a non-solvent which promotes the formation of solid regions around the trapped or condensed water on surface, yielding higher porosities and enabling the evaporation of the remaining solvent.

High temperatures cause a faster evaporation of the solvent, reducing the development of beaded structures [80]. It is also known that the viscosity of a polymer in solution is inversely proportional to the temperature [93]. So, by decreasing or raising the temperature, the polymer solution becomes thicker or thinner, respectively. Therefore, a reduction in fiber diameter is expected in warmer environments [39], [101].

### 1.2.5. Application of electrospun non-wovens.

As result of the versatility of the electrospinning process in converting materials into products with desired and advantageous characteristics including high surface area, tuneable porosity, and enhanced thermal and mechanical properties, various approaches have been applied to find suitable applications of electrospun non-wovens. Almost two-thirds of the proposed application of electrospun materials have been addressed towards biomedical applications related to tissue engineering, wound dressing, drug delivery, immobilization of active agents, and vascular graft implants. Among the remaining applications, their potential uses are in filtration, biotechnology, defence, environmental engineering, energy storage, nanosensors, catalysis, bioreactors, affinity membranes, and cosmetics [18], [41], [52], [57], [102], [103]. Figure 1-6 displays the pie chart for the distribution of the applications of electrospun non-wovens in each field.

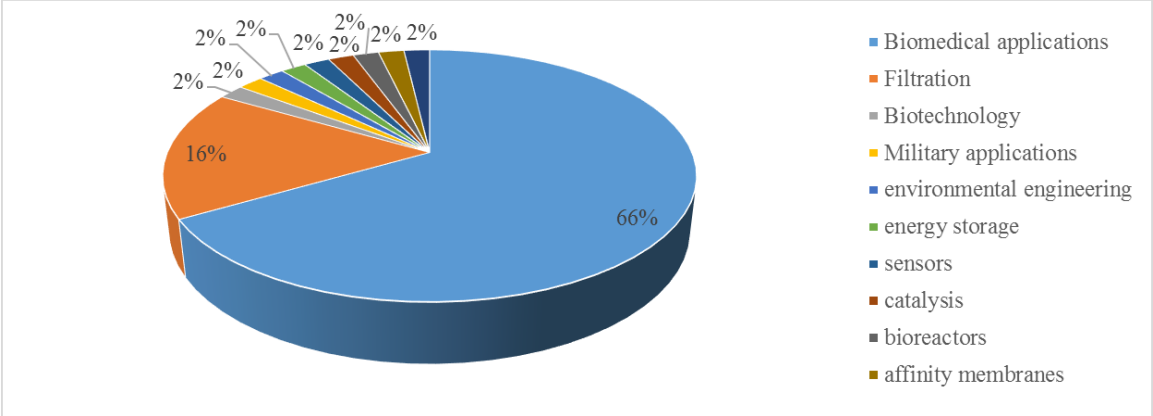


***FIGURE 1-6.*** Pie diagram for the application of electrospun materials among different fields. Adapted from [18], [102].

Increased demand for more sophisticated materials with enhanced surface and mechanical properties that cannot be obtained through conventional electrospinning processes, has led to innovative strategies and methodologies to address this need. These include modifications of the electrospinning setup, addition of fillers or reinforcing fibers, co-polymerization in solution, post-drawing, annealing, and solvent exchange [17], [18], [22], [57], [104]. These strategies have broadened the spectrum of application for electrospinning by yielding the production of polymers and composites that were previously unfeasible.

The use of fillers or reinforcing fibers in electrospinning, allows the incorporation of active molecules into the fiber, resulting in benefits like enhanced surface activity and mechanical strength, faster response to external stimuli, antibacterial properties, higher conductivity, increased porosity, and controlled release properties [5], [52], [61], [105]–[109]. For instance, Shi, *et al.* [108], developed an electrospun photosensitive biosensor with potential applications in optic-electronics, by embedding gold nanoparticles onto silica electrospun fibers. Figure 1-7 shows the dispersion of the nanoparticles along the an electrospun fiber.

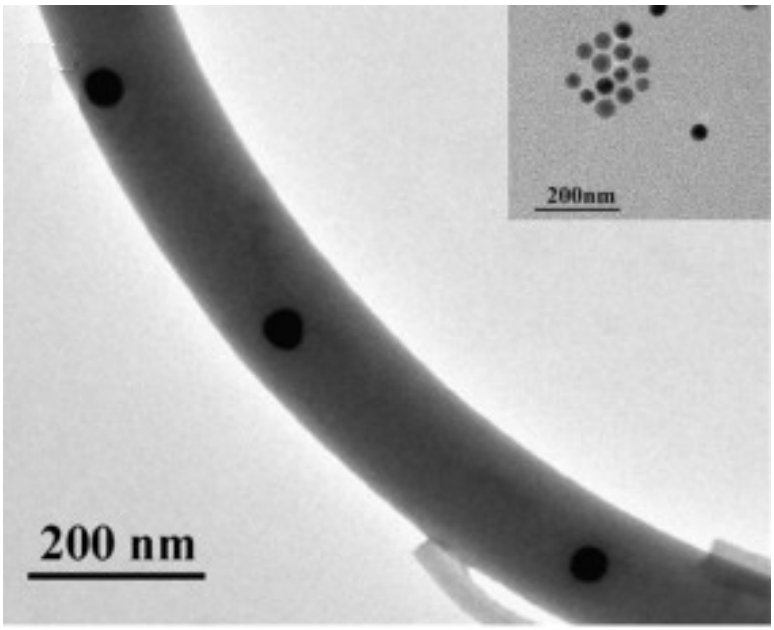


**FIGURE 1-7.** TEM image of embedded gold nanoparticles onto silica electrospun fiber, for improving the photoelectric response. Figure adapted from [108]. Copyright Elsevier 2009.

### 1.2.6. Challenges in electrospinning

Although electrospinning is a versatile, fairly simple, and relatively inexpensive process for the production of nanostructured fibrous composites at the laboratory scale, its industrial scaling-up has been a major challenge due to the sensitivity of the technique to slight chances in the processing parameters which are difficult to properly control on large scale [18]. Moreover, for the successful fabrication of many functionalized electrospun materials reported in the literature, an extremely low flow rate is required, which creates complications for a commercial-scale product [103].

Additionally, the optimization of processing parameters is an exhausting, iterative, but necessary task to produce nonwoven matrixes with desired morphologies and surface properties [110]. For instance, fiber orientation is one of the biggest challenge as consequence of the difficulty in controlling the direction and trajectory of polymer jets, hindering the implementation of this technique for applications where the randomness and anisotropy of the products must be avoided [57]. In textile engineering, it is well-known that fiber orientation leads to superior mechanical

properties, and appropriate control of this characteristic can broaden the relevance of this technique [103].

It has been observed that fiber diameters in the electrospinning process are usually limited to sizes up to tens of nanometers. This means that electrospinning by itself is not applicable for the fabrication of quantum wires or structures with dimensions below nanoscale, but through post-processing techniques these difficulties could be overcome [103], [111].

Finally, electrospun non-wovens are usually randomly oriented structures with anisotropic properties, so a consistent characterization of the mechanical properties using typical mechanical testing becomes tedious, and the isolation of a single electrospun fiber is nearly impossible because of the random nature of the technique [26]. Notwithstanding these limitations, characterization methods like nanoindentation have been explored for measuring mechanical properties of single fibers, but the feasibility of this technique is still under debate and strongly depends in the hardness of the tested product [112]–[116].

### 1.3. Silkworm silk

Silkworm silk is a natural polymer that has been used for thousands of years. The earliest evidence of the exploitation of silk can be traced to 3,200 years in the past coming from Zhejiang province in the southern China. Further investigations, however, have reported the utilization of silk during the early Neolithic era, around 5,000 years ago, and possibly earlier [1], [15], [117], [118]. According to archaeologic discoveries, the silkworm or *Bombyx mori* was domesticated in northern China, probably in the province of Shandong, where the primary food source of silkworm, the white mulberry, was first cultivated [6], [118]. Initially, silk was employed for manufacturing decorative artifacts, until the practice of boiling cocoons, also known as degumming, became common and enabled the production of continuous silk thread for textiles [1], [15]. It is assumed that degumming was crucial for the domestication of silkworm, as it allowed the manufacturing of luxurious and high-value added silk products and their further commercialization, which extended beyond China, through Asia and into parts of Europe, and became the one major trade product from China. The huge impact of the silk trade would later inspire the term “silk road” coined by the German geographer Baron Ferdinand von Richthofen, to describe a network that connected China, India and the Mediterranean regions through central Asia [119].

Even though, silk is mainly applied in textiles, it also has been employed in medicine as suture thread for wound closure and wound cloth, [7], [8], [120]. More innovative and prospective uses are currently under investigation [2].

### 1.3.1. Structure and composition

An isolated thread of *Bombyx mori* silk has an average diameter between 10 to 25 μm, and is mainly composed on a fibrous proteins called fibroin and an glue-like hydrophilic protein named sericine which keeps fibroin bundles together [3], [22], [28], [104], [117]. [121].

Fibroin is a hydrophobic block copolymer primarily composed of glycine, alanine and serine, based on a wide range of polypeptides and glycoproteins linked through disulphide bonds or hydrophobic interactions [2]. As consequence of its heterogeneity, fibroin presents a wide distribution of molecular weights with two principal units of 26 kDa and 390 kDa, which define a light and heavy segments within protein structure, which is held by disulphide linkage between the residue Cys-c20 from the heavy chain and Cys-172 on the light chain. Additionally, the glycoprotein P25, with an average molecular weight of around 25 kDa, is non-covalently linked to the heavy chain and composes an important segment within fibroin structure. It has been reported that the molar ratio between the heavy chain, light chain, and P25 is about 6:6:1 [2], [120], [122]–[124].

The heavy chain is formed by 12 domains which compose the crystalline region of silk, each randomly interconnected with non-repeating segments called linkers, that reduce the crystallinity. The length of crystalline domains within heavy chains are variable and can be composed of up to thousands of residues, built up in a sequence of hexapeptides with a general conformation defined as G-A-G-A-G-X, where G is glycine, A is alanine, and X can be serine, tyrosine or valine [125], [126]. The length of the linkers or amorphous domains does not vary much and is usually made up of 42 residues. The amino acids that make up the backbone of fibroin leads to a hydrophobic, highly crystalline, biodegradable, and biocompatible polymer [117].

Between 20% and 30% of the total mass in a single cocoon is sericine, which is a family of glycoprotein with high polydispersity whose molecular weight ranges from 20 kDa to 310 kDa, [15]. Sericine can adopt a random coil or β-sheet structure, which can be controlled by varying ambient and mechanical stresses. Random coils easily turn into β-sheets under mechanical stress

or high humidity, whereas the opposite occurs in aqueous solution at temperatures higher than 50° during which sericine adopts a soluble form [15], [127]. The sequence of amino acids that comprise sericine is variable, but most investigations agree that serine composes almost one-third of the total residues. Consequently, assorted types polypeptides with the ability of crosslinking can be found along the sericine structure [12], [128].

Table 1-1, presents the average weight percentage of each amino acid in natural silk, crystalline silk, amorphous silk, and sericine.

**TABLE 1-1.** Average weight percentage of amino acids in natural silk, crystalline silk, amorphous silk, and sericine. The crystalline and amorphous silk represent the non-water soluble and soluble portion of silk after enzymatic treatment. Adapted from [12].

| Amino acid | Natural Silk | Crystalline Silk | Amorphous Silk | Sericine |
|---|---|---|---|---|
| Alanine | 29.3 | 32.89 | 22.16 | 5.2 |
| Aspartic acid | 1.3 | 0.56 | 3.87 | 14.6 |
| Arginine | 0.5 | 0.18 | 1.29 | 2.8 |
| Cysteine (half) | 0.2 | 0.0 | 0.0 | 0.3 |
| Glutamic acid | 1.0 | 0.43 | 2.58 | 7.9 |
| Glycine | 44.5 | 48.5 | 36.85 | 13.5 |
| Histidine | 0.2 | 0.06 | 0.5 | 1.0 |
| Isoleucine | 0.7 | 0.13 | 1.80 | 0.6 |
| Leucine | 0.5 | 0.0 | 1.29 | 0.8 |
| Lysine | 0.3 | 0.2 | 0.77 | 4.3 |
| Methionine | 0.1 | 0.0 | 0.0 | 0.1 |
| Phenylalanine | 0.6 | 0.13 | 1.54 | 0.5 |
| Proline | 0.3 | 0.0 | 1.03 | 0.5 |
| Serine | 12.1 | 14.97 | 7.54 | 33.1 |
| Threonine | 0.9 | 0.36 | 2.32 | 8.3 |
| Thryptophan | 0.2 | 0.0 | 0.0 | 0.3 |
| Tyrosine | 5.2 | 1.40 | 10.8 | 3.1 |
| Valine | 2.2 | 0.64 | 5.67 | 3.1 |

### 1.3.2. Polymorphisms and crystalline structure of silk fibroin

As previously mentioned, because of its complex structure sericine can adopt a β-sheet or random coil conformation, depending on the applied environmental and mechanical stresses. Similarly, fibroin can assume assorted conformations also related to the applied stresses. The

polymorphisms of fibroin are commonly referred as Silk I, Silk II and Silk III. Silk I is the water-soluble state of fibroin, where the majority of secondary structures are random coils or α-helixes [129]. Silk II represents the dry and organized state of fibroin, where the secondary structures undergo a transition to β-sheets when Silk I is dried, heated, or stressed. This transition occurs naturally during the silkworm spinning process, when the solution of silk contained in the glands of the insect are ejected, yielding shear stresses that organize the structure of silk and pulls the water out [130]. It has been observed that Silk I transforms to Silk II under exposure to methanol or through changes in the ionic strength or pH of the silk solution [117], [131]. Finally, Silk III is a type of helical structure produced at the air-water interface of silk thread during the spinning process [2], [14], [132].

Commonly, the amorphous regions within the silk structure represent approximately 35% of the total volume, and are made up of randomly ordered peptide chains that provide deformability and elasticity to silk threads. In contrast, the crystalline regions are segments of β-sheets or α-helixes which provide structural joints and toughness to the protein. β-sheets structures are preferable in terms of mechanical, chemical and thermal resistance, as result of their asymmetric spatial organization of the protein chains, where one side of is entirely occupied by hydrogens coming from the glycine residues, whereas the other is covered with methyl groups from the alanine residues. This structure allows for the interaction between methyl groups and hydrogen molecules between chains facing opposite directions, enabling the formation of an antiparallel protein network stabilized through intermolecular hydrogen bonds and Van der Waals forces. Subsequently, protein networks in the same plane can be linked through the same mechanism to finally form a tightly packed, non-water soluble, and thermodynamically stable crystalline structure with the ability to exclude water, while being soluble in acids, bases, or chaotropic agents in aqueous solution [2], [28], [120], [133]. Figure 1-8, shows a schematic representation of the of the intermolecular interactions in β-sheets; whereas Figure 1-9 displays the antiparallel arrangement exhibited by β-sheets. While the dissolution in acid and bases may produce the denaturalization of the protein, the dissolution in chaotropic agents is preferred as these type of reagents preserve the structure of the protein, owing to their ability to only generate the breaking up of the hydrogen bonding network among water molecules. Such effect, leads an increased number of free molecules of solvent that screen the hydrophobic interactions between protein chains that stabilize that stabilize the main structure [134].

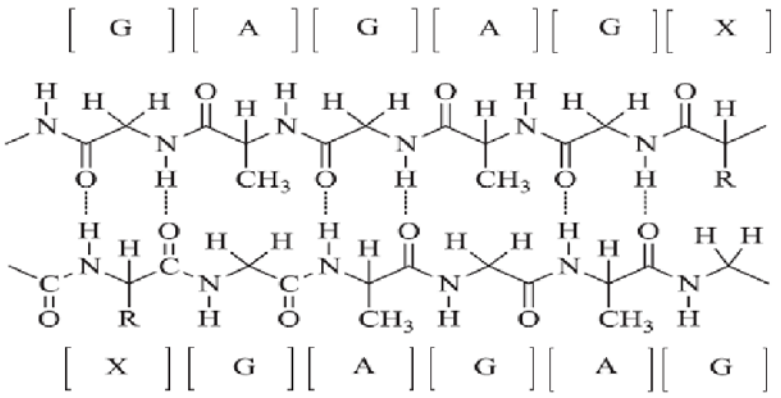


**FIGURE 1-8.** Intermolecular interactions between protein chains in fibroin β sheet structures. Figure adapted from [28]. Copyright Elsevier 2012.

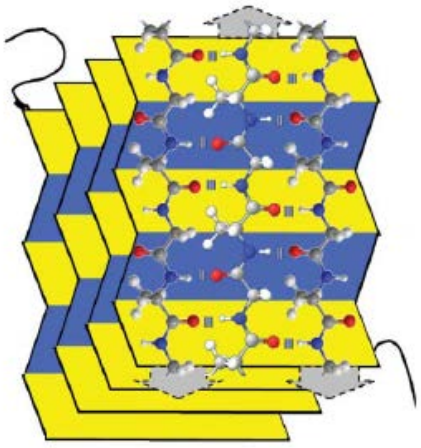

**FIGURE 1-9.** Antiparallel stacking pattern of silk fibroin protein chains in β sheet structures. Figure adapted from [133]. Copyright Springer Nature 2013.

Furthermore, as result of the diversity of amino acids located along silk fibroin backbone, several conformations of the crystalline structure can be assigned to this protein. However, the most commonly reported structure corresponds to the orthorhombic conformation between β-strands with the same molecular structure as shown in Figure 1-8. Where the intramolecular distances between glycine-glycine residues and alanine-alanine residues are in the order of 3.87 Å and 5.33 Å, respectively. While, the intermolecular distance between chain-chain in plane and the chain-chain perpendicular to the strand are 4.70 Å and 9.20 Å, respectively [12], [117].

### 1.3.3. Applications

For thousands of years, silk cocoons have been employed as staple for textile production as the principal application of this material. Since that time, the demand for silk clothing has been stimulated by the superior luster, softness, toughness, and quality of silk wovens, as well as for its direct association with wealth, luxury, and sumptuousness [3], [6]. In addition to textiles, silk has been used in biomedical applications as suture threads for wound closure, due to its good biocompatibility, degradability, and healing capacity [20], [135]. Silk based materials may also be used in electronic and optical devices, reinforcing fillers, wound dressings, tissue-engineering, and filtration [7], [8], [18], [20]–[22], [120]. However, the inability of silk threads to be processed into different shapes, along with the increasing demand for silkworm cocoons by the textile industry have restrained the implementation of silk in other fields.

In order to use silk for any application the removal of sericine by boiling the cocoons in a heating bath of water or in a mildly alkali solution has become a standard procedure. This process removes around 25-30% of the total silk mass, and the resulting product, also known as degummed silk, is the detached silk fibers [1], [15], [136]. These fibers can be directly used for textiles, as high performance filaments, or isolated as a solution of regenerated silk, which can be further processed into assorted forms and/or blended with other compounds [17].

Since the intrinsic properties of regenerated silk closely mimic the features of natural silk fiber, including biodegradability, biocompatibility, non-cytotoxicity, non-inflammatory reaction, there has been a great deal of effort in the utilization of regenerated silk among due to its processability and availability for surface modification, which are key factors that hinder the applicability of natural silk [3], [5], [18], [20]–[22], [104], [137], [138].

Recently, most research projects have explored the suitability of using silk for the production of biomedical devices to be used for general applications in biomedicine. For instance, silk fibroin has been recognized as an ideal candidate for tissue engineering, as it fulfils most of the biological requirements such as minimal inflammatory reactions, improvement of cell activity and cell ingrowth, tuneable biodegradability, and biocompatibility. In addition, the processing techniques can control the morphology and surface characteristics to mimic the features of the extracellular matrix. This, allows the production of bone tissue, organs, arteries, and ligament replacements [3], [139].

Another noteworthy approach is the use of silk fibroin in place of typical materials used to produce biosensors. Since most of the supports for biosensors are made up of silicon, the devices can be too rigid to properly mimic the flexibility of human tissues. Silk fibroin has shown an ability to hold circuits without side effects [3], [140]. A current application of silk in biosensing is in the production of glucose sensors, fabricated via immobilization of glucose oxidase onto a solvent-cast film of regenerated silk solution, attached to an oxygen electrode surface [135].

Supplementary investigations have focused on the production of silk fibroin substrates for the immobilization of macromolecules or bioactive compounds. One of the first reports tested the capacity of silk to immobilize enzymes was developed in the late 1970's. In this work, the surface of woven degummed silk was modified using acids and hydrazine. The modified silk was able to immobilize aspartate aminotransferase and alkali phosphatase, and successfully maintained the phosphatase activity for more than 90 days [141]. The immobilization of invertase, protease, and glucose oxidase, onto silk fibroin matrixes have been achieved using solvent-cast films or freeze-dried powders. Interestingly, for glucose oxidase, an enhancement in the detection time was observed when compared against the available sensors [142], [143]. Moreover, the capacity to immobilize glucose oxidase on silk fibroin supports was compared against gelatin substrates. Accordingly, a better detection activity was noticed when silk fibroin was employed as a support. Other investigations have reported an improvement in immobilization capacity and thermal stability for silk biosensor, when the protein is pretreated by dipping it into a methanol bath [144]. In addition, an extensive amount of reports and developments on the immobilization of enzymes on silk fibroin matrixes have been demonstrated the feasibility silk fibroin for this application [2], [143], [144]-[146].

Furthermore, as result of the semi-rigidity of silk chains in solution, they are able to assume nematic liquid crystalline organization and exhibit outstanding optical properties. This, makes silk a potential material for producing electronic displays or contact lenses [22].

Finally, current investigations and projects to explore the uses of silk fibroin, as well as the new processing techniques like electrospinning, 3D printing, and freeze drying, have broadened the alternative applications of silk including drug delivery devices, culture medium for cell ingrowth, anticoagulants, manmade organs, tympanic membrane, and use as a model protein for miscellaneous researches [3], [5], [20], [21], [25], [30], [137], [138], [140]. As a recent benchmark, the pharmaceutical industry took advantage of the interesting set of properties of silk, and has

produced microcapsules of silk fibroin with controlled release of drugs [3]. Figure 1-10 displays the different techniques suitable to process regenerated silk into various shapes.

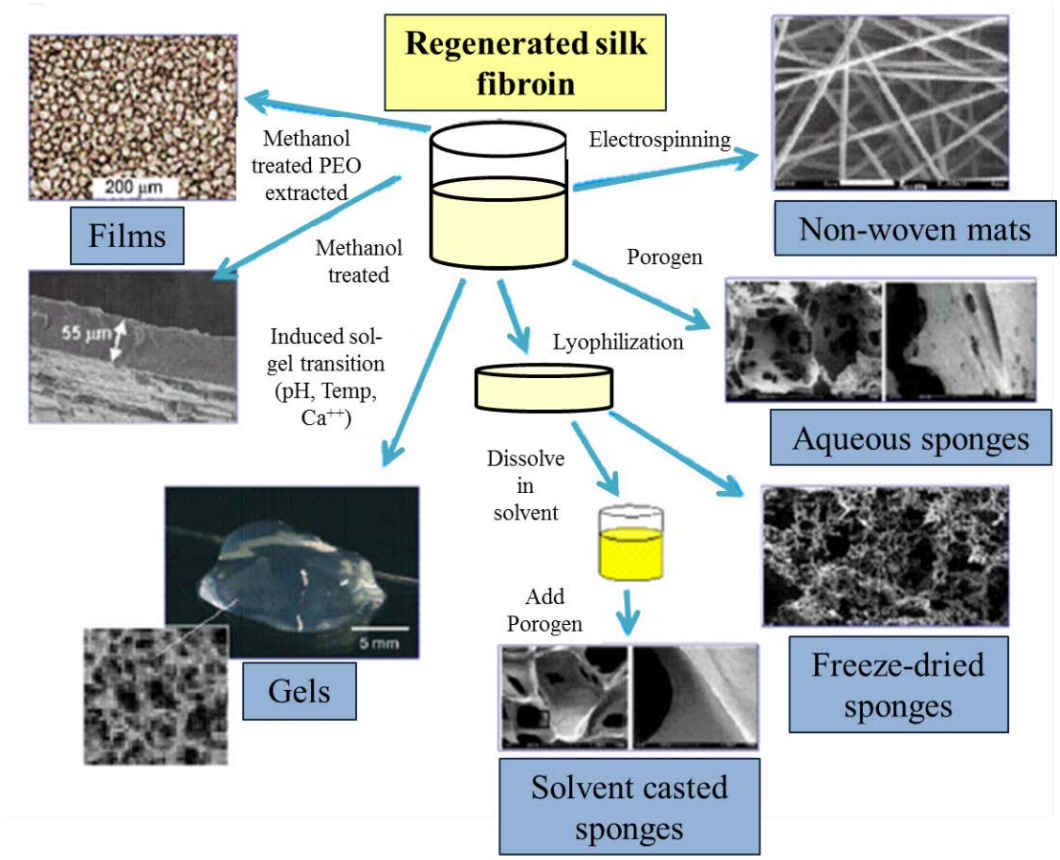


**FIGURE 1-10**. Techniques and methods to process regenerated silk fibroin into different shapes. Figure adapted from [2]. Copyright Elsevier 2007.

### 1.3.4. Challenges for the application of silk

As previously mentioned, natural silk is a strong fibrous material widely used in textiles and biomedicine, but given its properties, the applications of silk may not be restricted just to traditional approaches, but may include innovative and alternative uses for high-value added products. Notwithstanding, difficulties regarding processability have hampered its implementation [2], [3], [13], [14]. To overcome this problem, a dissolved form of silk called regenerated silk fibroin can be easily obtained by solving natural or degummed silk fibers with mildly acidic or basic solution, or by using chaotropic salts dissolved in water. Regenerated silk

can be shaped into miscellaneous forms depending on the processing technique; however, the regeneration process involves the disruption of most OH-bonds and Van der Waals forces that stabilize the β-sheets and conferred the superior mechanical resistance to silk, then turning regenerated silk fibroin in dry state into a hard and brittle material [2], [3], [20], [25]. Additionally, it has been noticed that regenerated silk exhibits a poor degradation rate. For this reason it is important to blend this material with other sources to achieve the desired conditions [21], [104].

Ideally, to address the shortcomings regarding the mechanical performance of regenerated silk the induction of β-sheet structures should be the pathway to follow. These structures can be achieved through controlling the pH, temperature, and ionic strength of the solution, by the introduction of mechanical stresses, removing entrapped water using a methanol bath, or through the addition of fillers or active agents which serve as nuclei for crystallization [117], [130], [131]. Yet, the likelihood of utilizing fillers or active compounds is encouraged due to the induction of silk crystallization to form β-sheet structures, and the possibility to endow silk with other characteristics and attributes provided by the addition of functionalized molecules [17], [20], [21], [26], [29]. Even so, the costs, stability, biocompatibility, biodegradability, dispersibility, aggregation, and poor interaction of some fillers with silk fibroin matrixes make their applicability unacceptable to completely fulfil the requirements for reinforcing silk [2], [17], [19], [14], [20], [27], [140].

In addition, when the degumming process is not properly carried out, remaining sericine in the silk fibers or in the regenerated silk solution may lead to inflammatory responses when silk is used as biomaterial. Also, sericine residues in silk solutions may hinder the crystallization process of silk fibroin, and subsequently lower the mechanical performance of silk products after processing, or reduce the stability of the regenerated silk solution [16], [136], [148]. Finally, it is important to point out that silk as a degradable material, is more susceptible to degradation in its regenerated form as consequence of the reduction in crystalline structures, thus the life span and stability of silk in solution is significantly lower, and closely depends on the temperature and pH of the solution [117], [120].

## 1.4. Cellulose

Cellulose is a natural, renewable and biodegradable material widely used in the textile, paper, forest products and engineering applications for thousands of years [22], [29]. Cellulose can be obtained from sources like trees, plants, some marine creatures, algae and bacteria, and depending on the source and the treatment, different forms of cellulose will be obtained.

Cellulose is a linear chain of glucose molecules linked through glycosidic bond from carbon 1 (C1) of one glucose ring to carbon 4 (C4) from the adjacent glucose. This kind of bounding is known as β-1,4-glucosidic [29] bound or beta-D-glycopyranose, where beta refers to the isoform of cellulose where the hydroxyl group linked to C1 lies in the equatorial position, while D or dextrorotatory denotes that the molecule is able to rotate the plane of polarized light clockwise [22], [121]. The hydrogen bonds between the adjacent cellulose molecules, provide structural stability and the formation of a cellulose chain. The number of repeat units of glucose depends on the cellulose source, which can go from 10000 to 15000 units [29].

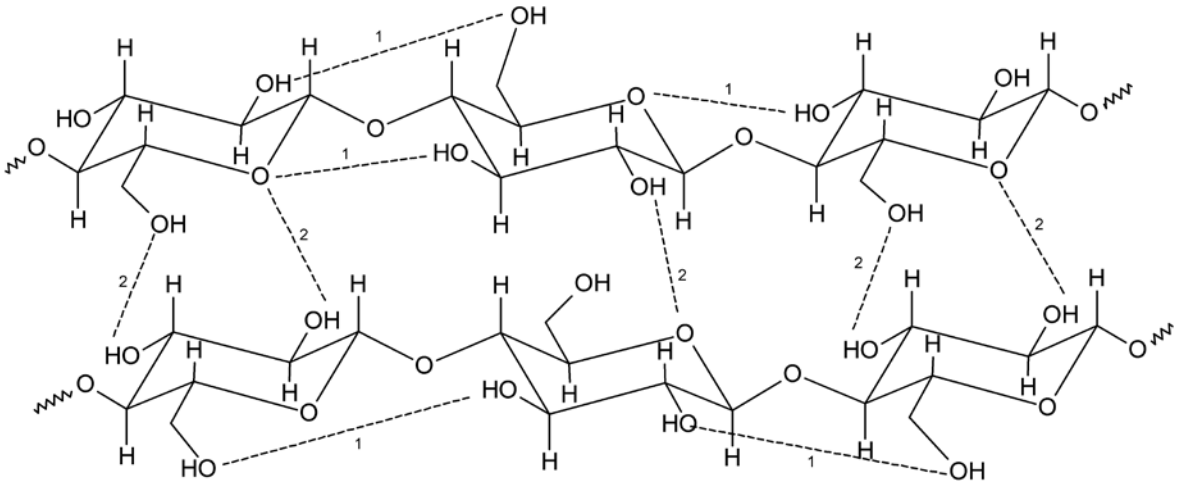

**FIGURE 1-11.** Intra- and inter-molecular bonding patter on cellulose I molecule. Reference: [29].

During the cellulose biosynthesis, the Van der Waals and the intermolecular hydrogen bounds promote the parallel assembly of multiple cellulose chains producing elementary fibers which consequently aggregate into microfibrils. The assembly process of elementary fibrils into microfibrils depends on the terminal enzyme complexes, which are spots located in the cell wall,

composed on several subunits that contain many catalytic sites where cellulose chains are polymerized and whose configuration dictates the final arrangement of the elementary fibrils. The configuration of the subunits in the terminal enzyme complexes variate along species, and it has implications in the aggregation process of the elementary fibrils which has impact on the crystallinity, morphology, aspect ratio, and crystalline structure of the final microfibril. For instance, in wood, the subunits in the terminal enzyme complexes are arranged into six-membered rosettes, each of them producing 6-member cellulose chain, which are later stacked into 36-member cellulose microfibrils, containing crystalline and amorphous regions [29], [149], [150].

Additionally, cellulose can form polymorphs referred to as cellulose I, II, III and IV. Cellulose I is sometimes referred to as natural cellulose and is produced by natural organisms such as trees, plants, algae, tunicates and bacteria. Cellulose I can be converted into cellulose II or III. Cellulose II is the most thermodynamically stable structure, and can be produce a regeneration process or mercerization. This kind of structure has been widely used in the paper industry for decades. Cellulose III can be produced from cellulose I or II through liquid ammonia treatment, and then can be converted into cellulose IV using a thermal treatment [29].

### 1.4.1. Cellulose nanocrystals

Cellulose is an abundant and renewable resource which exhibits properties such as moisture absorbency, biodegradability, biocompatibility, hydrolytic stability (liquid crystalline organization), chelating capacity and high mechanical resistance [20], [22], [104], [29]. These properties provide this material with an outstanding potential for applications in engineering fields.

The intra and inter molecular forces which bind the cellulose provide a stable and stiff structure [21]. Furthermore, the hydroxyl groups promote intramolecular hydrogen bonds that stiffen the chains and facilitate the intermolecular hydrogen bonding with other polymers, leading to chemical stable composites with novel functions and properties [22].

Cellulose nanocrystals are usually between 5-50 nm in diameter and hundreds of nanometers in length, low density, and a highly reactive surface populated of hydroxyl groups that facilitate grafting of other species to achieve different surface functionalization, including an easier self-assembly, controlled dispersion, and control of the particle-particle and particle-matrix bounding [29].

Special attention has been focused on cellulose nanocrystals as a reinforcing material, with mechanical properties that can be compared with those from carbon nanotubes, a greater elastic modulus than kevlar, high aspect ratio, and a strong interfacial adhesion, [3], [5], [20], [25], [29], [30], [151].

### 1.4.2. Cellulose nanocrystals preparation

The isolation of any kind of cellulose source is based in two phases. The first one is a purification and homogenization pretreatment process. This process will depend on the cellulose source and the desired morphology. In the case of wood or plants, purification is performed by the partial or complete removal of lignin and hemicellulose, and the isolation of individual fibers.

The second stage, is the separation of the individual cellulose fibers into their microfibers or crystalline compounds. The basic approaches to separate the cellulose are mechanical treatment, acid hydrolysis and enzymatic hydrolysis. Each of these methods can be used separately or combined to reach a desired cellulose morphology [29].

Within the mechanical processes are high-pressure homogenization, grinding/refining, cryocrushing, high intensity ultrasonic treatment, and microfluidization. Generally, these processes use high shear rates to produce the cleavage along the directional axis of cellulose fibrils, resulting in separated cellulose microfibrils. After each subsequently mechanical step, the particles become smaller and more homogeneous, but less crystalline. Following this treatment, a filtration process is included to remove the unfibrillated and partially fibrillated fraction. And additional chemical step can be performed in order to eliminate the amorphous region or functionalize the particle surfaces.

In acid hydrolysis, the cellulose fibrils are disrupted by a controlled process in which the amorphous region within cellulose structure is removed, leading to rod-like nanostructures called cellulose nanocrystals or cellulose nano-whiskers. [20], [31], [135], [34]. Sulfuric acid is the typical reactive used in this process, but other type of acids like hydrochloric, phosphoric and maleic have been employed as well [29].

### 1.4.3. Applications

Cellulose has been used for textile, pulp and paper, and forest products applications for hundreds of years [22], [29], [121]. The potential applications of cellulose nanomaterials include but are not limited to flexible displays, reinforcement for polymers, biomedical, pharmaceutical, drug delivery, textiles, electronic devices, separation membranes, thickening agent, and food packing [22], [29].

Within cellulose materials, cellulose nanocrystals (CNC) have arisen as a promising filler for polymers or matrix reinforcement, with superior mechanical properties attributed to their high aspect ratio, crystallinity and strong surface activity, resulting in performance comparable to carbon nanotubes or fiberglass [3], [5], [20], [25], [29], [30]. Depending on the cellulose source and conditions for the acid hydrolysis, assorted shapes and surface characteristics are obtained, leading to variations in mechanical performance and stability. For instance, CNC produced through acid hydrolysis with hydrochloric acid exhibits poor dispersability in water, whereas, hydrolysis with sulphuric acid induces higher dispersibility via charge repulsion from grafted sulphate ester groups, but reduces CNC thermal stability [31]–[33]. Therefore, several strategies for enhancing stability of CNC without compromising their potential reinforcing capability have been tested [32]. In addition to the characteristics of CNC surface, the surface area, orientation and concentration of crystals in a polymer solution will govern the interactions filler-matrix and filler-filler, and therefore, the ability of the filler to form a continuous reinforcing network. This phenomenon is modelled by an statistical-geometrical approach named “percolation” which predicts the number of particles required to go from a discrete dispersion to an infinite connection of elements when the reinforcing capacity is maximum [152]. Because of the relevance of this phenomenon for the current research, it is presented in a separate section where the basic fundament of this model is described for CNC.

Special attention has been paid to cellulose based materials as a replacement for synthetic polymers to develop immunodiagnostic assays, due to their interesting properties such as hydrophilicity, high stability, low toxicity abundance, renewability, biocompatibility, biodegradability, and mechanical properties [20], [29], [153]. The first report of about the use of cellulose material to produce a diagnostic test, comes from 1957, when Free et al. [154] impregnated a strip of stiff paper with glucose oxidase, peroxidase and orthotolidine for detection

of glucose in urine. After this first approach, many studies have focused their efforts on the production of diagnostic tests employing the concept of permeable porous matrix with entrapped molecules, especially for laminar flow tests for immunodiagnostic analysis where an antigen is bound to entrapped enzymes, within cellulose matrix [155]–[158]. Zul et al. [159] reported the design of a paper strip test for detection of drugs in human fluids, via the immobilization of immunochromatographic enzymes which were moved through capillary migration in the presence of theophylline. In the review written by Krska and Molinelli [160], the authors mentioned a method for measuring mycotoxins in food using a nitrocellulose based membrane in which a labeled antibody is entrapped and is used as a signal reagent. Also, Cheng et al. [161] produced an enzyme-linked immunosorbent assay (ELISA) performed in a 96-microzone plate fabricated in paper with potential to reduce the time and steps required in typical ELISA assays. This paper based ELISA demonstrated the capacity to detect glucose, total proteins and several enzymes.

### 1.4.4. Cellulose nanocrystals as reinforcing agent: Percolation model.

Percolation is a term coined by Hammerley in 1957, to describe the likelihood of the components in a heterogeneous system to turn from a completely disperse to an infinite association state, by increasing the amount of contact points or elements of one component in the system [162], [163]. In between these two states there is a transitional range whose upper limit represents the ultimate concentration of elements required to cross from one state to the other. This limit is known as the percolation threshold, and closely depends on the number of elements of each species in a multicomponent system, the chemical behavior of each species, and the orientation and aspect ratio of the elements [164], [164], [165], [166].

This approach has been widely employed to explain the reinforcing effect of cellulose nanocrystals in different polymers, by relating the aspect ratio and volume percentage of CNC, to its ability to form a tight reinforcing network of cellulose mainly linked by hydrogen bonds [167], [168]. According to the model developed by Favier, *et al*. [169], the minimum volume fraction is described for rod-like shape cellulose fibers to successfully generate geometrical percolation. It was found that the volume fraction is inversely proportional to the aspect ratio of cellulose, and strongly diminishes upon minimal variation in the length or diameter of the fiber. The model for

the calculation of the percolation threshold proposed by Favier is presented in the following equation.

$$\nu_{RC} = \frac{0.7}{L/D}$$

Where $\nu_{RC}$ is the minimum volume fraction, and L and D are the length and diameter of the cellulose fibers respectively.

Although, this approach leads to very accurate values for the volume fraction of cellulose to generate geometrical and electrical percolation, mechanical percolation is a completely different phenomenon. Unlike in the geometrical and electrical percolation, in mechanical percolation the formation of a continuous network of rigid elements across the entire system does not ensure the rigidity of the whole structure. It also depends on the type of chemical and physical interactions between elements, which are not included in the model [152], [170]. Additionally, the equation proposed by Frazier was formulated for non-branched fibers with homogeneous aspect ratios, which in practice has been observed to result in lower values of volume fraction [171]. Nevertheless, the values drawn by this equation help to set standard points to begin studying the mechanical percolation phenomenon of CNC.

Even so, a more precise calculation of the percolation threshold can be performed by evaluating the changes in the rheological behavior of polymer in solution, as a function of the weight percentage of filler. This method is based on the theory of filler reinforcement postulated by Eugene Guth [172], who observed that the changes in the elastic modulus and viscosity of a polymer reinforced with a filler, followed the same behavior as a function of the reinforcing agent content. He hypothesized that when a solution with a reinforcing agent is subjected to stress, the suspended particles of filler would perturb the propagation of the stress through the matrix by absorbing part of the forces, thus increasing the elastic energy and modulus of the material. Thereafter, taking advantage of the mathematical approach performed by Lorentz and Smoluchowski to describe the interaction of spherical particles embedded in a moving phase, Guth postulated the following equation, using K as the stress-strain relation at small strains, when the Young's modulus becomes a parameter

$$\frac{K'^*}{K'} = 1 + 2.5c + 14.1c^2$$

Where K'* and K' are the stress-strain relations of the reinforced and unreinforced system respectively, and "c" is the concentration of the filler in the system. This equation states that the addition of reinforcing elements would make the stress-strain curve increase by a factor of K'*/K, as a function of the filler concentration. Therefore, any deviation in this behavior may be caused by other effects like crystallization, changes in the volume under stress, or by the formation of a filler network. Subsequently, Guth realized that above certain concentrations, the equation was not valid to predict the sharp increments in the Young's modulus of the material. Further investigation in this area concluded that the rapid enhancement in the elastic properties of the solution were the result of the changes in the viscoelastic properties of the fluid, when a transition from liquid to solid-like state happens as consequence of the formation of a percolation network [172], [173], [174], [175].

Consequently, by surveying at small strains the changes in the elastic modulus of the reinforced solution as a function of the concentration, the amount of filler to achieve a percolation network can be found when an abrupt enhancement of the modulus occurs. Figure 1-12, shows the result of a study conducted by Fangming, *et al*. [174] related to the changes in the storage modulus of a solution of polymethyl methacrylate upon the increasing addition of carbon nanotubes. In this work, the viscosity of the polymer without a reinforcing agent was too low for the sensitivity of the equipment. From this figure, a sharp increase in the modulus is observed at low frequency or shear rate, when the concentration of carbon nanotubes was increased from 0.1% to 0.2%. Therefore, the percolation threshold was assumed to be within both concentrations.

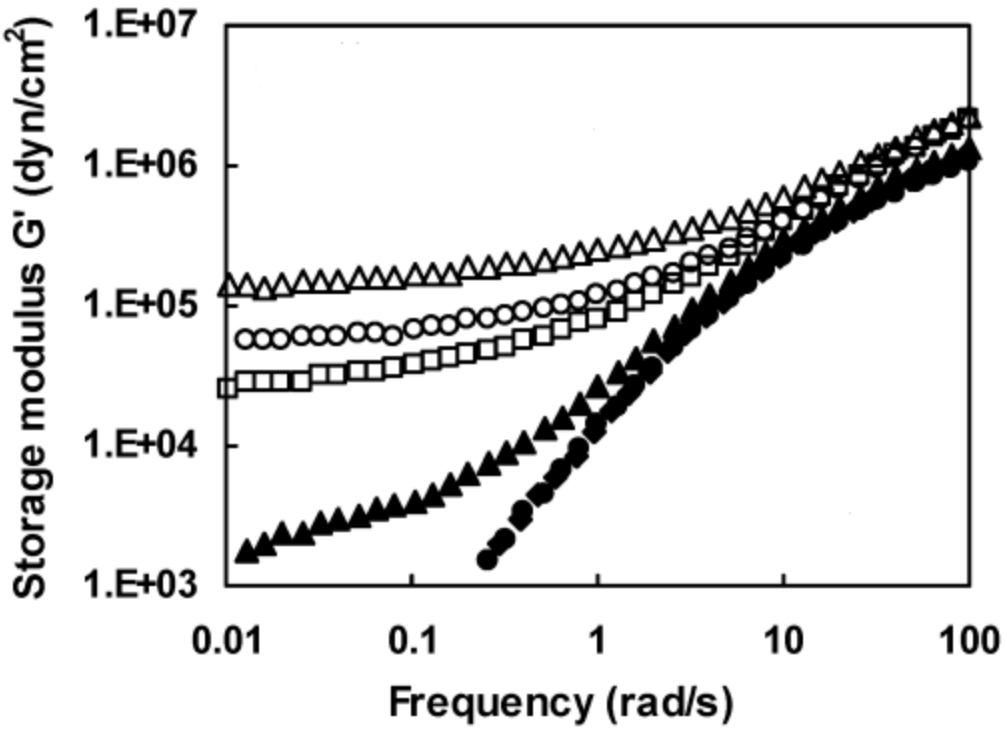


**FIGURE 1-12.** Storage modulus of a solution of polymethyl methacrylate as a function of the mass fraction carbon nanotubes (CNT) content. (●) 0.1% CNT, (▲) 0,2% CNT, (□) 0.5%, (○) 1.0% CNT, (∧) 2.0% CNT. Figure adapted from [174]. Copyright (2004) American Chemical Society.

Besides, in order to obtain an absolute value for the percolation threshold, instead of a range, a mathematical approach can be conducted at these conditions, where the mechanical properties and electrical conductivity strongly depends on the amount of filler added. Therefore, by replacing the electrical conductivity with the elastic modulus in the relationship discussed elsewhere by Benoit, *et al*. [176], the following expression to calculate the percolation threshold can be used.

$$G' \propto (m - m_C)^{\beta}$$

Where "m" is the concentration of the filler, G' is the elastic modulus at the given concentration of filler, "$m_c$" is the concentration at the percolation threshold, and β is a parameter. Thus, when values of elastic modulus at low frequency are available, via turning the former

expression into an equality and extrapolating the value of "m" when G' is zero, the value of the percolation threshold and β, can be obtained. Figure 1-13 displays the calculation for the numerical value of the percolation threshold for the study conducted by Fangming, *et al*. [174]. For this case, as mentioned in figure 1-12, the percolation threshold effectively was between 0.1% and 0.2%.

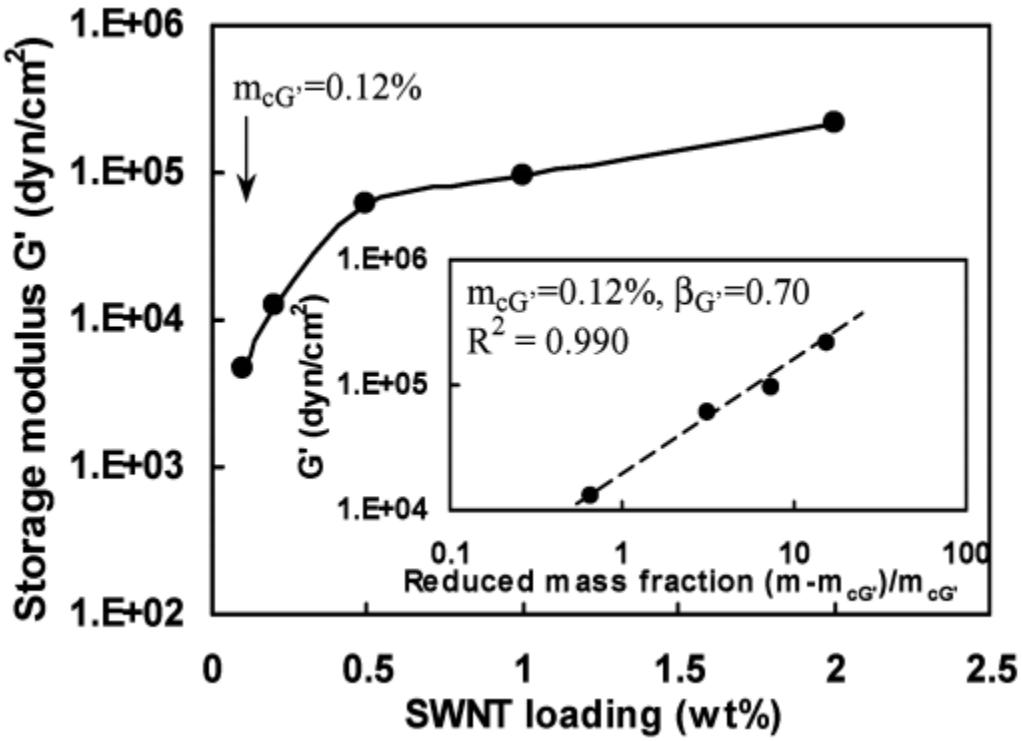


**FIGURE 1-13**. Storage modulus of a solution of polymethyl methacrylate measured at 0.5 rad/s, as a function of the mass fraction of carbon nanotubes (CNT) content. Figure adapted from [174]. Copyright (2004) American Chemical Society.

Finally, this approach is much more reliable than the theoretical value, as it considers the whole set of interactions that the solution experiences with the filler. Notwithstanding, the theoretical approach obtained by Favier's equation, may help to obtain an initial value.

### 1.5. Silk fibroin-cellulose nanocrystals composites

Recently, some studies have investigated the outcomes of blending silk fibroin with cellulose nanocrystals or nanofibrils, changing the solvents, and silk fibroin-cellulose ratios and processing systems, yielding composites with diverse morphologies and physicochemical and

mechanical properties. For instance, Huang, *el al.* [20], successfully improved tensile strength and reduced the fiber width of electrospun silk fibroin mats by adding up to 4% w/w of cellulose nanocrystals (also known as cellulose nanowhiskers). Nevertheless, a reduction in the strain at breaking was observed as CNC content increased. Likewise, Park, *et al.* [5], produced silk fibroin/bacterial cellulose nanocrystal (BCN) composites via electrospinning, accomplishing higher Young's modulus and tensile strengths as BCN content was increased up to 7%. Interestingly, the elongation at break was not affected by the addition of BCN. In addition, Lee, *et al.* [34], fabricated wet-spun fibers of silk fibroin/TEMPO-oxidized cellulose nanofibrils (TO-CNF), employing formic acid as a solvent and methanol as coagulating agent. It was found that TO-CNF decreased the drawing ratio of the fibers and the crystalline index of the composite, as TO-CNF might have restricted the crystallization of silk fibroin. Also, Yao, *et al.* [35], blended cellulose pulp and silk fibroin in different ratios by dissolving the compounds into 1-butyl-3-methylimidazolium chloride to render microfibers via jet-dry wet spinning. The tensile strength, elastic modulus, crystallinity, and drawing ratio decreased as silk fibroin content increased, however, all fibers exhibited outstanding mechanical performance. Correspondingly, Liu and Yao [36], reinforced silk fibroin wet-spun fibers by adding cellulose nanocrystals at various ratios into SF aqueous solutions before coagulation in a methanol bath. Regardless, regenerated silk fibroin has lower crystallinity and degradation temperature than degummed silk fibroin. The incorporation of CNC significantly increased these properties, resulting in higher crystallinity and thermal degradation in reinforced silk fibroin fibers compared with degummed silk. Additionally, it was observed that reinforced SF fibers exhibited superior Young's modulus and tensile strength compared with regenerated silk fibroin and degummed silk fibers. As well, Shefa *et al.* [37], developed SF-TO-CNC composites with wound healing capability by blending regenerated silk fibroin in a solution with TO-CNC at different ratios and cross-linking the components via amination of TO-CNC for grafting primary amine groups in silk fibroin onto the TO-CNC surface, followed by freeze drying. SF-TO-CNC composites exhibited biocompatibility, preferable water uptake capacity, and accelerated wound healing (related to percentage of wound closure), compared with other wound dressing materials.

### 1.5.1. Applications

Previous studies intended to entrap enzymes, chemicals, or cells into silk fibroin/cellulose based materials have also demonstrated the utility of these kinds of blends for food, pest control, and pharmaceutical applications. Qiong *et al*. developed a silk fibroin and cellulose acetate bilayer electrode which estimated the freshness of fish by incorporating xanthine oxidase into the silk fibroin layer. The sensor displayed high sensitivity for detection, stability in time, and capacity for reuse. The sensing values were in agreement with those from commercially available products, as well [177]. Guan *et al*. embedded bifenthrin, a chemical for termite control, in a silk fibroin matrix and then photoimmobilized the matrix on a wood surface with ultraviolet light. The device showed high-term stability and an appropriate bifenthrin release rate for termite control, providing an environmentally benign solution for pest control that protects materials that otherwise might be attacked [178]. Moreover, Drachuk *et al*. designed a biofilm of bacterial cellulose as a residue produced by *Gluconoacetobacter xylinus* in which recombinant *Escherichia coli* cells were cultured and finally immobilized using a silk fibroin coating, generating a composite of silk fibroin-bacterial cellulose where both types of cells were confined. The biofilm provided the necessary conditions to promote cell ingrowth and resilience to encapsulation. Also, the film displayed properties such as elasticity, fine porosity, high water retention, and the ability to absorb UV light [179].

Likewise, silk fibroin and cellulose based composites have been successfully processed through different techniques and in various shapes like films, fibers, powders, non-woven, and gels [2], [5], [21], [22] [20], [29], [34], [36], [104], [121]

## 1.6. References


[1] Y. Gong, L. Li, D. Gong, H. Yin, and J. Zhang, "Biomolecular Evidence of Silk from 8 , 500 Years Ago," *PLoS One*, vol. 11, no. 12, pp. 1–9, 2016.

[2] C. Vepari and D. L. Kaplan, "Silk as a biomaterial," *Prog. Polym. Sci.*, vol. 32, no. 8–9, pp. 991–1007, 2007.

[3] M. Elices, J. Perez Rigueiro, G. R. Plaza, and G. V. Guinea, "Usos médicos de la seda," *Investig. Cienc.*, pp. 28–35, 2011.

[4] L. Liu and J. M. Yao, "Wet-spinning of reinforced artificial silk hybrid fibres by cellulose whiskers," *Adv. Mater. Res.*, vol. 175–176, pp. 272–275, 2011.

[5] D. J. Park, Y. Choi, S. Heo, S. Y. Cho, and H.-J. Jin, "Bacterial Cellulose Nanocrystals-Embedded Silk Nanofibers," *J. Nanosci. Nanotechnol.*, vol. 12, no. 7, pp. 6139–6144, 2012.

[6] G. Shelach-Lavi, *The Archaeology of Early China, from prehistory to the Han dynasty*. 2015.

[7] D. L. Dunn, "Wound closure manual." Ethicon Products, Minnesota, pp. 1–127, 2005.

[8] Y. Cao and B. Wang, "Biodegradation of silk biomaterials," *Int. J. Mol. Sci.*, vol. 10, no. 4, pp. 1514–1524, 2009.

[9] B. N. Singh, N. N. Panda, R. Mund, and K. Pramanik, "Carboxymethyl cellulose enables silk fibroin nanofibrous scaffold with enhanced biomimetic potential for bone tissue engineering application," *Carbohydr. Polym.*, vol. 151, pp. 335–347, 2016.

[10] J. Pérez-Rigueiro, C. Viney, J. Llorca, and M. Elices, "Mechanical properties of silkworm silk in liquid media," *J. Appl. Polym. Sci.*, vol. 75, no. 10, pp. 1270–1277, 2000.

[11] H. P. Zhao, X. Q. Feng, S. W. Yu, W. Z. Cui, and F. Z. Zou, "Mechanical properties of silkworm cocoons," *Polymer (Guildf).*, vol. 46, no. 21, pp. 9192–9201, 2005.

[12] B. Lotz and F. Colonna Cesari, "The chemical structure and the crystalline structures of Bombyx mori silk fibroin," *Biochimie*, vol. 61, no. 2, pp. 205–214, 1979.

[13] Q. Zhang, S. Yan, and M. Li, "Silk fibroin based porous materials," *Materials (Basel).*, vol.

2, no. 4, pp. 2276–2295, 2009.

[14] G. H. Altman *et al.*, “Silk-based biomaterials,” *Biomaterials*, vol. 24, no. 3, pp. 401–416, 2003.

[15] R. I. Kunz, R. M. C. Brancalhao, L. D. F. C. Ribeiro, and M. R. M. Natali, “Silkworm Sericin: Properties and Biomedical Applications,” *Biomed Res. Int.*, vol. 2016, 2016.

[16] D. N. Rockwood, R. C. Preda, T. Yücel, X. Wang, M. L. Lovett, and D. L. Kaplan, “Materials fabrication from Bombyx mori silk fibroin,” *Nat. Protoc.*, vol. 6, no. 10, pp. 1612–1631, 2011.

[17] J. G. Hardy and T. R. Scheibel, “Composite materials based on silk proteins,” *Prog. Polym. Sci.*, vol. 35, no. 9, pp. 1093–1115, 2010.

[18] N. Bhardwaj and S. C. Kundu, “Electrospinning: A fascinating fiber fabrication technique,” *Biotechnol. Adv.*, vol. 28, no. 3, pp. 325–347, 2010.

[19] X. Zhang, M. R. Reagan, and D. L. Kaplan, “Electrospun silk biomaterial scaffolds for regenerative medicine,” *Adv. Drug Deliv. Rev.*, vol. 61, no. 12, pp. 988–1006, 2009.

[20] J. Huang, L. Liu, and J. Yao, “Electrospinning of Bombyx mori silk fibroin nanofiber mats reinforced by cellulose nanowhiskers,” *Fibers Polym.*, vol. 12, no. 8, pp. 1002–1006, 2011.

[21] W. Zhou, J. He, S. Du, S. Cui, and W. Gao, “Electrospun silk fibroin/cellulose acetate blend nanofibres: structure and properties,” *Iran. Polym. J.*, vol. 20, no. 5, pp. 389–397, 2011.

[22] E. Marsano, M. Canetti, G. Conio, P. Corsini, and G. Freddi, “Fibers based on cellulose-silk fibroin blend,” *J. Appl. Polym. Sci.*, vol. 104, no. 4, pp. 2187–2196, 2007.

[23] T. Kitagawa and K. Yabuki, “Physical properties of silk fibroin/chitosan blend films,” *J. Appl. Polym. Sci.*, vol. 80, no. 7, pp. 928–934, 2001.

[24] L.-D. Koh *et al.*, “Structures, mechanical properties and applications of silk fibroin materials,” *Prog. Polym. Sci.*, vol. 46, pp. 86–110, 2015.

[25] U. J. Kim, J. Park, C. Li, H. J. Jin, R. Valluzzi, and D. L. Kaplan, “Structure and properties of silk hydrogels,” *Biomacromolecules*, vol. 5, no. 3, pp. 786–792, 2004.

[26] A. Baji, Y. W. Mai, S. C. Wong, M. Abtahi, and P. Chen, “Electrospinning of polymer

nanofibers: Effects on oriented morphology, structures and tensile properties," *Compos. Sci. Technol.*, vol. 70, no. 5, pp. 703–718, 2010.

[27] S. Fujisawa, T. Ikeuchi, M. Takeuchi, T. Saito, and A. Isogai, "Superior reinforcement effect of TEMPO-oxidized cellulose nanofibrils in polystyrene matrix: optical, thermal, and mechanical studies.," *Biomacromolecules*, vol. 13, no. 7, pp. 2188–2194, 2012.

[28] S. Shang, L. Zhu, and J. Fan, "Intermolecular interactions between natural polysaccharides and silk fibroin protein," *Carbohydr. Polym.*, vol. 93, no. 2, pp. 561–573, 2013.

[29] R. J. Moon, A. Martini, J. Nairn, J. Simonsen, and J. Youngblood, *Cellulose nanomaterials review: structure, properties and nanocomposites*, vol. 40, no. 7. 2011.

[30] J. G. Hardy, L. M. Romer, and T. R. Scheibel, "Polymeric materials based on silk proteins," *Polymer (Guildf).*, vol. 49, no. 20, pp. 4309–4327, 2008.

[31] M. Mariano, N. El Kissi, and A. Dufresne, "Cellulose nanocrystals and related nanocomposites: Review of some properties and challenges," *J. Polym. Sci. Part B Polym. Phys.*, vol. 52, no. 12, pp. 791–806, 2014.

[32] Y. Habibi, L. A. Lucia, and O. J. Rojas, "Cellulose Nanocrystals : Chemistry , Self-Assembly , and Applications," *Chem. Rev.*, vol. 110, no. 6, pp. 3479–3500, 2010.

[33] A. Isogai, T. Saito, and H. Fukuzumi, "TEMPO-oxidized cellulose nanofibers," *Nanoscale*, vol. 3, no. 1, pp. 71–85, 2011.

[34] J. H. Lee, C. H. Bae, B.-D. Park, and I. C. Um, "Preparation of Cellulose Nanofibril/Regenerated Silk Fibroin Composite Fibers," *Int. J. Ind. Entomol.*, vol. 26, no. 2, pp. 81–88, 2013.

[35] Y. Yao *et al.*, "Morphology and properties of cellulose/silk fibroin blend fiber prepared with 1-butyl-3-methylimidazolium chloride as solvent," *Cellulose*, vol. 22, no. 1, pp. 625–635, 2015.

[36] L. Liu, X. Yang, H. Yu, C. Ma, and J. Yao, "Biomimicking the structure of silk fibers via cellulose nanocrystal as β-sheet crystallite," *R. Soc. Chem. Adv.*, vol. 4, no. 27, p. 14304, 2014.

[37] A. A. Shefa *et al.*, “In vitro and in vivo evaluation of effectiveness of a novel TEMPO-oxidized cellulose nanofiber-silk fibroin scaffold in wound healing,” *Carbohydr. Polym.*, vol. 177, no. April, pp. 284–296, 2017.

[38] L. L. Guo, Y. B. Liu, and J. B. Yao, “A Review on Existing Tecgnology of Electrospinning at Large Scale,” *Proc. 2010 Int. Conf. Inf. Technol. Sci. Manag. Vols 1-2*, pp. 279–282, 2010.

[39] L. M. Duque Sánchez, L. Rodriguez, and M. López, “Electrospinning: The Nanofibers Age,” *Rev. Iberoam. Polímeros Vol. Iber. Polímeros*, vol. 14, no. 141, pp. 10–27, 2014.

[40] J. F. Cooley, “Apparatus for electrically dispersing fluids,” US Patent 692,631, 1902.

[41] J. Stranger, N. Tucker, and M. Staiger, “Electrospinnin.” pp. 1–218, 2005.

[42] W. J. Morton, “Method of dispersing fluids,” US Patent705,691, 1902.

[43] J. Zeleny, “The electrical discharge from liquid points, and a hydrostatic method of measuring the electrical intensity at their surfaces,” *Physycal Rev.*, vol. 3, no. 2, pp. 69–91, 1914.

[44] A. Formhals, “Process and apparatus for preparing artificial threads,” US Patent 1,975,504, 1934.

[45] anton Formhals, “Artificial Fiber Construction,” US Patent 2,109,333, 1938.

[46] A. Formhals, “Method of Producing Artificial Fibers,” US Patent 2,158,415, 1939.

[47] A. Formhals, “Method and apparatus for spinning,” US Patent 2,160,962, 1939.

[48] A. Formhals, “Artificial thread and method of producing same,” US Patent2,187,306, 1940.

[49] A. Formhals, “Production of artificial fibers from fiber forming liquids,” 2,323,025, 1943.

[50] A. Formhals, “Method and apparatus for spinning,” US Patent 2,349,950, 1944.

[51] T. Subbiah, G. S. Bhat, R. W. Tock, S. Parameswaran, and S. S. Ramkumar, “Electrospinning of nanofibers,” *J. Appl. Polym. Sci.*, vol. 96, no. 2, pp. 557–569, 2005.

[52] M. Mirjalili and S. Zohoori, “Review for application of electrospinning and electrospun nanofibers technology in textile industry,” *J. Nanostructure Chem.*, vol. 6, no. 3, pp. 207–213, 2016.

[53] G. Taylor, “Disintegration of water drops in an electric field,” *Proc. R. Soc. London A*, vol. 280, no. 22, pp. 383–397, 1964.

[54] G. Taylor and M. D. Van Dyke, “Electrically driven jets,” *Proc. R. Soc. London A.*, vol. 313, pp. 453–475, 1969.

[55] J. Doshi and D. H. Reneker, “Electrospinning process and applications of electrospun fibers,” *Conf. Rec. 1993 IEEE Ind. Appl. Conf. Twenty-Eighth IAS Annu. Meet.*, vol. 35, pp. 151–160, 1993.

[56] S. Y. Chew, Y. Wen, Y. Dzenis, and K. W. Leong, “The role of electrospinning in the emerging field of nanomedicine.,” *Curr. Pharm. Des.*, vol. 12, no. 36, pp. 4751–70, 2006.

[57] Z.-M. Huang, Y.-Z. Zhang, M. Kotaki, and S. Ramakrishna, “A review on polymer nanofibers by electrospinning and their applications in nanocomposites,” *Compos. Sci. Technol.*, vol. 63, no. 15, pp. 2223–2253, 2003.

[58] M. M. Hohman, M. Shin, G. Rutledge, and M. P. Brenner, “Electrospinning and electrically forced jets. I. Stability theory,” *Phys. Fluids*, vol. 13, no. 8, pp. 2201–2220, 2001.

[59] D. H. Reneker, A. L. Yarin, H. Fong, S. Koombhongse, and D. H. Reneker, “Bending instability of electrically charged liquid jets of polymer solutions in electrospinning,” *J. Appl. Phys.*, vol. 87, no. 9, pp. 4531–4548, 2000.

[60] Y. M. Shin, M. M. Hohman, M. P. Brenner, and G. C. Rutledge, “Experimental characterization of electrospinning: the electrically forced jet and instabilities,” *Polymer (Guildf).*, vol. 42, no. 25, pp. 9955–9967, 2001.

[61] A. Greiner and J. H. Wendorff, “Electrospinning: A fascinating method for the preparation of ultrathin fibers,” *Angew. Chemie - Int. Ed.*, vol. 46, no. 30, pp. 5670–5703, 2007.

[62] A. J. Dekker, *Electrical engineering materials*, Prentice-Hall. Minnesota: Prentice-Hall INC., 1959.

[63] S. Kidoaki, I. K. Kwon, and T. Matsuda, “Mesoscopic spatial designs of nano- and microfiber meshes for tissue-engineering matrix and scaffold based on newly devised multilayering and mixing electrospinning techniques,” *Biomaterials*, vol. 26, no. 1, pp. 37–

46, Jan. 2005.

[64] J. J. Stankus, J. Guan, K. Fujimoto, and W. R. Wagner, “Microintegrating smooth muscle cells into a biodegradable, elastomeric fiber matrix,” *Biomaterials*, vol. 27, no. 5, pp. 735–744, Feb. 2006.

[65] S. Agarwal, J. H. Wendorff, and A. Greiner, “Use of electrospinning technique for biomedical applications,” *Polymer (Guildf).*, vol. 49, no. 26, pp. 5603–5621, 2008.

[66] R. Sahay, V. Thavasi, and S. Ramakrishna, “Design modifications in electrospinning setup for advanced applications,” *J. Nanomater.*, vol. 2011, 2011.

[67] F. E. Ahmed, B. S. Lalia, and R. Hashaikeh, “A review on electrospinning for membrane fabrication: Challenges and applications,” *Desalination*, vol. 356, pp. 15–30, 2015.

[68] W. E. Teo and S. Ramakrishna, “A review on electrospinning design and nanofibre assemblies,” *Nanotechnology*, vol. 17, no. 14, pp. R89–R106, Jul. 2006.

[69] P. Gupta, C. Elkins, T. E. Long, and G. L. Wilkes, “Electrospinning of linear homopolymers of poly(methyl methacrylate): exploring relationships between fiber formation, viscosity, molecular weight and concentration in a good solvent,” *Polymer (Guildf).*, vol. 46, no. 13, pp. 4799–4810, Jun. 2005.

[70] E. P. S. Tan, S. Y. Ng, and C. T. Lim, “Tensile testing of a single ultrafine polymeric fiber,” *Biomaterials*, vol. 26, no. 13, pp. 1453–1456, May 2005.

[71] J. . Deitzel, W. Kosik, S. . McKnight, N. . Beck Tan, J. . DeSimone, and S. Crette, “Electrospinning of polymer nanofibers with specific surface chemistry,” *Polymer (Guildf).*, vol. 43, no. 3, pp. 1025–1029, Feb. 2002.

[72] L. Larrondo and R. St. John Manley, “Electrostatic fiber spinning from polymer melts. I. Experimental observations on fiber formation and properties,” *J. Polym. Sci. Polym. Phys. Ed.*, vol. 19, no. 6, pp. 909–920, Jun. 1981.

[73] A. K. Haghi and M. Akbari, “Trends in electrospinning of natural nanofibers,” *Phys. status solidi*, vol. 204, no. 6, pp. 1830–1834, Jun. 2007.

[74] H. Fong, I. Chun, and D. . Reneker, “Beaded nanofibers formed during electrospinning,”

*Polymer (Guildf).*, vol. 40, no. 16, pp. 4585–4592, Jul. 1999.

[75] I. Hayati, A. . Bailey, and T. . Tadros, “Investigations into the mechanisms of electrohydrodynamic spraying of liquids: I. Effect of electric field and the environment on pendant drops and factors affecting the formation of stable jets and atomization,” *J. Colloid Interface Sci.*, vol. 117, no. 1, pp. 205–221, May 1987.

[76] N. A. M. Barakat, M. A. Kanjwal, F. A. Sheikh, and H. Y. Kim, “Spider-net within the N6, PVA and PU electrospun nanofiber mats using salt addition: Novel strategy in the electrospinning process,” *Polymer (Guildf).*, vol. 50, no. 18, pp. 4389–4396, Aug. 2009.

[77] R. Jalili, S. A. Hosseini, and M. Morshed, “The Effects of Operating Parameters on the morphology of electrospun polyacrilonitile nanofibres,” *Iran. Polym. J.*, vol. 14, no. 12, pp. 1074–1081, 2005.

[78] K. H. Lee, H. Y. Kim, M. S. Khil, Y. M. Ra, and D. R. Lee, “Characterization of nano-structured poly(ε-caprolactone) nonwoven mats via electrospinning,” *Polymer (Guildf).*, vol. 44, no. 4, pp. 1287–1294, Feb. 2003.

[79] Y. Zhang, H. Ouyang, C. T. Lim, S. Ramakrishna, and Z.-M. Huang, “Electrospinning of gelatin fibers and gelatin/PCL composite fibrous scaffolds,” *J. Biomed. Mater. Res.*, vol. 72B, no. 1, pp. 156–165, Jan. 2005.

[80] M. . Demir, I. Yilgor, E. Yilgor, and B. Erman, “Electrospinning of polyurethane fibers,” *Polymer (Guildf).*, vol. 43, no. 11, pp. 3303–3309, May 2002.

[81] V. Sencadas *et al.*, “Determination of the parameters affecting electrospun chitosan fiber size distribution and morphology,” *Carbohydr. Polym.*, vol. 87, no. 2, pp. 1295–1301, Jan. 2012.

[82] K.-H. Kim *et al.*, “Biological efficacy of silk fibroin nanofiber membranes for guided bone regeneration,” *J. Biotechnol.*, vol. 120, no. 3, pp. 327–339, Nov. 2005.

[83] X. Zong, K. Kim, D. Fang, S. Ran, B. S. Hsiao, and B. Chu, “Structure and process relationship of electrospun bioabsorbable nanofiber membranes,” *Polymer (Guildf).*, vol. 43, no. 16, pp. 4403–4412, Jul. 2002.

[84] C. S. Ki, D. H. Baek, K. D. Gang, K. H. Lee, I. C. Um, and Y. H. Park, “Characterization of gelatin nanofiber prepared from gelatin–formic acid solution,” *Polymer (Guildf).*, vol. 46, no. 14, pp. 5094–5102, Jun. 2005.

[85] J. S. Lee *et al.*, “Role of molecular weight of atactic poly(vinyl alcohol) (PVA) in the structure and properties of PVA nanofabric prepared by electrospinning,” *J. Appl. Polym. Sci.*, vol. 93, no. 4, pp. 1638–1646, Aug. 2004.

[86] X. Wang, I. C. Um, D. Fang, A. Okamoto, B. S. Hsiao, and B. Chu, “Formation of water-resistant hyaluronic acid nanofibers by blowing-assisted electro-spinning and non-toxic post treatments,” *Polymer (Guildf).*, vol. 46, no. 13, pp. 4853–4867, Jun. 2005.

[87] J. Doshi and D. H. Reneker, “Electrospinning process and applications of electrospun fibers,” *J. Electrostat.*, vol. 35, no. 2–3, pp. 151–160, Aug. 1995.

[88] J. . Deitzel, J. Kleinmeyer, D. Harris, and N. . Beck Tan, “The effect of processing variables on the morphology of electrospun nanofibers and textiles,” *Polymer (Guildf).*, vol. 42, no. 1, pp. 261–272, Jan. 2001.

[89] K. W. Kim, K. H. Lee, M. S. Khil, Y. S. Ho, and H. Y. Kim, “The effect of molecular weight and the linear velocity of drum surface on the properties of electrospun poly(ethylene terephthalate) nonwovens,” *Fibers Polym.*, vol. 5, no. 2, pp. 122–127, Jun. 2004.

[90] C. S. Ki *et al.*, “Electrospun three-dimensional silk fibroin nanofibrous scaffold,” *J. Appl. Polym. Sci.*, vol. 106, no. 6, pp. 3922–3928, Dec. 2007.

[91] C. J. Thompson, G. G. Chase, A. L. Yarin, and D. H. Reneker, “Effects of parameters on nanofiber diameter determined from electrospinning model,” *Polymer (Guildf).*, vol. 48, no. 23, pp. 6913–6922, Nov. 2007.

[92] S. Zhao, X. Wu, L. Wang, and Y. Huang, “Electrospinning of ethyl-cyanoethyl cellulose/tetrahydrofuran solutions,” *J. Appl. Polym. Sci.*, vol. 91, no. 1, pp. 242–246, Jan. 2004.

[93] G. L. Wilkes, “An Overview of the Basic Rheological Behavior of Polymer Fluids with an Emphasis on Polymer Melts,” *J. Chem. Educ.*, vol. 58, no. 11, p. 880-, 1981.

[94] L. C. Cheryl, J. S. Stephens, G. Tassi, Nancy, D. B. Chase, and J. F. Rabolt, “Controlling Surface Morphology of Electrospun Polystyrene Fibers: Effect of Humidity and Molecular Weight in the Electrospinning Process,” *Macromolecules*, vol. 37, no. 2, pp. 573–578, 2003.

[95] P. K. Baumgarten, “Electrostatic spinning of acrylic microfibers,” *J. Colloid Interface Sci.*, vol. 36, no. 1, pp. 71–79, May 1971.

[96] S. A. Theron, A. L. Yarin, E. Zussman, and E. Kroll, “Multiple jets in electrospinning: experiment and modeling,” *Polymer (Guildf).*, vol. 46, no. 9, pp. 2889–2899, Apr. 2005.

[97] D. Li and Y. Xia, “Electrospinning of Nanofibers: Reinventing the Wheel?,” *Adv. Mater.*, vol. 16, no. 14, pp. 1151–1170, Jul. 2004.

[98] M. Li, M. J. Mondrinos, M. R. Gandhi, F. K. Ko, A. S. Weiss, and P. I. Lelkes, “Electrospun protein fibers as matrices for tissue engineering,” *Biomaterials*, vol. 26, no. 30, pp. 5999–6008, Oct. 2005.

[99] J. Pelipenko, J. Kristl, B. Janković, S. Baumgartner, and P. Kocbek, “The impact of relative humidity during electrospinning on the morphology and mechanical properties of nanofibers,” *Int. J. Pharm.*, vol. 456, no. 1, pp. 125–134, Nov. 2013.

[100] E. S. Medeiros *et al.*, “Electrospun Nanofibers of Poly(vinyl alcohol) Reinforced with Cellulose Nanofibrils,” *J. Biobased Mater. Bioenergy*, vol. 2, no. 3, pp. 231–242, Sep. 2008.

[101] C. Mit-uppatham, M. Nithitanakul, and P. Supaphol, “Ultrafine Electrospun Polyamide-6 Fibers: Effect of Solution Conditions on Morphology and Average Fiber Diameter,” *Macromol. Chem. Phys.*, vol. 205, no. 17, pp. 2327–2338, Nov. 2004.

[102] C. Burger, B. S. Hsiao, and B. Chu, “NANOFIBROUS MATERIALS AND THEIR APPLICATIONS,” *Annu. Rev. Mater. Res.*, vol. 36, no. 1, pp. 333–368, Aug. 2006.

[103] S. Ramakrishna *et al.*, “Science and engineering of electrospun nanofibers for advances in clean energy, water filtration, and regenerative medicine,” *J. Mater. Sci.*, vol. 45, no. 23, pp. 6283–6312, Dec. 2010.

[104] E. Marsano, P. Corsini, M. Canetti, and G. Freddi, “Regenerated cellulose-silk fibroin blends fibers,” *Int. J. Biol. Macromol.*, vol. 43, no. 2, pp. 106–114, 2008.

[105] H. Hou and D. H. Reneker, “Carbon Nanotubes on Carbon Nanofibers: A Novel Structure Based on Electrospun Polymer Nanofibers,” *Adv. Mater.*, vol. 16, no. 1, pp. 69–73, Jan. 2004.

[106] H. Ma, J. Zeng, M. L. Realff, S. Kumar, and D. A. Schiraldi, “Processing, structure, and properties of fibers from polyester/carbon nanofiber composites,” *Compos. Sci. Technol.*, vol. 63, no. 11, pp. 1617–1628, Aug. 2003.

[107] Y. Liu, S. Sagi, R. Chandrasekar, L. Zhang, N. E. Hedin, and H. Fong, “Preparation and Characterization of Electrospun SiO2 Nanofibers,” *J. Nanosci. Nanotechnol.*, vol. 8, no. 3, pp. 1528–1536, Mar. 2008.

[108] W. Shi, W. Lu, and L. Jiang, “The fabrication of photosensitive self-assembly Au nanoparticles embedded in silica nanofibers by electrospinning,” *J. Colloid Interface Sci.*, vol. 340, no. 2, pp. 291–297, Dec. 2009.

[109] M. S. Peresin, Y. Habibi, J. O. Zoppe, J. J. Pawlak, and O. J. Rojas, “Nanofiber Composites of Polyvinyl Alcohol and Cellulose Nanocrystals: Manufacture and Characterization,” *Biomacromolecules*, vol. 11, no. 3, pp. 674–681, Mar. 2010.

[110] P. Bhattarai, K. B. Thapa, R. B. Basnet, and S. Sharma, “Electrospinning: How to Produce Nanofibers Using Most Inexpensive Technique? An Insight into the Real Challenges of Electrospinning Such Nanofibers and Its Application Areas,” *Int. J. Biomed. Adv. Res.*, vol. 5, no. 09, pp. 401–405, 2014.

[111] X. Shi *et al.*, “Electrospinning of Nanofibers and Their Applications for Energy Devices,” *J. Nanomater.*, vol. 2015, pp. 1–20, May 2015.

[112] V. Kumar and A. Rawal, “Elastic moduli of electrospun mats: Importance of fiber curvature and specimen dimensions,” *J. Mech. Behav. Biomed. Mater.*, vol. 72, no. February, pp. 6–13, 2017.

[113] L. Y. Wan, H. Wang, W. Gao, and F. Ko, “An analysis of the tensile properties of nanofiber mats,” *Polym. (United Kingdom)*, vol. 73, pp. 62–67, 2015.

[114] A. C. Fischer-Cripps, *Nanoindentation*, Third edit. Springer US, 2011.

[115] S. Ghosh, S. T. Parker, X. Wang, D. L. Kaplan, and J. A. Lewis, “Direct-Write Assembly of Microperiodic Silk Fibroin Scaffolds for Tissue Engineering Applications,” *Adv. Funct. Mater.*, vol. 18, no. 13, pp. 1883–1889, Jul. 2008.

[116] M. Wang, H.-J. Jin, D. L. Kaplan, and G. C. Rutledge, “Mechanical Properties of Electrospun Silk Fibers,” *Macromolecules*, vol. 37, no. 18, pp. 6856–6864, Sep. 2004.

[117] Y. X. He *et al.*, “N-terminal domain of Bombyx mori fibroin mediates the assembly of silk in response to pH decrease,” *J. Mol. Biol.*, vol. 418, no. 3–4, pp. 197–207, 2012.

[118] Q. Xia *et al.*, “Complete resequencing of 40 genomes reveals domestication events and genes in silkworm (Bombyx).,” *Science*, vol. 326, no. 5951, pp. 433–6, Oct. 2009.

[119] D. Christian, “Silk Roads or Steppe Roads? The Silk Road in World History,” *J. world Hist.*, vol. 11, no. 1, pp. 1–26, 2000.

[120] D. D. N. Rockwood, R. R. C. Preda, T. Yücel, X. Wang, M. L. Lovett, and D. L. Kaplan, “Materials fabrication from Bombyx mori silk fibroin,” *Nat. Protoc.*, vol. 6, no. 10, pp. 1–43, 2011.

[121] S. Hirano, N. Tamayo, M. Zhang, M. Nakagawa, M. Yoshikawa, and T. Midorikawa, “Wet-spun blend biofibers of cellulose-silk fibroin and cellulose-chitin-silk fibroin,” *Carbohydr. Polym.*, vol. 47, no. 2, pp. 121–124, 2002.

[122] S. Inoue, K. Tanaka, F. Arisaka, S. Kimura, K. Ohtomo, and S. Mizuno, “Silk Fibroin of Bombyx mori is Secreted, Assembling a High Molecular Mass Elementary Unit Consisting of H-chain, L-chain, and P25, with a 6:6:1 Molar Ratio,” *J. Biol. Chem.*, vol. 275, no. 51, pp. 40517–40528, Dec. 2000.

[123] K. Tanaka *et al.*, “Determination of the site of disulfide linkage between heavy and light chains of silk fibroin produced by Bombyx mori,” *Biochim. Biophys. Acta - Protein Struct. Mol. Enzymol.*, vol. 1432, no. 1, pp. 92–103, Jun. 1999.

[124] M. Chevillard, P. Couble, and J. C. Prudhomme, “Complete nucleotide sequence of the gene encoding the Bombyx mori silk protein P25 and predicted amino acid sequence of the protein.,” *Nucleic Acids Res.*, vol. 14, no. 15, pp. 6341–2, Aug. 1986.

[125] C. Z. Zhou, F. Confalonieri, M. Jacquet, R. Perasso, Z. G. Li, and J. Janin, “Silk fibroin: structural implications of a remarkable amino acid sequence.,” *Proteins*, vol. 44, no. 2, pp. 119–22, Aug. 2001.

[126] L. P. Gage and R. F. Manning, “Internal structure of the silk fibroin gene of Bombyx mori. I The fibroin gene consists of a homogeneous alternating array of repetitious crystalline and amorphous coding sequences.,” *J. Biol. Chem.*, vol. 255, no. 19, pp. 9444–50, Oct. 1980.

[127] S. K. Rajput and M. Kumar Singh, “Sericin - A Unique Biomaterial,” *J. Polym. Text. Eng.*, vol. 2, no. 3, pp. 29–35, 2015.

[128] Y.-Q. Zhang, “Applications of natural silk protein sericin in biomaterials,” *Biotechnol. Adv.*, vol. 20, no. 2, pp. 91–100, 2002.

[129] S. He, R. Valluzzi, and S. P. Gido, “Silk I structure in bomyx mori silk foams,” *Int. J. Biol. Macromol.*, vol. 24, pp. 187–195, 1999.

[130] H.-J. Jin and D. L. Kaplan, “Mechanism of silk processing in insects and spiders,” *Nature*, vol. 424, no. 6952, pp. 1057–1061, Aug. 2003.

[131] S. Rammensee, U. Slotta, T. Scheibel, and A. R. Bausch, “Assembly mechanism of recombinant spider silk proteins,” *Proc. Natl. Acad. Sci.*, vol. 105, no. 18, pp. 6590–6595, May 2008.

[132] A. Motta, L. Fambri, and C. Migliaresi, “Regenerated silk fibroin films: Thermal and dynamic mechanical analysis,” *Macromol. Chem. Phys.*, vol. 203, no. 10–11, pp. 1658–1665, Jul. 2002.

[133] P. Cebe *et al.*, “Beating the heat-fast scanning melts silk beta sheet crystals,” *Sci. Rep.*, vol. 3, pp. 1–7, 2013.

[134] G. Salvi, P. De Los Rios, and M. Vendruscolo, “Effective interactions between chaotropic agents and proteins,” *Proteins Struct. Funct. Genet.*, vol. 61, no. 3, pp. 492–499, Sep. 2005.

[135] J. Y. Rongji Li, Yanhong Zhang, Liangjun Zhu, “Fabrication and Characterization of Silk Fibroin/Poly(ethylene glycol)/Cellulose Nanowhisker Composite Films,” *J. Appl. Polym. Sci.*, vol. 124, pp. 2080–2086, 2012.

[136] L. S. Wray *et al.*, “Effect of processing on silk-based biomaterials: Reproducibility and biocompatibility,” *J. Biomed. Mater. Res. - Part B Appl. Biomater.*, vol. 99 B, no. 1, pp. 89–101, 2011.

[137] I. C. Um, H. Y. Kweon, K. G. Lee, D. W. Ihm, J. H. Lee, and Y. H. Park, “Wet spinning of silk polymer: I. Effect of coagulation conditions on the morphological feature of filament,” *Int. J. Biol. Macromol.*, vol. 34, no. 1–2, pp. 89–105, 2004.

[138] H. J. Cho, Y. J. Yoo, J. W. Kim, Y. H. Park, D. G. Bae, and I. C. Um, “Effect of molecular weight and storage time on the wet- and electro-spinning of regenerated silk fibroin,” *Polym. Degrad. Stab.*, vol. 97, no. 6, pp. 1060–1066, 2012.

[139] B. Kundu, R. Rajkhowa, S. C. Kundu, and X. Wang, “Silk fibroin biomaterials for tissue regenerations,” *Adv. Drug Deliv. Rev.*, vol. 65, no. 4, pp. 457–470, 2013.

[140] P. Wongpanit, O. Pornsunthorntawee, and R. Rujiravanit, *Chapter 11: Silk Fibre Composites*, vol. 1, no. 1. The royal Society of Chemistry, 2012.

[141] L. Grasset, D. Cordier, and A. Ville, “Woven Silk as a Carrier for the Immobilization of Enzymes,” *J. Biotecnol. Bioeng.*, vol. 19, pp. 611–618, 1977.

[142] Y. Q. Zhang, “Natural silk fibroin as a support for enzyme immobilization,” *Biotechnol. Adv.*, vol. 16, no. 5–6, pp. 961–971, 1998.

[143] H. Yoshimizu and T. Asakura, “Preparation and Characterization of Silk Fibroin Powder andApplication to Enzyme Immobilization,” *J. Appl. Polym. Sci.*, vol. 40, no. 1–2, pp. 127–134, 1990.

[144] Kuzuhara A, Asakura T, Tomoda R, and Matsunaga T, “Use of silk fibroin for enzyme membrane,” *J. Biotechnol.*, vol. 5, no. 3, pp. 199–207, May 1987.

[145] M. Demura and T. Asakura, “Porous membrane of Bombyx mori silk fibroin: structure characterization, physical properties and application to glucose oxidase immobilization,” *J. Memb. Sci.*, vol. 59, no. 1, pp. 39–52, 1991.

[146] Y. Q. Zhang, J. Zhu, and R. a Gu, “Improved biosensor for glucose based on glucose oxidase-immobilized silk fibroin membrane.,” *Appl. Biochem. Biotechnol.*, vol. 75, pp.

215–233, 1999.

[147] H. Zhang *et al.*, “Preparation and characterization of silk fibroin as a biomaterial with potential for drug delivery,” *J. Transl. Med.*, vol. 10, no. 1, p. 117, 2012.

[148] M. P. Ho, H. Wang, and K. T. Lau, “Effect of degumming time on silkworm silk fibre for biodegradable polymer composites,” *Appl. Surf. Sci.*, vol. 258, no. 8, pp. 3948–3955, 2012.

[149] R. M. Brown, “The biosynthesis of cellulose,” *J. Macromolecurar Sci. Part A*, vol. 33, no. 10, pp. 345–351, Oct. 1996.

[150] I. M. Saxena and R. M. Brown, “Cellulose Biosynthesis: Current Views and Evolving Concepts,” *Ann. Bot.*, vol. 96, no. 1, pp. 9–21, Jul. 2005.

[151] L. Liu and J. M. Yao, “Wet-Spinning of Reinforced Artificial Silk Hybrid Fibres by Cellulose Whiskers,” *Adv. Mater. Res.*, vol. 175–176, pp. 272–275, 2011.

[152] A. Dufresne, *Nanocellulose: From natural to high performance tailored materials*. Berlin: De Gruyter, 2012.

[153] R. Pelton, “Bioactive paper provides a low-cost platform for diagnostics,” *TrAC - Trends Anal. Chem.*, vol. 28, no. 8, pp. 925–942, 2009.

[154] A. H. Free, E. C. Adams, M. L. Kercher, H. M. Free, and M. H. Cook, “Simple specific test for urine glucose.,” *Clin. Chem.*, vol. 3, no. 3, pp. 163–168, 1957.

[155] H. Orelma, *Cellulose based bio- interfaces for immunodiagnostic applications*. 2012.

[156] K. Abe, K. Suzuki, and D. Citterio, “Inkjet-printed microfluidic multianalyte chemical sensing paper,” *Anal. Chem.*, vol. 80, no. 18, pp. 6928–6934, 2008.

[157] E. M. Fenton, M. R. Mascarenas, G. P. López, and S. S. Sibbett, “Multiplex lateral-flow test strips fabricated by two-dimensional shaping,” *ACS Appl. Mater. Interfaces*, vol. 1, no. 1, pp. 124–129, 2009.

[158] A. W. Martinez, S. T. Phillips, G. M. Whitesides, and E. Carrilho, “Diagnostics for the developing world: Microfluidic paper-based analytical devices,” *Anal. Chem.*, vol. 82, no. 1, pp. 3–10, 2010.

[159] R. F. ZuI *et al.*, “Enzyme Immunochromatography-AQuantitativeImmunoassayRequinng

No Instrumentation," *Clin. Chem.*, vol. 3117, no. 7, pp. 1144–1150, 1985.

[160] R. Krska and A. Molinelli, "Rapid test strips for analysis of mycotoxins in food and feed," *Anal. Bioanal. Chem.*, vol. 393, no. 1, pp. 67–71, 2009.

[161] C. M. Cheng *et al.*, "Paper-based elisa," *Angew. Chemie - Int. Ed.*, vol. 49, no. 28, pp. 4771–4774, 2010.

[162] J. M. Hammersley, "Percolation processes," *Math. Proc. Cambridge Philos. Soc.*, vol. 53, no. 03, p. 642, Jul. 1957.

[163] S. R. Broadbent and J. M. Hammersley, "Percolation processes," *Math. Proc. Cambridge Philos. Soc.*, vol. 53, no. 03, p. 629, Jul. 1957.

[164] I. Balberg, N. Binenbaum, and N. Wagner, "Percolation Thresholds in the Three-Dimensional Sticks System," *Phys. Rev. Lett.*, vol. 52, no. 17, pp. 1465–1468, Apr. 1984.

[165] A. Dufresne, "Comparing the Mechanical Properties of High Performances Polymer Nanocomposites from Biological Sources," *J. Nanosci. Nanotechnol.*, vol. 6, no. 2, pp. 322–330, 2006.

[166] M. A. S. Azizi Samir, F. Alloin, and A. Dufresne, "Review of recent research into cellulosic whiskers, their properties and their application in nanocomposite field," *Biomacromolecules*, vol. 6, no. 2, pp. 612–626, 2005.

[167] J. Bras, D. Viet, C. Bruzzese, and A. Dufresne, "Correlation between stiffness of sheets prepared from cellulose whiskers and nanoparticles dimensions," *Carbohydr. Polym.*, vol. 84, no. 1, pp. 211–215, 2011.

[168] W. Helbert, J. Y. Cavaillé, and A. Dufresne, "Thermoplastic nanocomposites filled with wheat straw cellulose whiskers. Part I: Processing and mechanical behavior," *Polym. Compos.*, vol. 17, no. 4, pp. 604–611, Aug. 1996.

[169] V. Favier, R. Dendievel, G. Canova, J. Y. Cavaille, and P. Gilormini, "Simulation and modeling of three-dimensional percolating structures: Case of a latex matrix reinforced by a network of cellulose fibers," *Acta Mater.*, vol. 45, no. 4, pp. 1557–1565, Apr. 1997.

[170] L. Flandin, J. Y. Cavaillé, G. Bidan, and Y. Brechet, "New nanocomposite materials made

of an insulating matrix and conducting fillers: Processing and properties," *Polym. Compos.*, vol. 21, no. 2, pp. 165–174, Apr. 2000.

[171] I. Balberg and N. Binenbaum, "Computer study of the percolation threshold in a two-dimensional anisotropic system of conducting sticks," *Phys. Rev. B*, vol. 28, no. 7, pp. 3799–3812, Oct. 1983.

[172] E. Guth, "Theory of filler reinforcement," *J. Appl. Phys.*, vol. 16, no. 1, pp. 20–25, 1945.

[173] M. Takayanagi, S. Uemura, and S. Minami, "Application of Equivalent Model Method to Dynamic Rheo-Optical Properties of Crystalline Polymers," *J. Polym. Sci. Part C*, vol. 5, pp. 113–122, 1964.

[174] F. Du, R. C. Scogna, W. Zhou, S. Brand, J. E. Fischer, and K. I. Winey, "Nanotube networks in polymer nanocomposites: Rheology and electrical conductivity," *Macromolecules*, vol. 37, no. 24, pp. 9048–9055, 2004.

[175] N. E. Marcovich, M. L. Auad, N. E. Bellesi, S. R. Nutt, and M. I. Aranguren, "Cellulose micro/nanocrystals reinforced polyurethane," *J. Mater. Res.*, vol. 21, no. 4, pp. 870–881, 2006.

[176] J. M. Benoit, B. Corraze, and O. Chauvet, "Localization, Coulomb interactions, and electrical heating in single-wall carbon nanotubes/polymer composites," *Phys. Rev. B*, vol. 65, no. 24, p. 241405, Jun. 2002.

[177] C. Qiong, P. Tuzhi, and Y. Liju, "Silk fibroin/cellulose acetate membrane electrodes incorporating xanthine oxidase for the determination of fish freshness," *Anal. Chim. Acta*, vol. 369, no. 3, pp. 245–251, 1998.

[178] Y. Q. Guan, J. M. Chen, Z. Bin Li, Q. L. Feng, and J. M. Liu, "Immobilisation of bifenthrin for termite control," *Pest Manag. Sci.*, vol. 67, no. 2, pp. 244–251, 2011.

[179] I. Drachuk, S. Harbaugh, R. Geryak, D. L. Kaplan, V. V. Tsukruk, and N. Kelley-Loughnane, "Immobilization of Recombinant E. coli Cells in a Bacterial Cellulose-Silk Composite Matrix to Preserve Biological Function," *ACS Biomater. Sci. Eng.*, vol. 3, no. 10, pp. 2278–2292, 2017.

# Chapter 2

## Formulation and characterization of regenerated silk fibroin/cellulose nanocrystals in solution

### 2.1. Introduction

This chapter covers the processing to obtain silk fibroin (SF) in aqueous solution, hereafter referred to as regenerated silk fibroin (RSF), including the removal of sericine, dissolution, and concentration, as well as its properties in liquid related to molar mass, rheological behavior, conductivity, pH, and density. These characteristics, along with the processing parameters, control the mechanism of production and tailor the properties of electrospun materials (which will be elaborated in chapter 3) [18], [38], [39], [41], [52], [61], [68]. Therefore, understanding the behavior of RSF in solution provides a starting point for the explanation and optimization of the end-properties of the electrospun nonwovens made up of RSF.

In addition, this section describes results in the rheological behavior, conductivity, and pH of RSF solutions in response to the addition of cellulose nanocrystals (CNC) in different loadings, with the objective of improving the processability of RSF solution in electrospinning and enhancing the final properties of RSF electrospun nonwovens. Consequently, the mechanism explaining the increase in the characteristics of RSF solutions and electrospun nonwovens was approached through the formation of a percolation network above a critical concentration of CNC, defined as the minimum concentration for percolation (MCP) or percolation threshold (PT). This

phenomenon was investigated by the theoretical model proposed by Favier for rod-like particles [169], and changes in the storage modulus and dynamic viscosity of RSF solutions upon addition of CNC, according to the principle postulated by Guth [172].

## 2.2. Materials

Partially degummed silkworm cocoons from a waste stream were kindly provided by Corseda (Popayan, Colombia). Sodium carbonate anhydrous was purchased from VWR (West Chester, PA). Lithium bromide was supplied by Oak Chemical (Columbia). Polyethylene glycol (MW≈10,000) was bought from Merck (Darmstadt, Germany). Ultrapure water (0.055 μs/cm, 18 mΩ-cm) was employed for every procedure, except for degumming and dialysis, where distilled water was utilized.

Additionally, cellulose nanocrystals in an aqueous slurry produced by the sulfuric acid hydrolysis of a feedstock pulp containing small residues of regenerated cellulose (Cellulose II), with a total solid concentration of 10.26% w/w was provided by the USDA Forest Product Laboratory (Madison, WI). The average length and diameter of the crystals were 125 nm and 4.5 nm, respectively. Figure 2-1 shows an image of the cellulose nanocrystals obtained through atomic force microscopy.

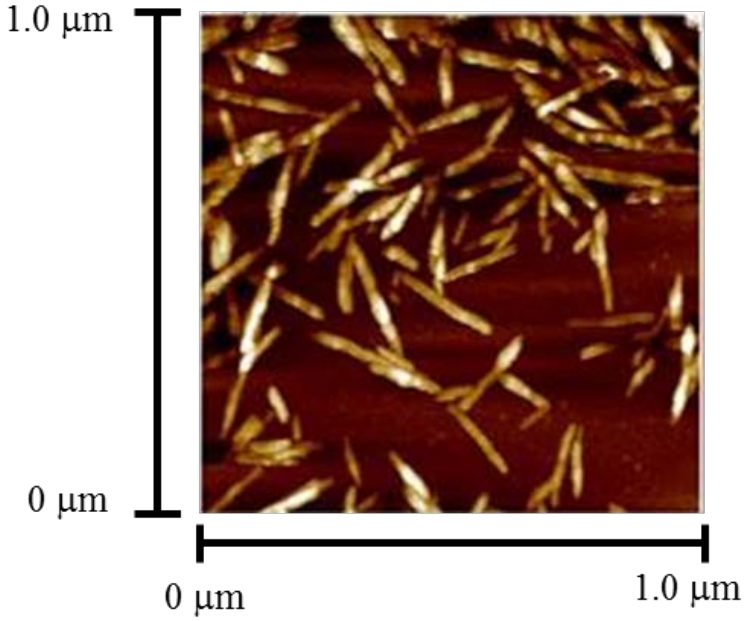


**FIGURE 2- 1.** Cellulose nanocrystals employed during the project**.**

## 2.3. Methods

### 2.2.1. Silkworm cocoon degumming

Silkworm cocoons from industrial waste were initially untangled to increase the contact area of the fiber. Then, the remaining sericine in the silk was removed by soaking the untangled threads in a bath of boiling aqueous solution of 0.02 M sodium carbonate, under constant stirring for 30 minutes. Subsequently, the silk was rinsed with boiling distilled water followed by distilled water at room temperature. This process was performed twice, where the 30 minutes of soaking were strictly controlled to ensure the complete removal of sericine and to avoid further complications associated with the degradation of silk properties [8], [16], [136], [148], [180]. Afterwards, the silk without sericine or degummed silk, was dried at 60 °C for 24 hours.

### 2.2.2. Isolation of silk fibroin

Degummed silk was isolated by dissolving the fibers in an aqueous solution of lithium bromide (LiBr) 9.3M at 60 °C, under constant stirring rate of 240 rpm, during 4 hours. This process requires a very strict temperature control, as it can lead to changes in the length of the resulting silk structures in the solution [181]. Next, the silk in solution or regenerated silk fibroin (RSF) was filtered with filter paper grade 1 (Whatman$^{TM}$, GE life science, USA) and dialyzed for 48 hours using dialysis membranes with MWCO 3.5 kDa (Spectra/Por 3, Spectrum labs, USA) in order to remove the lithium bromide. Distilled water was utilized as dialysis medium, and it was changed after 1 hour, 2 hours, 4 hours, 8 hours, and every 8 hours thereafter until constant conductivity values were obtained. Then, the dialyzed solution was centrifuged at 9000 rpm, 4 °C for 20 minutes; this process was carried out two times. Later, the solution was micro filtrated through cellulose acetate filter membranes, 0.45 μm pore size (Ahlstrom, Germany), and stored at 7 °C to improve the stability of the solution. Next, aliquots of RSF solution were weighed in wet and in dry conditions after drying at 105 °C for 24 hours, to determine the percentage of solids in sample, referred as the percentage of silk in solution [16]. Finally, solutions with a total concentration of silk between 3-5% were obtained. Figure 2-2, displays the different stages of silkworm cocoons processing, prior to and after degumming, and in regenerated form.


**FIGURE 2- 2**. Presentation of silk through various steps. a) Partially degummed silk cocoons form industrial waste; b) Degummed silk, c) Regenerated silk fibroin.

### 2.2.3. Concentration of regenerated silk fibroin solution

Previous works report that it is required a minimum concentration of regenerated silk in the solution of 20% w/w or a viscosity above 0.13 Pa*s to successfully obtain continuous fibers through electrospinning [182], [183]. In our case, the resulting solutions of RSF exhibited a very low concentration after isolation. Therefore, the RSF solution was concentrated via reverse dialysis employing dialysis membranes MWCO 3.5 kDa (Spectra/Por 3, Spectrum labs, USA) against a concentrated aqueous solution of 25% w/w polyethylene glycol (10 kDa) at room temperature. The concentration of the solution in the dialysis membrane was constantly measured by calculating the difference between the weight in wet and dry in aliquots of the solution. This process proceeded until a final concentration of RSF in solution between 23-36% w/w was reached. A counter effect of this is that high concentrations of RSF in the solution cause protein jelling at ambient conditions [16], such that, fresh batches of concentrated regenerated silk were used for each test.

### 2.3.4. Rheological behavior of concentrated RSF in solution

The concentrated solution of RSF was first diluted to achieve a solid content of 20% w/w, in accordance to the minimum concentration needed to successfully produce regular shaped fibers of RSF through electrospinning [182], [183]. For this solution, a rheological test was performed employing a CVO rheometer (Bohlin Instrument, Cirencester, United Kingdom), within a range of shear rate from 0.1 to 1,000 1/s, using a cone-plate (4°/40 mm) geometry, and a gap of 150 μm,

at room temperature. The dynamic viscosity was potted as a function of the strain for the concentrated solution of RSF.

### 2.3.5. Determination theoretical percolation threshold for CNC

The minimum concentration of cellulose nanocrystals required to effectively create a continuous network of filler, which may result in the enhancement of the properties of RSF solution, was at first determined through equation 2.1 proposed by Favier *et. al*, to determine the theoretical percolation threshold for systems with fillers with a rod-like shape. For this approach, the concentration of filler in volume percentage ($v_{RC}$ in v/v %) to achieve formation of a percolation network, is only a function of its aspect ratio, where L = length and D = diameter of the filler [169].

$$v_{RC} = \frac{0.7}{L/D} \tag{2-1}$$

### 2.3.6. Preparation of RSF/CNC aqueous solutions and experimental determination of percolation threshold

Once the theoretical percolation threshold (PT) for CNC was calculated, in order to determine the experimental percolation threshold, two different solutions of RSF/CNC with a CNC concentration above the theoretical PT were prepared since below this value, the probability for the formation of a continuous CNC network is rather low. Accordingly, the total solid concentration of each solution was fixed at 20% w/w, whereas the selected weight ratios total solids for the RSF/CNC were 95/5 and 90/10, corresponding to RSF/CNC concentrations in solutions of 19/1% w/w and 18/2% w/w, respectively.

Before preparing the RSF/CNC solutions, an aqueous suspension of cellulose nanocrystals was prepared by diluting the cellulose nanocrystal aqueous slurry at 10.26% w/w with ultrapure-water, followed by dispersing CNC via sonication using a vibra-cell sonicator, series VC 750 (Sonic, Newtown, CT), operating at 750 W, with a ½" tip, and set at 20% amplitude for10 minutes.

For the preparation of the RSF/CNC solutions, the concentrated RSF was blended with the suspension of CNC, under the appropriated weight ratios to produce the desired solutions. The blends were mechanically stirred for at least 30 minutes.

At first, oscillatory strain-sweep test for the three solutions of RSF/CNC was performed employing a rheometer, CVO (Bohlin Instrument, Cirencester, United Kingdom), using a cone-plate (4°/40 mm) geometry, with a gap of 150 μm, at room temperature, and in strains between 0.1 and 1000%, to identify the linear viscoelastic region of each solution.

Once the linear viscoelastic region was determined, a frequency-sweep test for the solutions was carried out in a rheometer, CVO (Bohlin Instrument, Cirencester, United Kingdom), using a cone-plate (4°/40 mm) geometry, with a gap of 150 μm, at room temperature, employing a strain of 1%, and within frequencies of deformation from 0.1 to 1,000 rad/s. The storage moduli for each solution were potted as a function of the frequency.

To determine the experimental percolation threshold, the value of the storage modulus of the solution, at a strain of 0.5 rad/s, was plotted as a function of the concentration of CNC. At this strain, the value of the storage modulus falls in the linear viscoelastic region, where this property is independent of the strain. Then, the values of storage modulus for solutions with concentration of CNC of 1% and 2% w/w were adjusted to the function proposed by Benoit [176], displayed in equation 2.2.

$$G' = (x - x_{PT})^{\beta} \tag{2-2}$$

In this model, G' represents the storage modulus of a polymer with a loading of filler equal to "x" in weight percent (%w/w). The constants "β" and "$x_{PT}$" respectively correspond to a parameter of proportionality, and the concentration of filler to achieve the percolation thresholds for a pure polymer solution with negligible storage modulus.

In parallel, as the value of the storage modulus for the solution of RSF without CNC was different from cero, it was fit to a constant straight line along the x-axis until it intercepted the curved obtained with using the equation 2. The interception between both curves represented the minimal concentration of CNC to enhance the storage modulus of the RSF solution, which means the percolation threshold.

### 2.3.7. General characterization of the RSF/CNC solutions

The rheological behavior, density, pH, and conductivity for the RSF and each solution of RSF/CNC were measured to assess the outcomes of the addition of CNC in RSF and their potential effects on the spinability of the solutions. Their rheological behaviors were characterized employing a CVO rheometer (Bohlin Instrument, Cirencester, United Kingdom), within a range of shear rate from 0.1 to 1,000 1/s, using a cone-plate (4°/40 mm) geometry, and a gap of 150 μm, at room temperature. Conductivities and pH were recorded at room temperature employing a multi-meter Benchtop Symphony sb70 (VWR, Radnor, PA). Whereas, the densities were calculated as the weight per 1 milliliter of solution. Each measurement was performed in triplicate.

## 2.3. Results

### 2.3.1. Characterization of concentrated RSF solution

The rheological behavior of the concentrated solution of silk fibroin was characterized by evaluating the changes in the dynamic viscosity of the solution with the shear rate, the collected data is presented in Figure 2-3.

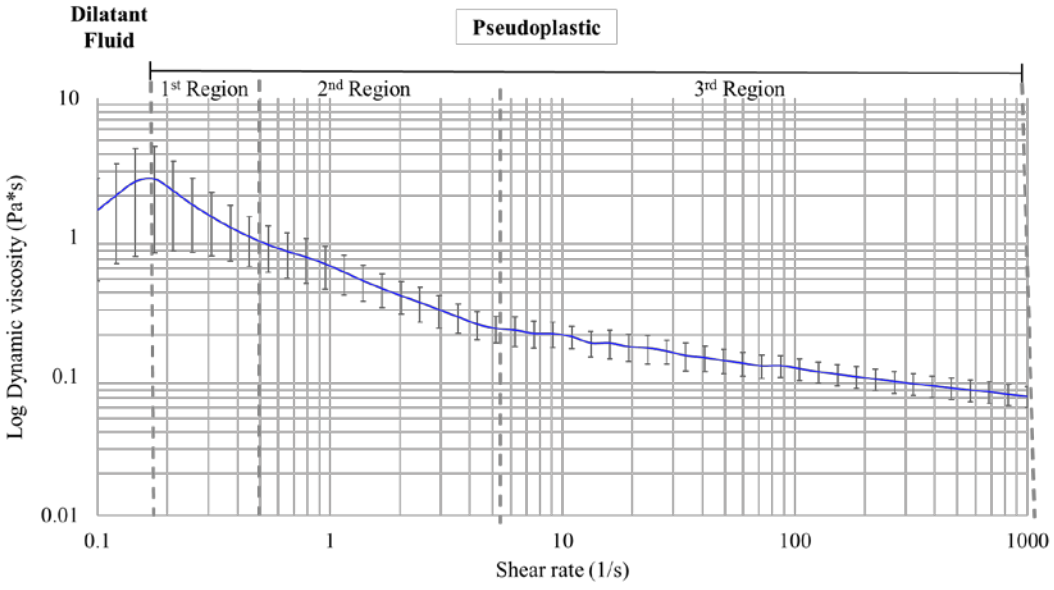


**FIGURE 2- 3.** Dynamic viscosity vs. shear rate for the concentrated solution of regenerated silk fibroin.

By assessing Figure 2-3, it was observed that the polymer in solution exhibited a dilatant or shear thickening behavior at very low shear rate, slightly below 0.20 rad/s; followed by a pseudoplastic or shear thinning behavior, which could be analyzed in three different regions.

The initial shear thickening behavior at low strain has been previously reported for solutions of silk fibroin in water. This phenomenon is thought to be related to the orientation, elongation, and disentanglement of polymer chains in the solution, in addition to the onset of the formation of silk fibroin clusters or aggregates in the solution, resulting from the rise in polymer mobility under a weak shear flow field, which facilitates the formation of intermolecular interactions or the agglomeration of the polymer in micelles, without disrupting the forces [184]–[188]. Interestingly, this behavior has been observed only in solutions of silk fibroin in water, where the polymer concentration is above 15% w/w, reported as the critical concentration of silk fibroin to avoid the jet breaking up during electrospinning. It is assumed that such concentration corresponds to the critical concentration of SF in water to maximize the interactions polymer-polymer, due to the higher number of molecules in solution, which increases the likelihood of interactions, producing a sudden raise in viscosity of the solutions. Usually, this phenomenon comes along with the development of a linear viscoelastic plateau, after the induced shear thickening [186], [189]. Notwithstanding, other report has assigned this behavior to inertial effects at the imposed shear rate, rather to an effective increase in the dynamic viscosity [182].

Afterwards, at slightly higher shear rates, the solution exhibited a transition to shear thinning or pseudoplastic fluid, where the dynamic viscosity of the solution diminished. The transitions to pseudoplastic and its behavior could be divided into three different regions in the flow curve, depending on the relation between and shear rate [190], [191].

In the first region, starting around ~0.20 $s^{-1}$ to ~0.55 $s^{-1}$, the fluid underwent a transition from dilatant to pseudoplastic fluid, characterized by a sharp drop in the viscosity of the solution. The second region within the pseudoplastic behavior was observed after the critical strain of 0.55 and extended to about 5.19 rad/s. On this region the dynamic viscosity experienced an almost negligible decrease in the order of 0.90 Pa*s, which highlighted the strength of the interactions and chain entanglement between molecules of silk [184], [186]. Finally, in the third region of the pseudoplastic behavior, which commenced nearby 5.19 and extended until 1,000 rad/s, the response of the solution to the shear rate became unstable and the dynamic viscosity did not experience a major variation. This transition from pseudoplastic to almost Newtonian Fluid may

be attributed to the formation of a liquid crystalline phase of silk fibroin promoted by the exclusion of water between polymer molecules under stronger shear flow field, which ultimately leads to the complete separation of the silk fibroin crystalline phase from the solvent [182], [184]. Previous investigations have reported the commencement for that phenomenon at shear rates between 0.50 $s^{-1}$ and 20 $s^{-1}$, where the onset of phase separation occurs at lower deformations when the concentration of silk fibroin increases [182], [184], [189], [192], [19], [93]. This effect could be produced by a greater chain entanglement and a closely tightened structure in accordance to higher concentrations, which enables more interaction and a faster production of crystalline networks at lower shear rate.

Likewise, the density, pH, and conductivity of the solution were measured in triplicate, and the results are summarized in Table 2-1. Curiously, the pH of the solution lies above the isoelectric point of silk fibroin which is typically found around 4.2 [184], depending on the different residues in the protein backbone. At this pH, the acidic residues on the silk fibroin structure are ionized and impose a net negative charge on silk fibroin chains, producing repulsive forces that hold the fibroin in an extended form or random coil conformation. Correspondingly, lowering the pH would lead to the protonation of the acidic residues, whose isoelectric points is around a pH pf 4.5, and consequently may cause the formation of micellar structures mainly composed of silk fibroin crystals, resulting from the folding of the protein chain [185], [117]. Figure 2-5 schematizes the transition of silk fibroin from an extended form to micellar structures with reduction in pH.

**TABLE 2- 1.** Density, pH and conductivity for the concentrated solution of RSF

| **Density (gr/cm$^3$)** | **pH** | **Conductivity (μs/cm)** |
|---|---|---|
| 1.157 ± 0.272 | 7.00 ± 0.01 | 268 ± 2 |

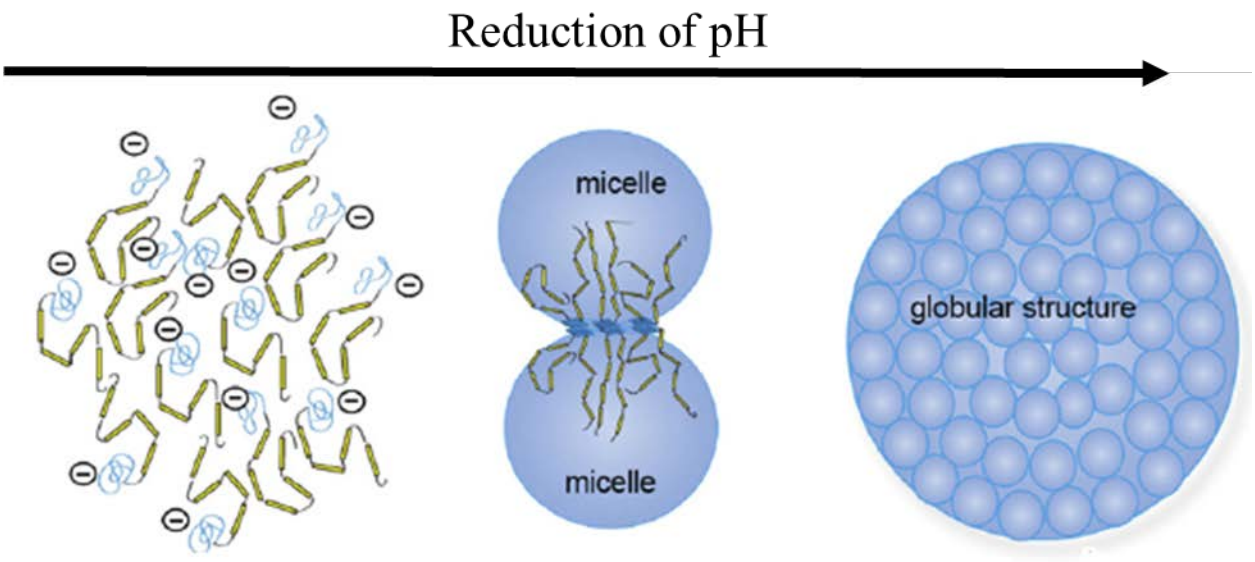


**FIGURE 2- 4.** Silk fibroin conformation as function of pH. Adapted from [117]. Copyright Elsevier Ltd. 2012.

### 2.3.2. Determination of percolation threshold and rheological behavior of RSF/CNC

In order to determine the minimum concentration of cellulose nanocrystals to achieve mechanical percolation, the equation 2.1 was used to stablish a referential value of filler loading to effectively produce an enhancement on the composite material performance (i.e. mechanical, thermal, and/or electrical properties). This theoretical approach assumes that fillers have a uniform cylindrical shape, and the formation of a percolation network is independent of the chemical behavior and likelihood of the filler to exhibit other interactions different than OH-bonds, like Van der Waals and/or interactions between filler-solvent. Accordingly, the concentration at the percolation threshold becomes solely a function of the aspect ratio of the filler [8], [52]-[54].

By introducing the average length and diameter of CNC in equation 2.1, a concentration 2.5% v/v in total solid content was obtained. The former fraction could be expressed in weight percentage through the theoretical density for CNC, of 1.60 g/cm$^3$ [29], [152], and the density of the RSF concentrated solution shown in Table 2-1. From this conversion, a value of 3.50% w/w in the total solid was calculated. The last, corresponds to the concentration of CNC in a solid polymer composite made up of regenerated silk fibroin and cellulose nanocrystals, which for a solution with a total solid content of 20% w/w, would represent 0.70% w/w of the solution.

To define the real percolation threshold of the filler, cellulose nanocrystals were added in solutions of RSF, using concentrations of filler above the theoretical percolation threshold. Solutions of RSF/CNC with loadings of CNC of 1% and 2% w/w were prepared, and their rheology, conductivity and pH were evaluated to assess the effects of the filler on RSF in solution.

At first, for the solutions of RSF/CNC with CNC loading of 1% and 2%, and for the solution of RSF without CNC, hereafter just referred as RSF, the linear viscoelastic region was investigated through an oscillatory strain-sweep test, by assessing the changes in the storage modulus of the solution at different strains, and by identifying the segment of the curves where the modulus was independent of the strain. The results of this test are shown in the Figure 2-5.

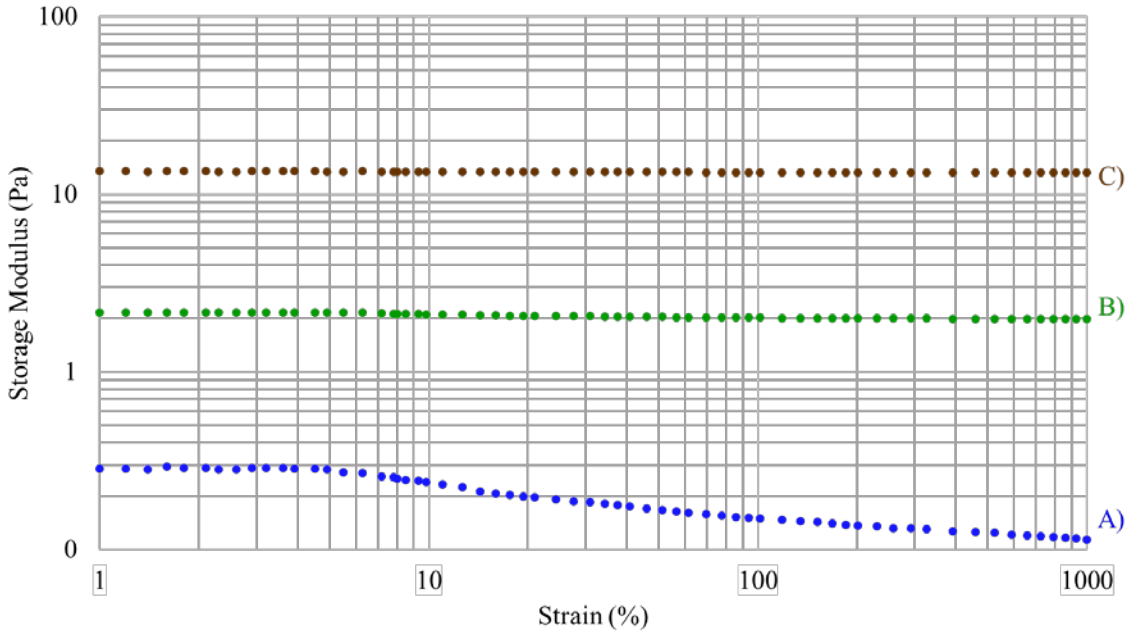


**FIGURE 2- 5.** Strain sweep curves for: A) RSF; and RSF/CNC solutions with loadings of CNC of: B) 1% w/w and C) 2% w/w.

The solution of RSF presented a critical strain between 5 and 5.5%, whereas, this value was not easy to identify in the solutions of RSF loaded with CNC, which seemed to fall in the linear viscoelastic region at every strain applied in this test. Interestingly, Hodgkinson, *et. al*, [16], in a rheological study for solutions of silk fibroin at different concentrations, found that for solutions with concentrations above 10%, the critical strain felt between 1 and 50% of strain, where the highest values belong to the more concentrated solutions. Therefore, for the solutions employed

in this work, working at a strain of 1% ensured that the further rheological tests were carried out in the linear viscoelastic region.

Once the linear viscoelastic region was established, frequency-sweep test for the solutions were carried out to observe their changes in their storage moduli against the frequency of deformation, at a strain of 1%. These results were plotted in Figure 2-6.

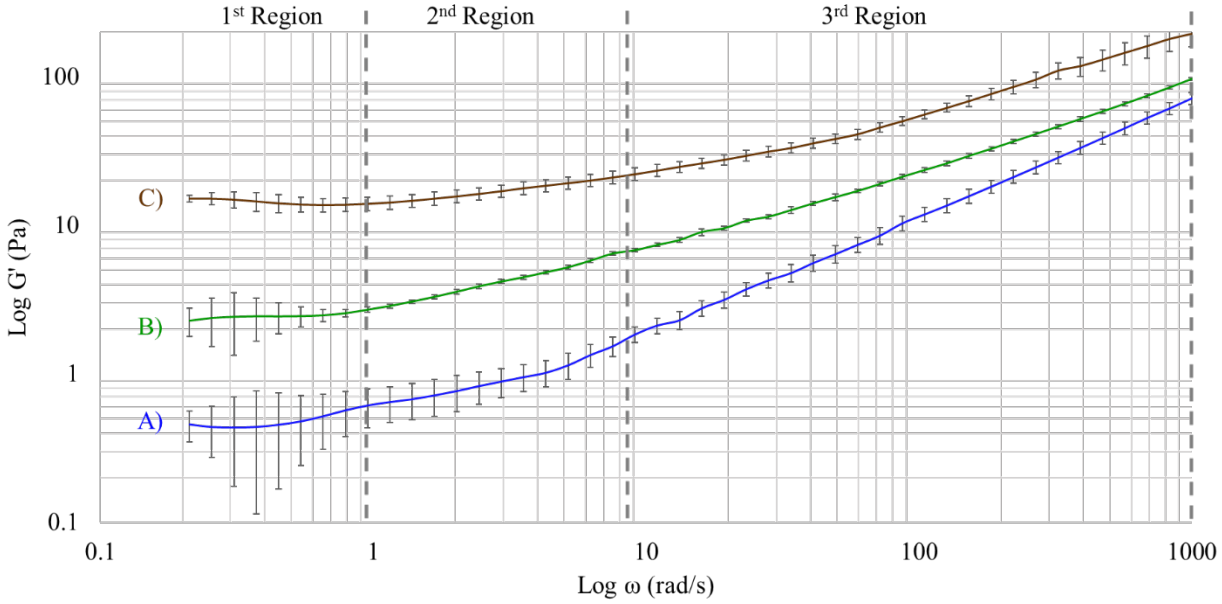


**FIGURE 2- 6.** Frequency-sweep curve for: A) concentrated solution of RSF; B) RSF/CNC solution with 1% w/w CNC, C) RSF/CNC solution with 2% w/w CNC.

By analyzing the behavior of RSF in Figure 2-6, three different transitions were observed, which could be extrapolated to the solutions of RSF with CNC. The first region has been associated with the formation of a dynamic equilibrium between the formation and disruption of polymer interactions, promoted by the flow field force, which produce the orientation and disentanglement of polymer chains and facilitates the contact between molecules, along with the disruption of intermolecular interactions under the imposed deformation. The end of the linear viscoelastic behavior has been defined as the critical shear, where the polymer chains have enough mobility to break down the equilibrium between the formation and interruption of interactions, thus reducing the resistance of the molecules to flow under the shear field force [182], [185], [186], [192]–[194].

For silk fibroin, Terry, *et al*. [184], reported a value for the critical shear rate of ~0.50 $s^{-1}$ for a solution of natural SF directly extracted from silk worm glands, with a concentration moderately above 25% w/w. The authors also reported that this value strongly depends on the polymer chain entanglement, molecular weight, concentration, and relaxation time. The lower the value for the critical strain, the lower the interactions and relaxation time, thus the lower the time and strain it takes to disentangle the molecules. The similarity between the values for the critical shear rate reported in the literature and the one obtained on this study, highlights the degree of resemblance between the polymers used in both studies.

In the second region, the behavior of the fluid is characterized by the disruption of the dynamic equilibrium between the formation and disruption of interactions, where the strong shear flow field disturbs the intermolecular bonds and limits the production of replacing bonds. The end of this region or commencement of the third region is appointed as the onset for the formation of a separate crystalline phase of silk fibroin caused by the shear induced crystallization of the polymer, which causes a sharp increment in the storage modulus [184].

For solution of RSF/CNC it has been reported that the location and extension of the regions changes with the addition of cellulose based fillers, as well as with its concentration [29], [175], [195], [196]. Two phenomena associated with the presence of interactions between polymer-filler and filler-filler could be noticed. The first one, related to the increase in storage modulus for RSF solutions with the addition of CNC. And the second one, identified as longer first regions for the solutions of RSF/CNC [197]–[199].

As evidence of the first phenomenon, by only adding 2% of CNC, the initial storage modulus for the solution of RSF experienced a raise of about 34 times their original values, changing from 0.44 Pa to 15.17 Pa for the storage modulus. The initial elastic modulus strongly depends on the molecular weight, chain entanglement, and polymer and filler concentration, but, as the polymer was the same for the three solution, the variations on this property was probably generated only by the introduction of fillers [182] ,[184].

Yet, the second phenomenon associated with interactions between both components, was related to the extension in the length of the first region, where the storage modulus was independent of the frequency of deformation, varying from a value of ~0.55 rad/s for RSF to almost 1.0 rad/s for the two solutions of RSF/CNC. The latter, could be a consequence of stronger interactions in the solution of RSF/CNC, as the components were able to hold the dynamic equilibrium between

the formation and disruption of interactions under higher frequencies of deformations [28], [200]. This result also implies a higher relaxation time for RSF, which could retard the recovery, relaxation, and motion of RSF chains, perhaps, due to the hindrances caused by the presence of CNC [189], [175], [201]. This effect has also been explained by the formation of a crystalline filler network that increases the resistance to flow until the strain is strong enough to overcome the opposing shear forces [175], [195], [197], [202], [174]. In a similar manner, the commencement of the third region shifted from around 5.19 $s^{-1}$ for RSF to 7.54 $s^{-1}$ for RSF/CNC. The delay in the development of phase separation might be attributed to stronger interactions between the components in the solution, which restrained the exclusion of water and the formation of a continuous crystalline phase of polymer.

As previously indicated, the addition of CNC at concentrations above the theoretical percolation threshold produce a sharp enhancement on the storage modulus (G'). This variation could be attributed to the effective formation of a continuous filler network, which restrained the mobility of polymer chains. This behavior has been employed to find the real percolation threshold of the filler in solution, accordingly, a region where the raise on this property only depends on the addition of filler and not on the frequency or on other properties must be carefully selected [172], [176], [175], [197] [174].

Within this region, a value of 0.50 rad/s was selected, and the values of storage moduli were plotted against the concentrations of CNC. The resulting graph is presented in Figure 2-7. Consequently, the values of storage moduli for the solutions with CNC were adjusted to the equation 2-2, whereas the value of the storage modulus for RSF was fit to a constant straight line with slope equal to zero. For the curve described by the equation 2-2, values for "$x_{PT}$" of and "β" of 0.61 and 1.36 were respectively obtained by reducing the squared difference between the experimental and theoretical data points. This previous results indicate that for a solution with an initial storage modulus close to zero, the mechanical percolation could be achieved at CNC concentrations above 0.61% w/w. Notwithstanding, as the initial value of the storage modulus for the solution was different to zero, the real percolation threshold corresponded to the concentration of CNC where the curve described by the equation 2-2 intercepted the straight line which described the initial storage modulus of RSF. The interception between the two curves indicated a value close to 0.83% w/w of CNC, which is slightly lower than the chosen standard values of 1% and 2% w/w, but greater than the theoretical value, which just takes into account the interactions via

hydrogen bonding and omits other types of interactions, such as Van der Waals or polymer-solvent, such might explain the differences between results [169]. The inset graph in Figure 2-7 shows the linear fit for the storage modulus vs the reduce mass fraction of CNC.

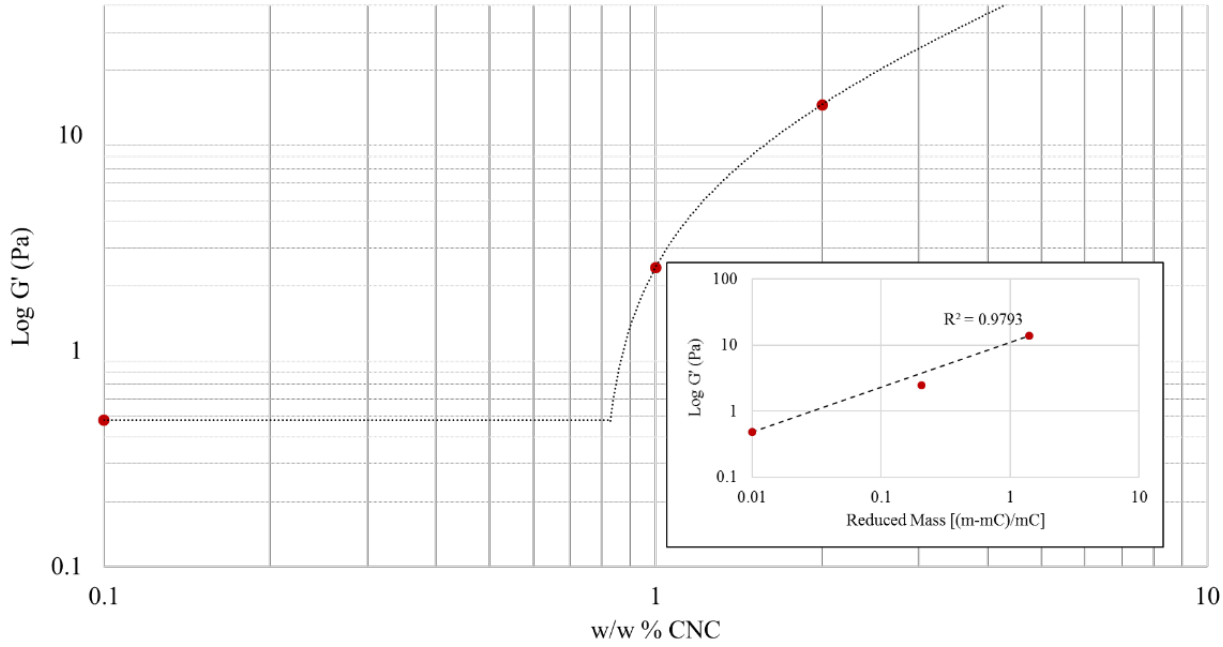


**FIGURE 2- 7.** Storage modulus (G') as a function of CNC loading, at a fixed strain of 0.5 rad/s. Inset graph: Log-Log plot of Storage modulus against reduced mass fraction.

After stablish the experimental value for the percolation threshold of CNC in the solution of RSF, the rheological behavior of the solutions of RSF with 1% and 2% of CNC, and without CNC was assessed against the shear rate, to observe the change in the flowability of RSF when the filler was added. Figure 2-8, presents the flow curves for these solutions. As it could be observed, the RSF/CNC solutions followed a similar rheological behavior described by RSF, identified by shear thickening at very low strains, followed by a transition to shear thinning fluid. In contrast to RSF, the two solutions of RSF/CNC showed an almost linear reduction in viscosity with the shear rate after the transition from dilatant to pseudoplastic, even at very high strain.

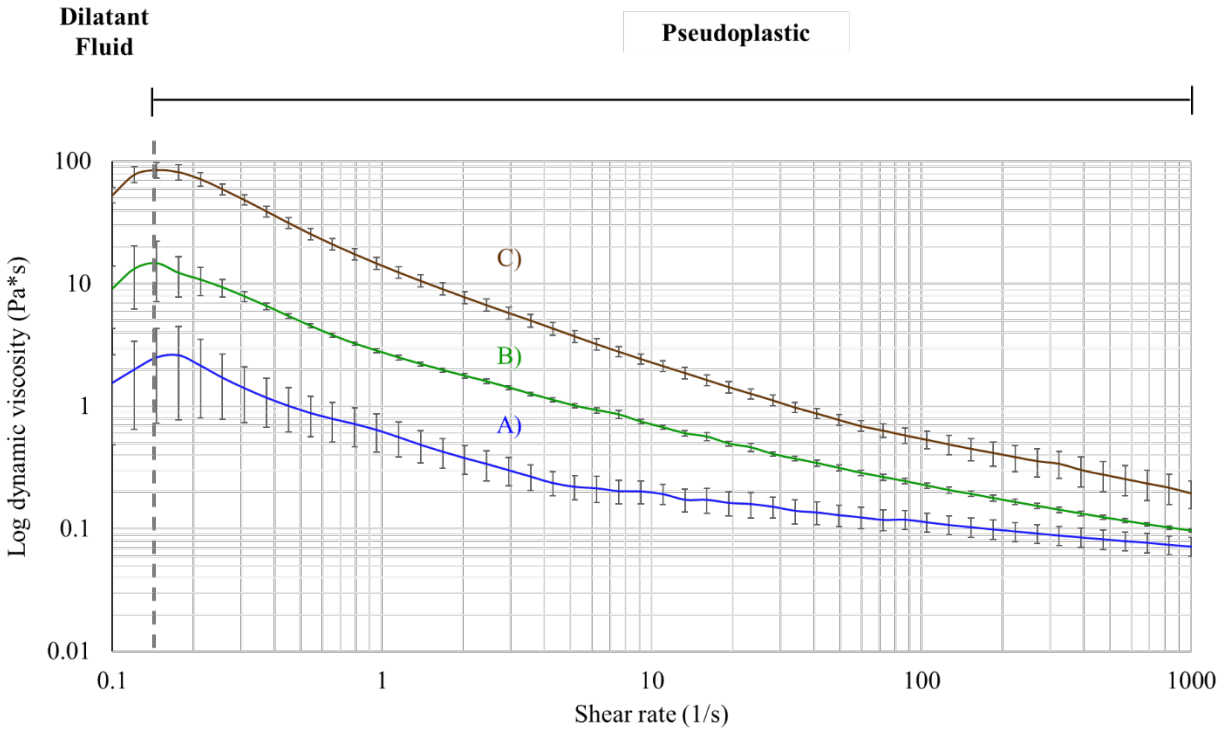


**FIGURE 2- 8.** Dynamic viscosity vs shear rate curves for: A) RSF; and RSF/CNC solutions with loadings of CNC of: B) 1% w/w and C) 2% w/w.

Likewise, the values of viscosity at the very high frequency (1000 rad/s) for these three systems did not variate much, changing from 0.19 Pa*s for the RSF/CNC with 2% of CNC, to 0.09 Pa*s for the solution with 1% of CNC, and finally to a viscosity of 0.07 Pa*s for the RSF solution without CNC. As previously stated, phase separation could occur at high frequency of deformation, where the strong shear forces inhibit the interaction within the components and with the solvent, lowering the resistance of the solution to flow. This variation in dynamic viscosity may be associated with the resistance produced by the CNC liquid crystalline phases [152], [203].

Finally, conductivity and pH of the RSF/CNC solutions were measured to evaluate the effects of the addition of CNC on these properties and their potential impacts on the processability of the solution through electrospinning. Table 2-2 displays the values of conductivity and pH for RSF and RSF/CNC solutions. The addition of CNC did not markedly impact pH, thus, apparently the protein preserved its initial shape in the solution. However, its conformation and entanglement could have varied due to contact with CNC, leading to the enhancement of other properties, such as viscosity. In contrast with pH, the conductivity of the solution increased upon increasing

loadings of CNC. It is assumed that this effect was the result of the increased amount of hydroxyl groups introduced into the solution when CNC was added and to the formation of a CNC electrical percolation network, which facilitated charge transfer within the system [29], [174], [32]. It is important to mention that the electrical percolation threshold is usually achieved at values of filler concentration higher than those required to produce mechanical percolation [176].

The changes in viscosity and conductivity in the RSF solution when CNC was added could yield benefits for the production of continuous fibers of RSF via electrospinning, as higher viscosities prevent the jet from breaking up and Rayleigh-Plateau instabilities in response to longer polymer relaxation times; whereas, an increment in the conductivity might lead to the reduction of second order instabilities, which occur with the low capacity of the polymer to transport the charges along its surface, and finally produce a faster jet breaking up. Additionally, changes in these two properties might lead to opposing outcomes during the electrospinning process, as the higher viscosity usually results in fiber with larger diameters and more narrow distributions of fiber diameter, but, very high viscosities might eventually hinder the process by the strong viscous forces or by jet blockage. On the other hand, raising conductivity leads to lower fiber diameter due to higher electrostatic repulsion, which ultimately promotes fiber stretching, but generates broader distributions of the fiber diameter size [26], [58], [71], [72].

**TABLE 2- 2.** Conductivity and pH for RSF and RSF/CNC solutions.

| RSF/CNC w/w % in solution | pH | Conductivity (μS/cm) |
|---|---|---|
| 20/0 | 7.00 ± 0.01 | 268 ± 2 |
| 19/1 | 7.06 ± 0.02 | 288 ± 1 |
| 18/2 | 7.11 ± 0.00 | 306 ± 2 |

## 2.4. Conclusions

RSF solution at 20% w/w exhibited dilatant behavior at very low rates of deformation, characterized by the reorientation, accommodation, and slow mobility of silk fibroin chains, which might have increased the contact between RSF molecules, and subsequently promoted inter- and intra-molecular interactions, increasing the resistance to flow. However, the solution behaved like a pseudoplastic fluid at most the rates of deformation.

According to the strain-sweep test, the solution of RSF felt in the linear viscoelastic region when strains approximately below 5.5% are applied. Whereas, this condition was successfully achieved for the solutions of RSF with 1% and 2% of CNC at every input strain for this test.

The behavior of RSF, in the frequency-sweep curve, could be summarized in three regions whose extension and onset strongly depends on the polymer chain entanglement, molecular weight, concentration of polymer, and relaxation time. Each region underlined particular phenomena, where the 1$^{st}$ region may be the result from the onset of a dynamic equilibrium between formation and disruption of interactions between silk fibroin strands, and between polymer-filler. The 2$^{nd}$ region could be caused by the disruption of the dynamic equilibrium, followed by the formation of a separate crystalline phase of SF in the 3$^{rd}$ region.

The values of critical shear rate for the RSF solution employed in this work was in agreement with the value reported in literature for a solution of natural silk fibroin at 25% w/w. These values are strongly influenced by the molecular weight, chain entanglement, and the strength of interactions within silk fibroin molecules. Therefore, the material used in this experiment was similar to natural silk fibroin. In a similar manner, the strain required to induce the crystallization of silk fibroin was between the threshold reported in literature, which also depends on the aforementioned properties and in the concentration of the solution, where higher concentrations, lower the value of the required strain to induce the crystallization, as a result of the higher probability of silk fibroin molecules to interact between each other.

The solutions of RSF and RSF/CNC exhibited similar rheological behavior, characterized by the same transitions from dilatant to pseudoplastic. However, at low shear rates, the sharp change in viscosity when CNC was added evidenced the formation of interactions between both components, and probably the development of a percolation network of filler, which enhanced the resistance of the solution to flow, evidenced in the flow curve, and caused the development of more extended first regions in the frequency-sweep curves for the blends.

For the concentration of CNC to develop a percolation network, the theoretical value of 0.70% w/w, showed a difference of about 15% respect to the real value of 0.83% w/w obtained through the frequency-sweep experiments. This deviation may be caused by the omission of other intermolecular different than hydrogen bonds. However, the theoretical

method may provide a close insight about to the real value of concentration to achieve mechanical percolation when it is not possible to perform an experimental run.

The increase in viscosity and conductivity of the solution when CNC was added might result in a better processability of RSF in solution via electrospinning, as the higher viscosity promoted the formation of continuous and more homogeneous fibers, while increased conductivity usually leads thinner fibers. These variations generally lower the Rayleigh-Plateau and secondary type of instabilities that produce the jet breaking up.

## 2.5. References


[1] N. Bhardwaj and S. C. Kundu, “Electrospinning: A fascinating fiber fabrication technique,” *Biotechnol. Adv.*, vol. 28, no. 3, pp. 325–347, 2010.

[2] L. L. Guo, Y. B. Liu, and J. B. Yao, “A Review on Existing Tecgnology of Electrospinning at Large Scale,” *Proc. 2010 Int. Conf. Inf. Technol. Sci. Manag. Vols 1-2*, pp. 279–282, 2010.

[3] L. M. Duque Sánchez, L. Rodriguez, and M. López, “Electrospinning: The Nanofibers Age,” *Rev. Iberoam. Polímeros Vol. Iber. Polímeros*, vol. 14, no. 141, pp. 10–27, 2014.

[4] J. Stranger, N. Tucker, and M. Staiger, “Electrospinnin.” pp. 1–218, 2005.

[5] M. Mirjalili and S. Zohoori, “Review for application of electrospinning and electrospun nanofibers technology in textile industry,” *J. Nanostructure Chem.*, vol. 6, no. 3, pp. 207–213, 2016.

[6] A. Greiner and J. H. Wendorff, “Electrospinning: A fascinating method for the preparation of ultrathin fibers,” *Angew. Chemie - Int. Ed.*, vol. 46, no. 30, pp. 5670–5703, 2007.

[7] W. E. Teo and S. Ramakrishna, “A review on electrospinning design and nanofibre assemblies,” *Nanotechnology*, vol. 17, no. 14, pp. R89–R106, Jul. 2006.

[8] V. Favier, R. Dendievel, G. Canova, J. Y. Cavaille, and P. Gilormini, “Simulation and modeling of three-dimensional percolating structures: Case of a latex matrix reinforced by a network of cellulose fibers” *Acta Mater.*, vol. 45, no. 4, pp. 1557–1565, Apr. 1997.

[9] E. Guth, “Theory of filler reinforcement,” *J. Appl. Phys.*, vol. 16, no. 1, pp. 20–25, 1945.

[10] Y. Cao and B. Wang, “Biodegradation of silk biomaterials,” *Int. J. Mol. Sci.*, vol. 10, no. 4, pp. 1514–1524, 2009.

[11] D. N. Rockwood, R. C. Preda, T. Yücel, X. Wang, M. L. Lovett, and D. L. Kaplan, “Materials fabrication from Bombyx mori silk fibroin,” *Nat. Protoc.*, vol. 6, no. 10, pp. 1612–1631, 2011.

[12] M. P. Ho, H. Wang, and K. T. Lau, “Effect of degumming time on silkworm silk fibre for

biodegradable polymer composites," *Appl. Surf. Sci.*, vol. 258, no. 8, pp. 3948–3955, 2012.

[13] L. S. Wray *et al.*, "Effect of processing on silk-based biomaterials: Reproducibility and biocompatibility," *J. Biomed. Mater. Res. - Part B Appl. Biomater.*, vol. 99 B, no. 1, pp. 89–101, 2011.

[14] T. Yongzhen, X. Weilin, Y. Yun, and Y. Cao, "Preparation and Characterization of Silk fibroin nanocrystals." .

[15] S. D. Aznar-Cervantes, D. Vicente-Cervantes, L. Meseguer-Olmo, J. L. Cenis, and A. A. Lozano-Pérez, "Influence of the protocol used for fibroin extraction on the mechanical properties and fiber sizes of electrospun silk mats," *Mater. Sci. Eng. C*, vol. 33, no. 4, pp. 1945–1950, 2013.

[16] T. Hodgkinson, Y. Chen, A. Bayat, and X.-F. Yuan, "Rheology and Electrospinning of Regenerated *Bombyx mori* Silk Fibroin Aqueous Solutions," *Biomacromolecules*, vol. 15, no. 4, pp. 1288–1298, 2014.

[17] H. J. Kim and I. C. Um, "Relationship between rheology and electro-spinning performance of regenerated silk fibroin prepared using different degumming methods," *Korea Aust. Rheol. J.*, vol. 26, no. 2, pp. 119–125, 2014.

[18] J. M. Benoit, B. Corraze, and O. Chauvet, "Localization, Coulomb interactions, and electrical heating in single-wall carbon nanotubes/polymer composites," *Phys. Rev. B*, vol. 65, no. 24, p. 241405, Jun. 2002.

[19] A. E. Terry, D. P. Knight, D. Porter, and F. Vollrath, "pH Induced Changes in the Rheology of Silk Fibroin Solution from the Middle Division of Bombyx mori Silkworm," 2004.

[20] J. Zhu, Y. Zhang, H. Shao, and X. Hu, "Electrospinning and rheology of regenerated Bombyx mori silk fibroin aqueous solutions: The effects of pH and concentration," *Polymer (Guildf).*, vol. 49, no. 12, pp. 2880–2885, 2008.

[21] B. N. Singh, N. N. Panda, and K. Pramanik, "A novel electrospinning approach to fabricate high strength aqueous silk fibroin nanofibers," *Int. J. Biol. Macromol.*, vol. 87, pp. 201–207, 2016.

[22] T. A. Witten and M. H. Cohen, “Crosslinking in shear-thickening ionomers,” *Macromolecules*, vol. 18, no. 10, pp. 1915–1918, Oct. 1985.

[23] G. Bokias, D. Hourdet, and I. Iliopoulos, “Positively Charged Amphiphilic Polymers Based on Poly(N-isopropylacrylamide): Phase Behavior and Shear-Induced Thickening in Aqueous Solution,” *Macromolecules*, vol. 33, no. 8, pp. 2929–2935, 2000.

[24] A. Ochi, K. Hossain, J. Magoshi, and N. Nemoto, “Rheology and Dynamic Light Scattering of Silk Fibroin Solution Extracted from the Middle Division of Bombyx mori Silkworm,” *Biomacromolecules*, vol. 3, no. 6, pp. 1187–1196, 2002.

[25] R. B. Bird, W. E. Stewart, and E. N. Lightfoot, *Trnasport Phenomena*. New York: John Willey & Sons Inc., 2007.

[26] T. Yamasaki and T. F. Irvine, “A comparative Capillary Tube Viscometer to Measure the Viscous Properties of Newtonian and Power-Law Fluids,” *Exp. Therm. Fluid Sci.*, vol. 3, pp. 458–462, 1990.

[27] H. Wang, Y. Zhang, H. Shao, and X. Hu, “Electrospun ultra-fine silk fibroin fibers from aqueous solutions,” *J. Mater. Sci.*, vol. 40, no. 20, pp. 5359–5363, 2005.

[28] H. Wang, H. Shao, and X. Hu, “Structure of silk fibroin fibers made by an electrospinning process from a silk fibroin aqueous solution,” *J. Appl. Polym. Sci.*, vol. 101, no. 2, pp. 961–968, 2006.

[29] J. Zhu, H. Shao, and X. Hu, “Morphology and structure of electrospun mats from regenerated silk fibroin aqueous solutions with adjusting pH,” *Int. J. Biol. Macromol.*, vol. 41, no. 4, pp. 469–474, 2007.

[30] X. Zhang, M. R. Reagan, and D. L. Kaplan, “Electrospun silk biomaterial scaffolds for regenerative medicine,” *Adv. Drug Deliv. Rev.*, vol. 61, no. 12, pp. 988–1006, 2009.

[31] G. L. Wilkes, “An Overview of the Basic Rheological Behavior of Polymer Fluids with an Emphasis on Polymer Melts,” *J. Chem. Educ.*, vol. 58, no. 11, p. 880-, 1981.

[32] Y. X. He *et al.*, “N-terminal domain of Bombyx mori fibroin mediates the assembly of silk in response to pH decrease,” *J. Mol. Biol.*, vol. 418, no. 3–4, pp. 197–207, 2012.

[33] R. J. Moon, A. Martini, J. Nairn, J. Simonsen, and J. Youngblood, *Cellulose nanomaterials review: structure, properties and nanocomposites*, vol. 40, no. 7. 2011.

[34] A. Dufresne, *Nanocellulose: From natural to high performance tailored materials*. Berlin: De Gruyter, 2012.

[35] N. E. Marcovich, M. L. Auad, N. E. Bellesi, S. R. Nutt, and M. I. Aranguren, "Cellulose micro/nanocrystals reinforced polyurethane," *J. Mater. Res.*, vol. 21, no. 4, pp. 870–881, 2006.

[36] M. A. S. Azizi Samir, F. Alloin, J.-Y. Sanchez, N. El Kissi, and A. Dufresne, "Preparation of Cellulose Whiskers Reinforced Nanocomposites from an Organic Medium Suspension," *Macromolecules*, vol. 37, pp. 1386–1393, 2004.

[37] M. M. de Souza Lima and R. Borsali, "Rodlike Cellulose Microcrystals: Structure, Properties, and Applications," *Macromol. Rapid Commun.*, vol. 25, no. 7, pp. 771–787, Apr. 2004.

[38] P. Pötschke, T. D. Fornes, and D. R. Paul, "Rheological behavior of multiwalled carbon nanotube/polycarbonate composites," *Polymer (Guildf).*, vol. 43, no. 11, pp. 3247–3255, May 2002.

[39] L. A. Utracki, "Flow and flow orientation of composites containing anisometric particles," *Polym. Compos.*, vol. 7, no. 5, pp. 274–282, Oct. 1986.

[40] J. M. Dealy and K. F. Wissbrun, "Rheology of Multiphase Systems," in *Melt Rheology and Its Role in Plastics Processing*, Dordrecht: Springer Netherlands, 1999, pp. 390–409.

[41] S. Shang, L. Zhu, and J. Fan, "Intermolecular interactions between natural polysaccharides and silk fibroin protein," *Carbohydr. Polym.*, vol. 93, no. 2, pp. 561–573, 2013.

[42] D. Tian *et al.*, "Conformations and Intermolecular Interactions in Cellulose/Silk Fibroin Blend Films: A Solid-State NMR Perspective," *J. Phys. Chem. B*, vol. 121, no. 25, pp. 6108–6116, 2017.

[43] L. H. Sperling, *Introduction to Physical Polymer Science*, Fourth Edi. New Jersey: John Wiley & Sons Ltd, 2006.

[44] M. Bercea and P. Navard, “Shear Dynamics of Aqueous Suspensions of Cellulose Whiskers,” *Macromolecules*, vol. 33, no. 16, pp. 6011–6016, 2000.

[45] M. I. Aranguren, E. Mora, J. V. DeGroot, and C. W. Macosko, “Effect of reinforcing fillers on the rheology of polymer melts,” *J. Rheol. (N. Y. N. Y).*, vol. 36, no. 6, pp. 1165–1182, Aug. 1992.

[46] F. Du, R. C. Scogna, W. Zhou, S. Brand, J. E. Fischer, and K. I. Winey, “Nanotube networks in polymer nanocomposites: Rheology and electrical conductivity,” *Macromolecules*, vol. 37, no. 24, pp. 9048–9055, 2004.

[47] Y. Habibi, L. A. Lucia, and O. J. Rojas, “Cellulose Nanocrystals : Chemistry , Self-Assembly , and Applications,” *Chem. Rev.*, vol. 110, no. 6, pp. 3479–3500, 2010.

[48] A. Baji, Y. W. Mai, S. C. Wong, M. Abtahi, and P. Chen, “Electrospinning of polymer nanofibers: Effects on oriented morphology, structures and tensile properties,” *Compos. Sci. Technol.*, vol. 70, no. 5, pp. 703–718, 2010.

[49] M. M. Hohman, M. Shin, G. Rutledge, and M. P. Brenner, “Electrospinning and electrically forced jets. I. Stability theory,” *Phys. Fluids*, vol. 13, no. 8, pp. 2201–2220, 2001.

[50] J. . Deitzel, W. Kosik, S. . McKnight, N. . Beck Tan, J. . DeSimone, and S. Crette, “Electrospinning of polymer nanofibers with specific surface chemistry,” *Polymer (Guildf).*, vol. 43, no. 3, pp. 1025–1029, Feb. 2002.

[51] L. Larrondo and R. St. John Manley, “Electrostatic fiber spinning from polymer melts. I. Experimental observations on fiber formation and properties,” *J. Polym. Sci. Polym. Phys. Ed.*, vol. 19, no. 6, pp. 909–920, Jun. 1981.

[52] A. Dufresne, *Nanocellulose: From natural to high performance tailored materials*. Berlin: De Gruyter, 2012.

[53] L. Flandin, J. Y. Cavaillé, G. Bidan, and Y. Brechet, “New nanocomposite materials made of an insulating matrix and conducting fillers: Processing and properties,” *Polym. Compos.*, vol. 21, no. 2, pp. 165–174, Apr. 2000.

[54] I. Balberg and N. Binenbaum, “Computer study of the percolation threshold in a two-

dimensional anisotropic system of conducting sticks," *Phys. Rev. B,* vol. 28, no. 7, pp. 3799–3812, Oct. 1983.

# Chapter 3

## Production and characterization of regenerated silk fibroin electrospun nanocomposites reinforced with cellulose nanocrystals

### 3.1. Introduction

This section describes the aspects regarding the production and characterization of regenerated silk fibroin (RSF) nanocomposites reinforced with cellulose nanocrystals (CNC) produced via electrospinning and solvent casting. The main goal of this work was the enhancement of the mechanical and thermal properties of RSF due to the process or by the addition of the filler. The first stage for this investigation was focused on finding the best conditions to carry out electrospinning. Such that, supported on literature review and on previous experimental work, the variables to produce continuous fibers of RSF via electrospinning were successfully obtained. Subsequently, to explore the effects of the process on the properties of regenerated silk fibroin (RSF), electrospun nonwovens and solvent-casted films were produced using an aqueous solution of RSF with 20% w/w. In parallel, to evaluate the consequence of the addition of cellulose nanocrystals (CNC) on RSF, the filler was added to solutions of RSF to generate RSF/CNC blends with a total solid content of 20% w/w, with RSF/CNC ratios in %w/w in solution of 19.5/0.5, 19/1, 18.5/1.5, 18/2. The chosen loadings of filler were carefully selected to investigate the effects of the addition of CNC in concentrations below and above the experimental percolation threshold,

determined via rheological studies, previously elaborated in Chapter 2. These solutions were used for the fabrication of the nanocomposites through electrospinning and solvent-casting.

The produced electrospun nonwovens were characterized in terms of their morphology via scanning electron microscopy (SEM), chemical conformation by Fourier transformed infra-red spectroscopy (FTIR), crystallinity by x-ray diffraction (XRD), and thermal resistance by thermogravimetric analysis (TGA). Whereas, the mechanical performance of the composites was assessed via dynamic mechanical analysis (DMA) in films rather than in the electrospun nonwovens, due to the brittleness and softness of the electrospun nanocomposites, which hindered the separation of the materials settle on the collector without damaging the structures. Such tests, provided good insights about the ideal amount of CNC to be added in a RSF to successfully reinforce the polymer.

## 3.2. Materials

Partially degummed silkworm cocoons from a waste stream were generously provided by Corseda (Popayan, Colombia). Cellulose nanocrystals aqueous slurry with a solid concentration of about 10.26% w/w, produced via acid hydrolysis of wood pulp with small residues of cellulose II, was donated by the USDA forest product laboratory (Madison, WI). Sodium carbonate anhydrous was purchased from VWR (West Chester, PA). Lithium bromide was supplied by Oak Chemical (Columbia). Polyethylene glycol (MW≈10,000) was bought from Merck (Darmstadt, Germany). Ultrapure water (0.055 μs/cm, 18 mΩ-cm) was employed for every procedure, except for degumming and dialysis, where distilled water was utilized.

## 3.3. Methods

### 4.3.1. Silkworm cocoon degumming

Silkworm cocoons from industrial wastes were untangled to increase the contact area of the fiber and were then dipped into a solution of sodium carbonate 0.02 M at a boiling temperature under constant stirring for 30 minutes. Subsequently, the fibers were washed with distilled water at a boiling temperature and later with distilled water at room temperature. This process was

performed twice, and the process time (30 minutes) was strictly controlled to ensure the complete removal of sericine and to avoid further complications associated with the degradation of silk properties [8], [16], [136], [148], [180]. Afterwards, the degummed silk was dried at 60 °C for 24 hours.

### 4.3.2. Isolation of silk fibroin

The degummed silk was dissolved in a 9.3M solution of lithium bromide (LiBr) at 60 °C, under a constant stirring rate of 240 rpm, for 4 hours [181]. Next, the solution was filtered through filter paper grade 1 (Whatman$^{TM}$, GE life science, USA) and dialyzed using a dialysis membrane MWCO 3.5 kDa (Spectra/Por 3, Spectrum labs, USA), until reaching a constant value of conductivity. Thereafter, the solution was centrifuged at 9000 rpm and 4 °C, for 20 minutes. The latter was performed two times. Finally, the solution was micro filtered d through cellulose acetate filter membranes 0.45 μm pore size (Ahlstrom, Germany) and stored at 7 °C.

The percentage of solids in the RSF was measured as the ratio between the dry and wet weight of the solution dried overnight at 105 °C.

### 4.3.3. Concentration of regenerated silk fibroin solution

The regenerated silk fibroin solution was concentrated via reverse dialysis. The RSF solution was placed in a dialysis membrane MWCO 3.5 kDa (Spectra/Por 3, Spectrum labs, USA) in an aqueous solution of 25% w/w polyethylene glycol (10 kDa) at room temperature. The concentration of the solution in the dialysis membrane was constantly measured by calculating the difference between the weight in wet and dry in aliquots of the solution. The process proceeded until a final concentration from 23% to 36% w/w for the RSF solution was obtained.

### 3.3.4. Preparation of RSF and RSF/CNC solutions

An aqueous CNC slurry was diluted in ultrapure-water and dispersed using a sonicator vibra-cell series VC 750 (Sonic, Newtown, CT) set at 750 W and 20% amplitude, for 10 minutes, using the ½” tip. Next, the concentrated solution of RSF was diluted to a total solid content of 20% w/w,

either by adding ultra-pure water or by mixing it with the suspension of CNC to produce the RSF/CNC solutions for electrospinning, with ratios of 19.5/0.5, 19/1, 18.5/1.5, and 18/2 in weight percent. Finally, both components were mechanically stirred until a homogeneous dispersion was achieved.

### 3.3.5. Characterization of the dispersions

The conductivity and pH of each solution were measured at room temperature employing a multi-meter Benchtop Symphony sb70 (VWR, Radnor, PA). Each property was recorded in triplicate to evaluate the variability.

### 3.3.6. Electrospinning parameters for RSF solution

The initial set of parameters for electrospinning were selected based on values reported in the literature for similar experimental works [19], [182], [185], [186], [192]–[194], [204], [205]. To establish the best conditions to fabricate defect-less RSF electrospun nonwovens, a RSF solution with a concentration of 20% w/w was introduced into 1 ml plastic syringes (BD, Franklin Lakes, NJ) with an inner diameter of 4.78 mm, attached to a metallic needle 21G x 1" (BD PrecisionGlide$^{TM}$, Franklin Lakes, NJ), whose sharpened end was previously removed. The syringe was placed on a single jet electrospinning system, and the metallic needle was connected to the anode of a power supply. A flat metallic sheet was wrapped with aluminum foil, ground connected, and placed in front of the electrospinning setup to be used as collector. The complete picture of the electrospinning set up is shown in Figure 3-1.

The electrospinning process was carried out at a flow rate of 0.1 ml/h for the electrospinning apparatus, a voltage of 10 kV and 20 kV, and a distance from the tip of the needle to the collector of 10 cm and 20 cm. The combinations of parameters are summarized in Table 3-1. These values of distance and voltage were selected in accordance with literature reports in order to keep a ratio voltage/distance between 2 and 1, where values close to 1 give the best conditions for electrospinning [182], [194], [205]. This ratio is established based on the relationship between the magnitude of the electric field and these two variables, where the first is directly proportional

to the voltage and inversely proportional to the square of the distance ($\alpha$ $V/D^2$) [18], [41]. The material produced was stored in dry conditions, and their morphology was analyzed via SEM.

**TABLE 3-1.** Combination of parameters to find the best conditions to produce defect-less electrospun RSF.

| Sample | Flow rate (ml/h) | Voltage (kV) | Distance (cm) |
|---|---|---|---|
| RSF-1 | 0.1 | 10 | 10 |
| RSF-2 | | 20 | 10 |
| RSF-3 | | 20 | 20 |

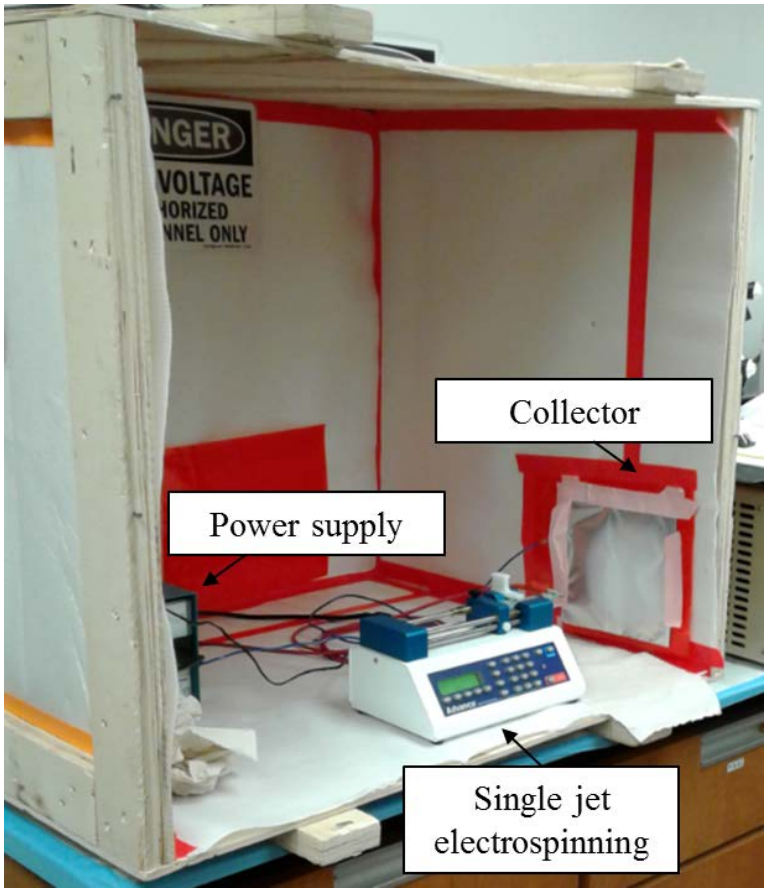


**FIGURE 3-1.** Electrospinning setup utilized in this work.

### 3.3.7. Production of RSF/CNC electrospun nonwovens

Once the best combination of parameters for electrospinning was established, the solutions of RSF with different loadings of CNC were processed. Each solution was introduced into 1 ml plastic syringes (BD, Franklin Lakes, NJ) with an inner diameter of 4.78 mm, attached to a metallic needle 21G x 1" (BD PrecisionGlide$^{TM}$, Franklin Lakes, NJ), whose sharpened end was previously removed. One syringe at a time was placed on a single jet electrospinning system with a flow rate of 0.1 ml/h, a voltage of 20 kV, and a distance from the tip of the needle to the collector of 20 cm. The process was allowed to run for at least 3 hours until a representative amount of material was produced, and the resulting products were stored in dry conditions. The name of each sample and their conditions are presented in Table 3-2.

**TABLE 3-2.** Processing parameters for electrospinning of RSF/CNC solutions.

| Sample | RSF/CNC %weight in solution | Flow rate (ml/h) | Voltage (kV) | Distance (cm) |
|---|---|---|---|---|
| RSF | 20/0 | 0.1 | 20 | 20 |
| RSF/CNC-0.5 | 19.5/0.5 | | | |
| RSF/CNC-1 | 19/1 | | | |
| RSF/CNC-1.5 | 18.5/1.5 | | | |
| RSF/CNC-2 | 18/2 | | | |

### 4.3.9. Production of RSF and RSF/CNC films

Solvent-cast films of RSF were produced in order to understand the effect of the electrospinning process and the addition CNC on the chemical structure and the thermo-mechanical performance of RSF. Aqueous solutions of RSF at 3-5% w/w were cast on plastic petri dishes and oven-dried at 25 °C for 48 hours, until a constant weight was reached. This process was carried out in accordance with the protocol reported by Asakura, *et al*. [206] to

produce regenerated silk fibroin films with a structure mainly composed of silk I or water soluble silk.

Additionally, RSF/CNC films were produced using the same RSF solutions with CNC loadings of 0%, 0.5%, 1%, 1.5%, and 2% w/w, as employed for the electrospinning process. The solutions were cast on plastic petri dishes and oven-dried overnight at 60 °C. These films were fabricated to evaluate the effects on the mechanical behavior of RSF with the addition of CNC.

### 3.3.10. Characterization of electrospun-nonwovens

#### 3.3.9.1. Morphological analysis

The morphology of the nanocomposites and fiber shape were analyzed for every sample via scanning electron microscopy (SEM). A representative amount of sample from each electrospun nonwoven was cut and taped to aluminum holders using a double-faced carbon conductive tape and sputter coated with gold for 2 minutes. The morphology of the samples was analyzed with a SEM EVO50 (ZEISS, Oberkochen, Germany) set at 20 kV under high vacuum. Images of the morphology were recorded at magnifications of 1 kX and 15 kX.

#### 3.3.9.2. Chemical characterization

The characteristic chemical structures of each sample were assessed through Fourier-transform Infrared spectroscopy (FTIR), using a Spectrum 400 FTIR-NIR (Perkin Elmer, Waltham, MA) equipped with a universal ATR accessory and a mid-infrared deuterated triglycine sulfate detector. For each spectrum, 1,024 scans with a resolution of 4 $cm^{-1}$, within a wavenumber range from 800 to 4,000 $cm^{-1}$ were collected Changes in the main chemical groups associated with the electrospinning process and the addition of CNC were evaluated.

#### 3.3.9.3. Crystallinity

The crystallinity of the nanocomposites and RSF films was studied with an X-ray diffractometer D2 Phaser (Bruker, Germany) equipped with a Cu $K_\alpha$ radiator (wavelength of

0.154 nm). The first order of reflection (n=1) was recorded at 30 kV and 10 mA, under a scanning rate of 0.5 sec/point within a diffraction range from 5° to 55°. The angle/angles where the constructive interference presented a maximum were determined (when Bragg's law was satisfied), and their associated d-spacing was calculated though Bragg's law (equation 3-1) and related to their particular crystalline structure.

$$\frac{n*\lambda}{2\sin(\theta)} \tag{3-1}$$

Where "n" is the order of reflection, λ is the wavelength of the x-ray source, and θ is the angle at maximum constructive interference.

Deconvolution of the diffraction patterns of each sample was performed to determine the area of the peaks associated to the diffraction pattern, and to evaluate the presence of unresolved peaks planes. The crystallinity for each sample was determined as the ratio between the sum of the area of the peaks associated with silk II and cellulose I, divided by the total area of the diffraction pattern [180], [36].

#### 3.3.9.4.Thermal stability

The resistance to thermal degradation of the RSF/CNC electrospun composites and the RSF film was evaluated via thermogravimetric analysis (TGA) with a TGA Pyris 1 (Perkin Elmer, Waltham, MA). Approximately 7 mg of sample was weighed and placed in an alumina pan and heated from 30 °C to 600 °C, with a heating ramp of 10 °C/min, under a continuously flowing nitrogen atmosphere set at 20 ml/min. The onset temperature of degradation and temperature of maximum degradation rate were recorded and compared to establish the sample with the best performance.

#### 3.3.9.5. Mechanical properties

The mechanical performance of the electrospun nonwovens was challenging to evaluate, due to the difficulties to remove the produced materials from the support without damaging the structure,

leading to biased measurements. Such that, the mechanical properties of the RSF/CNC composites were measured in films, via dynamic mechanical analysis (DMA) using a TA RSA3 DMA (TA instruments, New Castle, DE) in tensile mode at a constant deformation rate of 10 mm/min, with a span of 15 mm, and room conditions.

## 3.4. Results

### 3.4.1. Determination of parameters for electrospinning

The solution of RSF at 20% w/w was electrospun under the conditions shown in Table 3-1, beginning at a short distance and low voltage (10 cm and 10 kV), followed by a combination of short distance and high voltage (10 cm and 20 kV), and finishing at a long distance and high voltage (20 cm and 20 kV). The morphology of the produced electrospun nonwovens under a magnification of 1,000 X is presented in Figure 3-2.

According to literature reports, a minimum concentration of 20% w/w of silk fibroin in an aqueous solution must be used to provide enough viscous forces to support the formation of a continuous jet [19], [182], [193], [194]. However, as seen in Figure 3-2, the process parameters also played a key role in the morphology of the produced electrospun nonwoven. In the case of the nonwoven fabricated at short distance and low voltage (RSF-1), a combination of thin fibers and droplet-shaped structures or beads, were found. These results may be attributed to poor fiber stretching related to low electric forces and/or short distance, where the small electrostatic field was not sufficiently strong to completely overcome the viscous forces. In addition the short distance reduced the time of fly of the fiber, generating poor solvent evaporation and less room for fiber stretching [18], [41], [39], [72], [81], [84], [85].

The material produced at short distance and high voltage (RSF-2), did not present a defined structure, but rather fibers embedded in a polymer matrix. This type of structure is thought to be due to very strong electric fields in combination with a short working distance, where the polymer jet was able to stretch at under the electric field, but the short distance did not allow an adequate solvent evaporation, which led to the generation of extremely wet fibers. This caused an accumulation of solvent on the surface of the electrospun nonwoven, and the re-dissolution of the polymer and coalescence of the fiber on the collector [18], [39], [84], [85].

By working at long distance and high voltage (RSF-3), the product exhibited a continuous fibrous structure, where beads or fiber coalescence were not detected. This combination of parameters gave distances and electrostatic forces suitable to meet the requirements for jet drying and stretching for the production of continuous and regular fibers. Consequently, these conditions were selected for the production of the RSF/CNC electrospun nanocomposites.

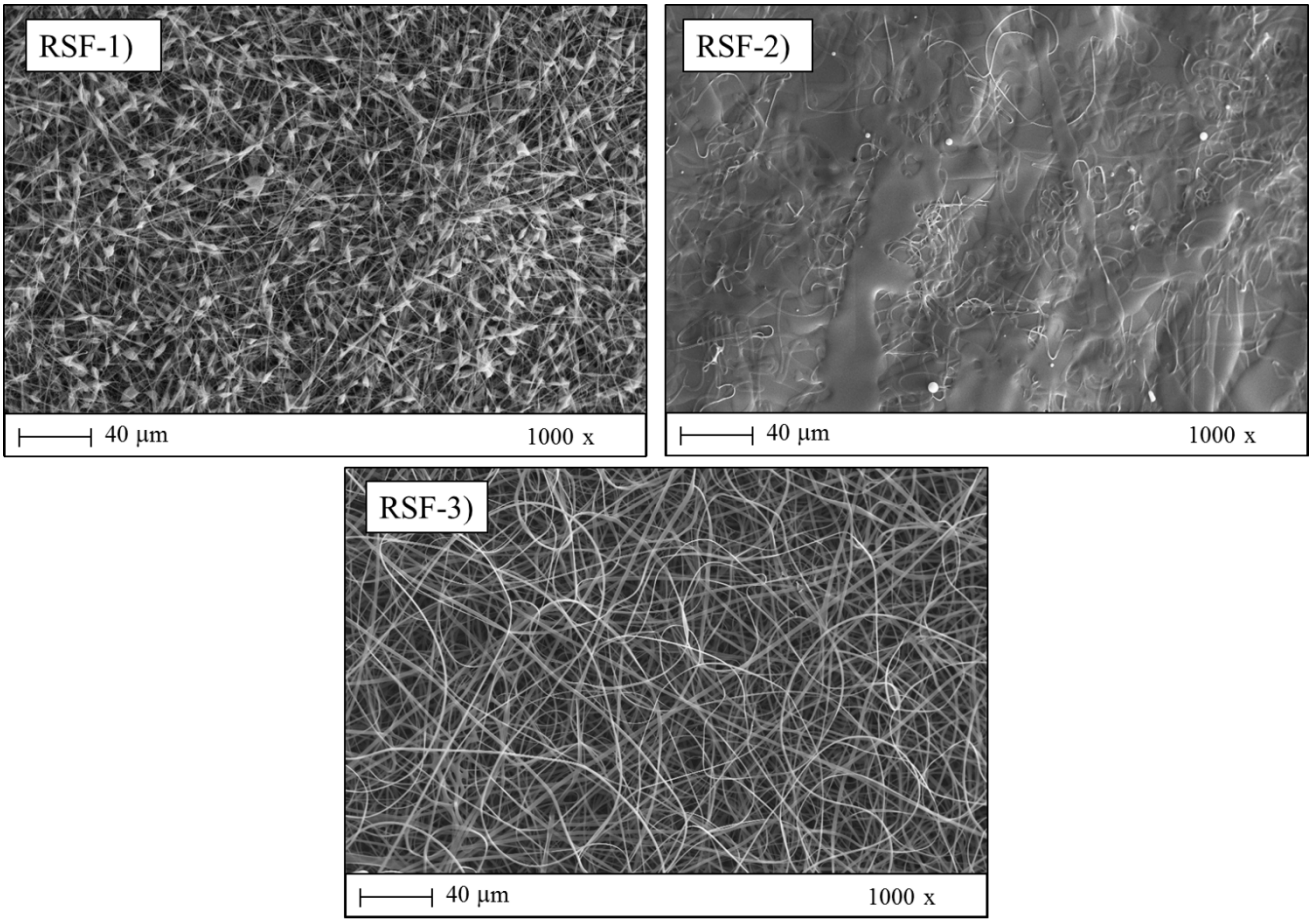


**FIGURE 3-2.** Morphology at 1,000 X of magnification for the RSF electrospun nonwovens processed at 20% w/w, 0.1 ml/h, and at distances and voltages of: RSF-1) 10 cm and 10 kV; RSF-2) 10 cm and 20 kV; RSF-3) 20 cm and 20 kV.

### 3.4.2. Production and characterization of RSF/CNC electrospun nanocomposites

Before producing electrospun nanocomposites, each solution of RSF and RSF with different loadings of CNC were characterized in terms of conductivity and pH, the results of which

are displayed in Table 3-3. As previously discussed the addition of CNC did not produce a major change in the pH of the solutions but raised the conductivity of the solutions. The increase in conductivity could be attributed to the increased number of hydroxyl groups in the solution endowed by CNC, along with the formation of an electrical percolation network of CNC, which facilitated the charge transference within the system [29], [32], [174].

Then, once the best combination of parameters for electrospinning was established, the RSF/CNC solutions were processed via electrospinning according to the conditions in Table 3-2, and the morphology, chemical structure, crystallinity, and thermal resistance of the produced nonwovens were characterized to evaluate the effects of the electrospinning process and the addition of CNC on RSF. The properties of the electrospun nanocomposites of RSF were compared against those form a RSF film mainly composed of silk I.

**TABLE 3-3.** Conductivity and pH of RSF and RSF/CNC solutions

| Sample | RSF/CNC %weight in solution | Conductivity (μS/cm) | pH |
|---|---|---|---|
| RSF | 20/0 | 268 ± 2 | 7.00 ± 0.01 |
| RSF/CNC-0.5 | 19.5/0.5 | 280 ± 2 | 7.01 ± 0.02 |
| RSF/CNC-1 | 19/1 | 288 ± 1 | 7.06 ± 0.02 |
| RSF/CNC-1.5 | 18.5/1.5 | 302 ± 1 | 7.09 ± 0.02 |
| RSF/CNC-2 | 18/2 | 306 ± 2 | 7.11 ± 0.01 |

#### 3.4.2.1. Morphological analysis

The morphology of the electrospun composites was analyzed in terms of the fiber shape and number of defects, related to beads and regularity of fiber. The morphology of each composite, produced according to the conditions in Table 3-2, are presented in Figure 3-3 and Figure 3-4, in magnifications of 1,000 X and 15,000 X, respectively. The distribution of fiber diameter of each sample is illustrated in Figure 3-5.

As observed in Figure 3-3, RSF/CNC electrospun nonwovens with continuous fibrous structures were obtained employing the processing parameters previously stablished. It was noticed that the CNC loading apparently influenced the average diameter size (mean) and

regularity of the fiber related to the standard deviation of fiber diameter. The RSF electrospun nonwoven without CNC exhibited the largest fiber diameter, the highest standard deviation, and consequently a wide distribution of dimeter size, as compared to the RSF/CNC electrospun nanocomposites. A small loading of CNC in the order of 0.5% w/w (SF/CNC-0.5) produced a sharp decrease in diameter and contributed to the production of more homogeneous fibers. Further increases in CNC loading led to bigger diameter and reduced homogeneity of the fibers size, or broadened distributions of fiber size.

The initial reduction in diameter and more homogeneous fibers for RSF when CNCs were added, may be attributed to the raise in the conductivity of the solution caused by the addition of CNC, which might have facilitated the charge transportation along the polymer jet, fostering the fiber stretching and the reduction in the second type of instabilities in electrospinning process, therefore, lessening the chances of jet breaking up [18], [41], [75], [76], [109]. Notwithstanding, an abrupt rise in the conductivity could lead to uncontrolled bending and whipping instabilities and to reductions in the regularity of the fiber or broader distributions of size [18]. The last, might explain the higher standard deviation in diameter size among the nanocomposites in response to the increasing loading of CNC in the electrospun material.

In addition, as it was observed during the rheological analysis of the solutions of RSF/CNC (see Chapter 2), the addition of CNC increased the initial dynamic viscosity of RSF solution, specially, at strains below 7.54 rad/s, equal to 1.20 1/s. To verify if the electrospinning process proceed at lower strains, the shear rate experienced by the RSF and RSF/CNC solutions during electrospinning was modelled as the deformation suffered by a Newtonian fluid as it flows through a capillary tube, described by equation 3-2. Where “Q” is the flow rate (0.1 ml/h), and “d” is the diameter of the capillary (0.051 cm for a 21G needle) [190], [207]. Form this equation, a value of 2.13 1/s, which corresponded to 13.40 rad/s, was obtained. At this conditions, the solutions behaved like pseudoplastic fluids, where the addition of CNC had a lower impact on the viscosity, but still produced a slight enhancement on this property among the solutions.

$$\gamma = \frac{32Q}{\pi d^3} \tag{3-2}$$

In theory, higher viscosities leads to thicker and more homogeneous fibers [72], [71], but, such effect was not observed when comparing the RSF/CNC nanocomposites with the RSF nonwoven without CNC. It could be the result of the higher conductivities and lower amounts of RSF in solution, when CNC were added. Where the first fostered fiber stretching, while the last reduced the viscous forces in the polymeric matrix. Furthermore, in spite that CNC enhanced the dynamic viscosity of the solutions, at the conditions of the electrospinning, such effect was attenuated by the high shear rate exercised by electrospinning. It is important to point out that the increase in viscosity caused by the addition of CNC, may have occurred due to the increase in the interactions polymer-filler and/or filler-filler, rather than in polymer-polymer interaction, which might result in smaller fiber sizes in the electrospun composites of RSF/CNC compared to RSF nonwovens [18]. In contrast, among the electrospun composites of RSF/CNC, the slight increase in viscosity produced by the higher loading of CNC, resulted in bigger and more heterogeneous fiber diameter.

In Figure 3-4, it was noticed that the shape of the fibers changed from a ribbon-like shape for the electrospun RSF without CNC, to more rounded fibers with increasing loading of CNC. This flattened shape is typically associated with poor or incomplete solvent evaporation, as a consequence of a very short distance and/or weak stretching forces. At these conditions, the remaining solvent in the fibers would allow the mobility of the polymer chains, which leads to the relaxation of the material in surface, leading to fattened or ribbon-shaped structures [18], [39], [84], [85]. However, as rounded-shaped fibers were produced using a working distance of 20 cm, the ribbon-like shape observed in the RSF electrospun nonwoven could be caused by poor fiber stretching in relation to lower conductivity of the polymer.

Finally, it is important to remark that the addition of CNC in RSF solutions, led to reduced diameters, less variability, and more rounded fibers. Such that, the addition of CNC could be advantageous for the production of electrospun composites of RSF with more regular structures.

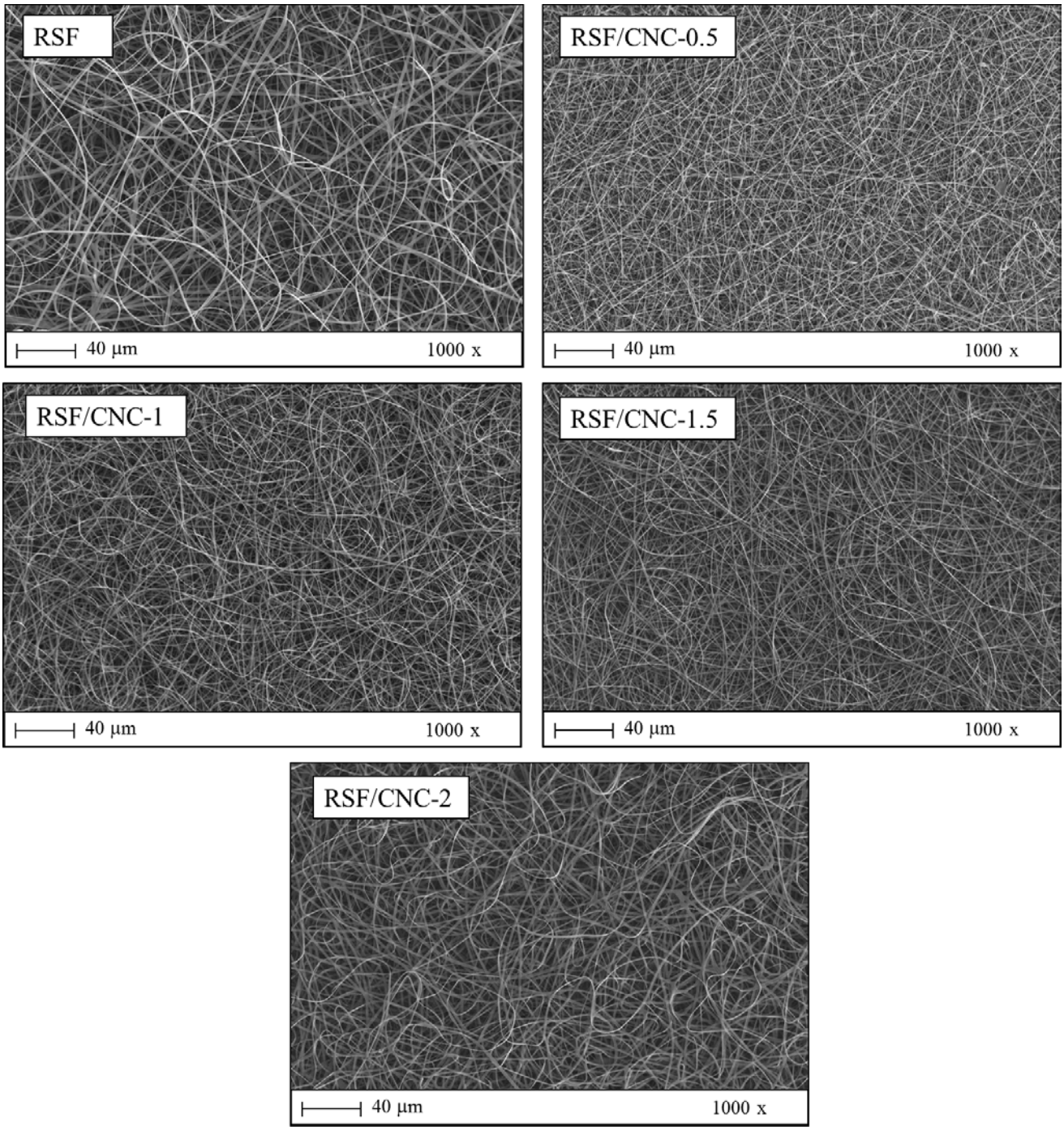


**FIGURE 3-3.** Morphology at 1,000 X of magnification for the electrospun nanocomposites produced at 0.1 ml/h, 20 kV, 20 cm.

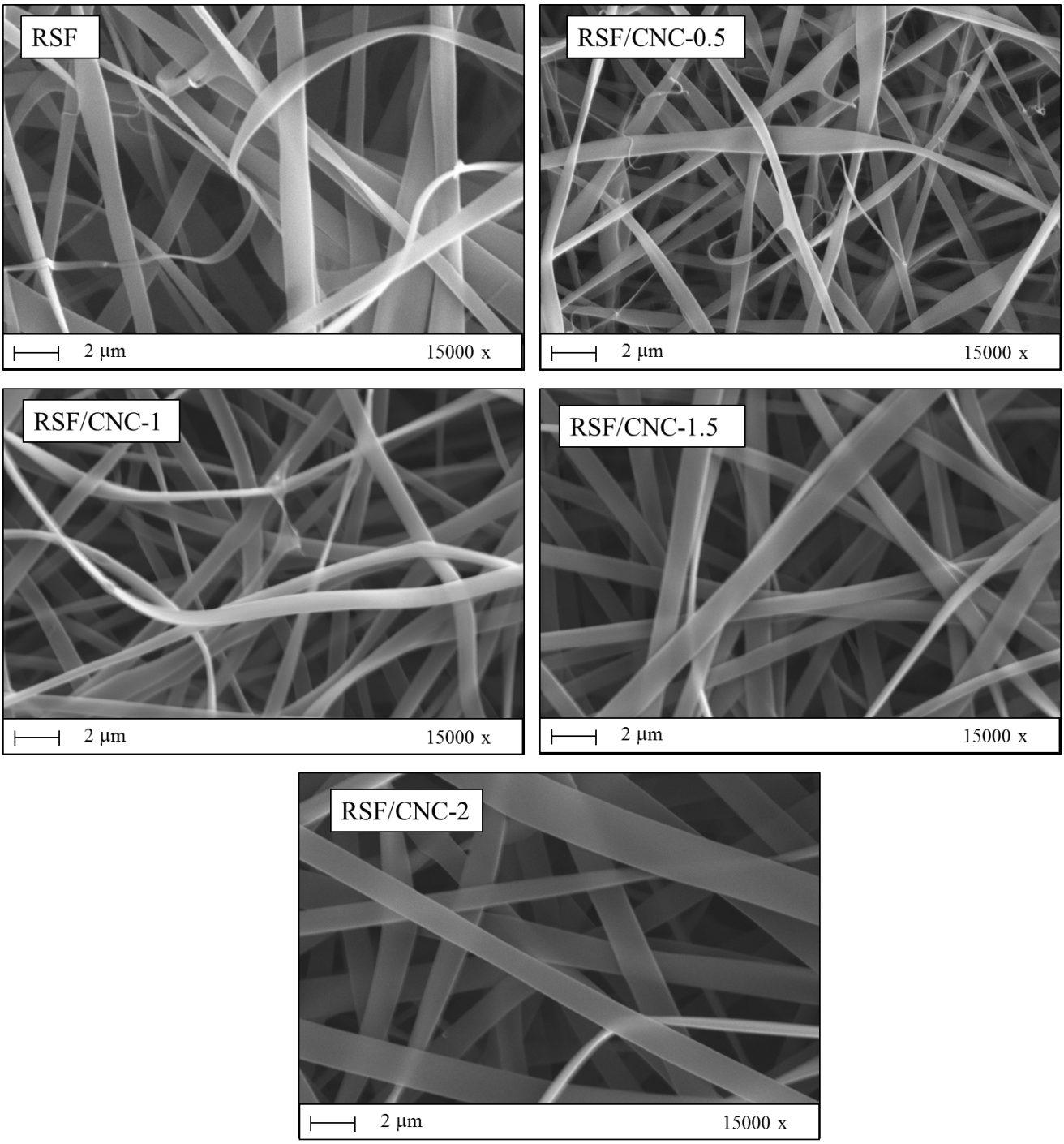


**FIGURE 3-4.** Morphology at 15,000 X of magnification for the electrospun nanocomposites produced at 0.1 ml/h, 20 kV, 20 cm.

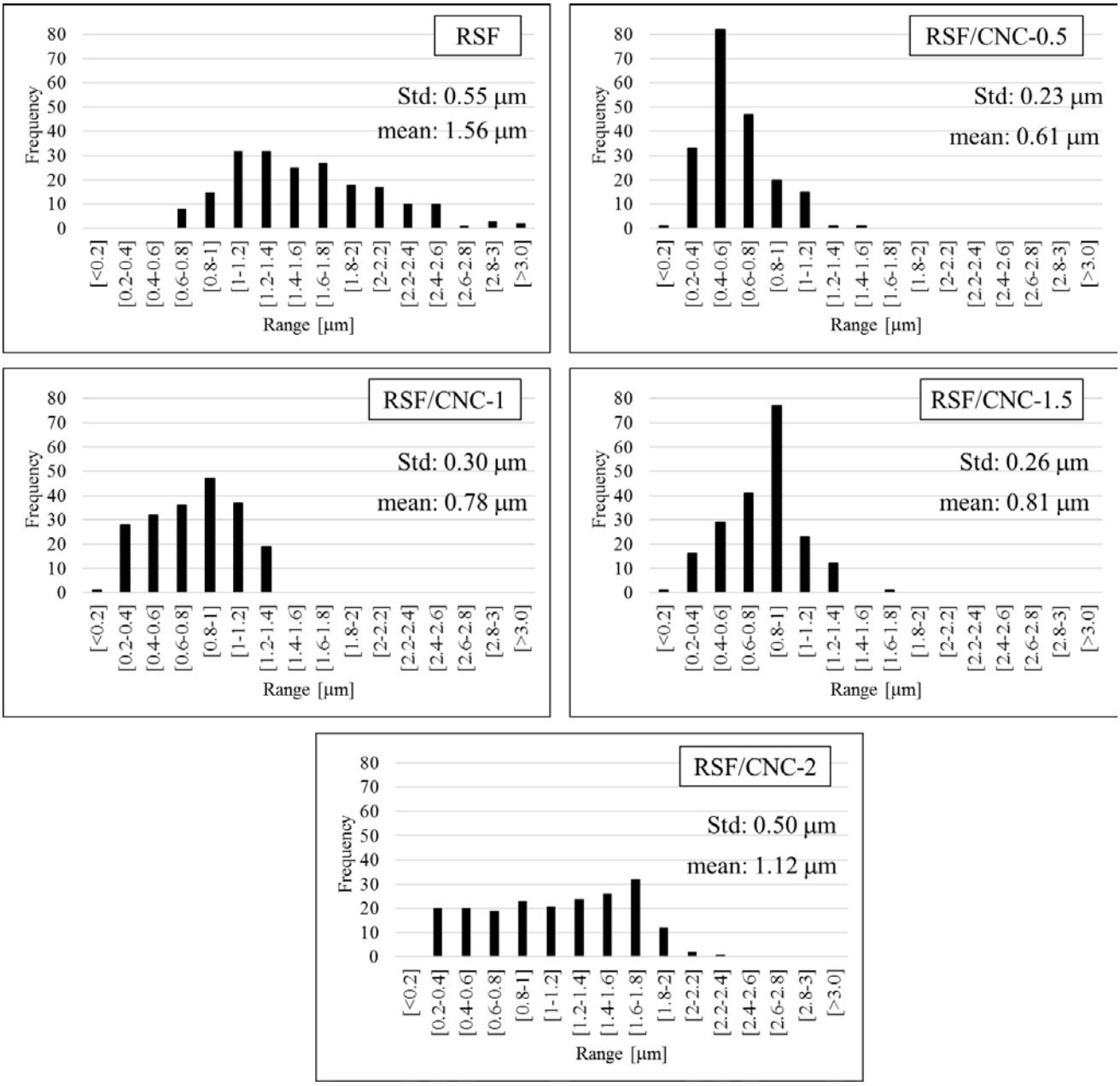


**FIGURE 3-5.** Distribution of diameter size, standard deviation (Std), and mean diameter size (mean) for RSF/CNC electrospun nanocomposites.

### 3.4.2.2. Chemical characterization

The analysis of the chemical structure of RSF was carried out in two parts, to observe the effects of processing and the addition of CNC. To analyze the effects of the process, the infrared

spectra of RSF in film produced by solvent casting and electrospun nonwoven of RSF were compared to detect differences between the chemical structures of both materials. Both spectra are presented in Figure 3-6, where the highlighted region corresponds to the bands or vibrational modes in RSF structure.

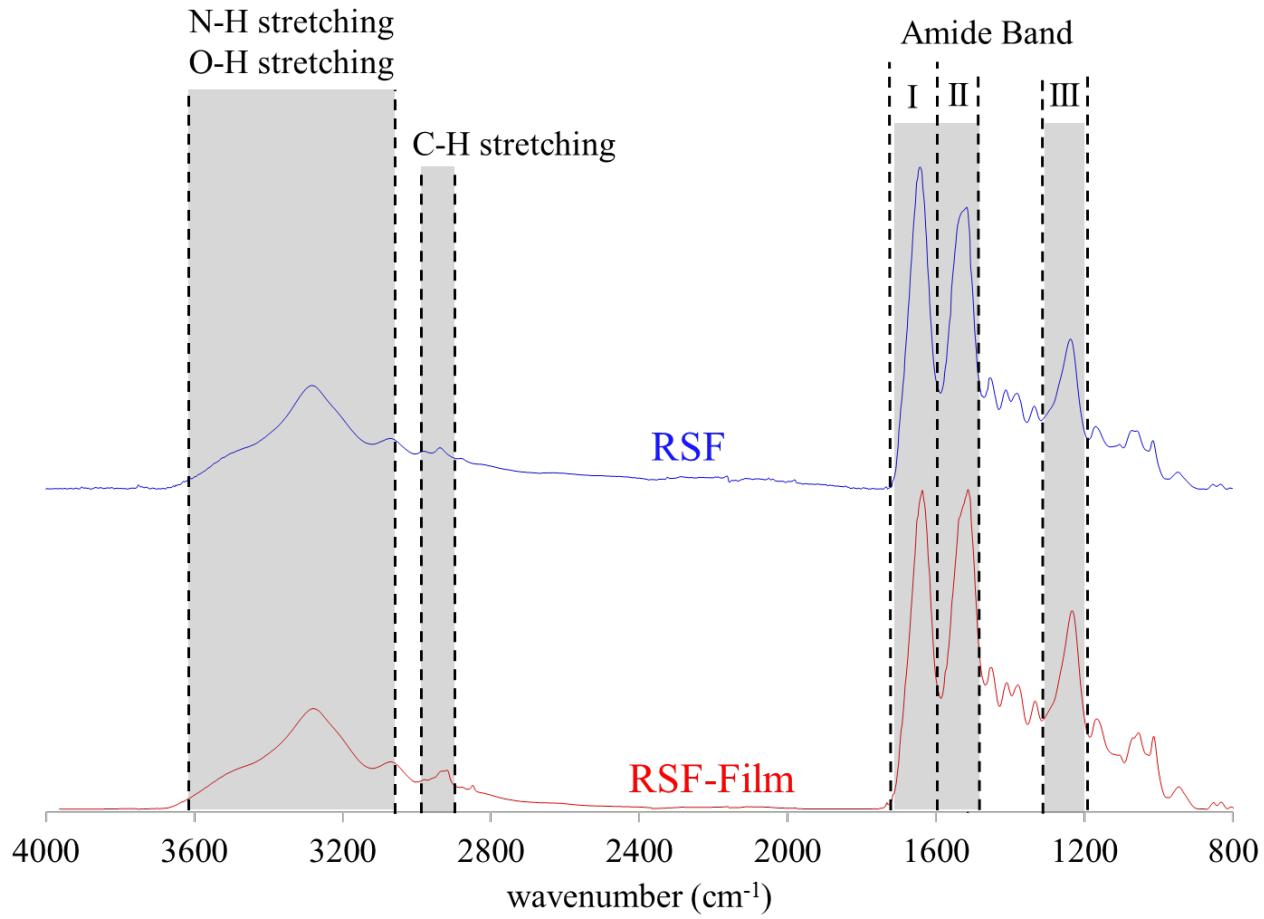


**FIGURE 3-6.** FTIR spectra of Electrospun RSF (RSF) and RSF in film (RSF-Film).

In Figure 3-6, two principal zones where most of the vibrational modes occurred could be identified in both samples. The first one, between 3500-2900 $cm^{-1}$, which corresponded to three different vibrational modes; and the second one, localized between 1700-1000 $cm^{-1}$, deemed as the amide band, which exhibited a several peaks, which principally depend on the backbone and secondary structures of the protein [208].

In the first zone, between 3500-2900 $cm^{-1}$, both samples exhibited analogous peaks with similar intensities, where a broad peak with medium intensity, and two other peaks with weak

intensity were identified. The first peak resulted from the N-H stretching from primary and secondary amines, usually located between 3500-3300 $cm^{-1}$, centered circa 3300 $cm^{-1}$. One of the weak intensity peaks with a center close to 3000 cm-1, could be attributed to the O-H stretching from carboxylic acids, which typically appears between 3300-2500 $cm^{-1}$. Finally, the second weak intensity peak with center around 2900 $cm^{-1}$ was produced by the C-H stretching from alkanes in the protein backbone, resulting from the saturated α carbon and the methyl pendant groups from alanine in the protein backbone. This vibrational mode is usually observed as low intensity scattered peaks between 3000-2850 $cm^{-1}$ [12], [125], [126], [209].

The analysis of the second zone, localized around 1700-1000 $cm^{-1}$, was more challenging due to the complexity of the vibrational modes from the primary and secondary structures that the protein experience at this threshold of frequencies. Within this region, the vibrational modes corresponding to amide I, II, and III are used to evaluate the changes in the protein structure. The amide I band, identified as a strong intensity peak located around 1700-1600 $cm^{-1}$, is predominantly produced by C=O stretching, and it has been widely employed to analyze quantitatively and qualitatively the amount of β-sheets (silk II), and α-helices and random structures (silk I). The assessment of β-turns in this region becomes difficult, as most of these structures vibrate at the same frequency of α-helices and β-sheets. The amide II band, found as a strong intensity peak between 1600-1500 $cm^{-1}$, is produced by the N-H bending and C-N stretching. This band provides more information about parallel and antiparallel arrangements of β-sheets, as well as a more accurate appreciation of random structures. As in amide I band, here, it is difficult to distinguish between β-turns and β-sheets. Finally, the region between 1350-1200 $cm^{-1}$ is deemed to the amide III, distinguished by weak intensity peaks from mixed vibrations. The evaluation of this band by itself is sometimes impractical and does not give many insights about the protein secondary structure. Although, when it is inspected along with amide I, it is feasible to discern between β-sheets and random structures [208], [147], [210]–[212].

In order to evaluate the structure of the protein in the second zone, Figure 3-7 shows the scope of the infrared spectra between 1700-1200 $cm^{-1}$. Accordingly, in the amide I band, the peaks located between 1630-1620 $cm^{-1}$, 1635-1645 $cm^{-1}$, and 1655-1662 $cm^{-1}$ are assigned to the presence of β-sheets, random coils, and α-helices, respectively. And an additional peak located near 1685-1700 $cm^{-1}$ results from the occurrence of antiparallel β-sheets, which is a clear indication of more stable structures [192], [206], [36], [208], [21], [28], [147], [210]–[215]. For

the amide II band, the peaks found between 1530-1520 $cm^{-1}$ and 1550-1535 $cm^{-1}$ are accurately attributed to the formation of silk II and silk I structures, respectively. The amide II band is not commonly employed to identify α-helices, but, in a comprehensive investigation about the identification of secondary structures in proteins through FTIR, Miyazawa and Blout [211] assigned a peak below 1520 $cm^{-1}$ to α-helices, whereas other authors assign this peak to antiparallel β-sheets [208], [212], [21]. Lastly, in the amide III, the peaks centered near 1260 $cm^{-1}$ and 1230 $cm^{-1}$ are commonly produced by the presence of non-water soluble silk (silk II) and water soluble silk (silk I), respectively. The identification of secondary structures within this band is complicated and inaccurate due to the weak intensity of the peaks and the number of miscellaneous vibrations that occur along these range of frequencies [206], [208], [213].

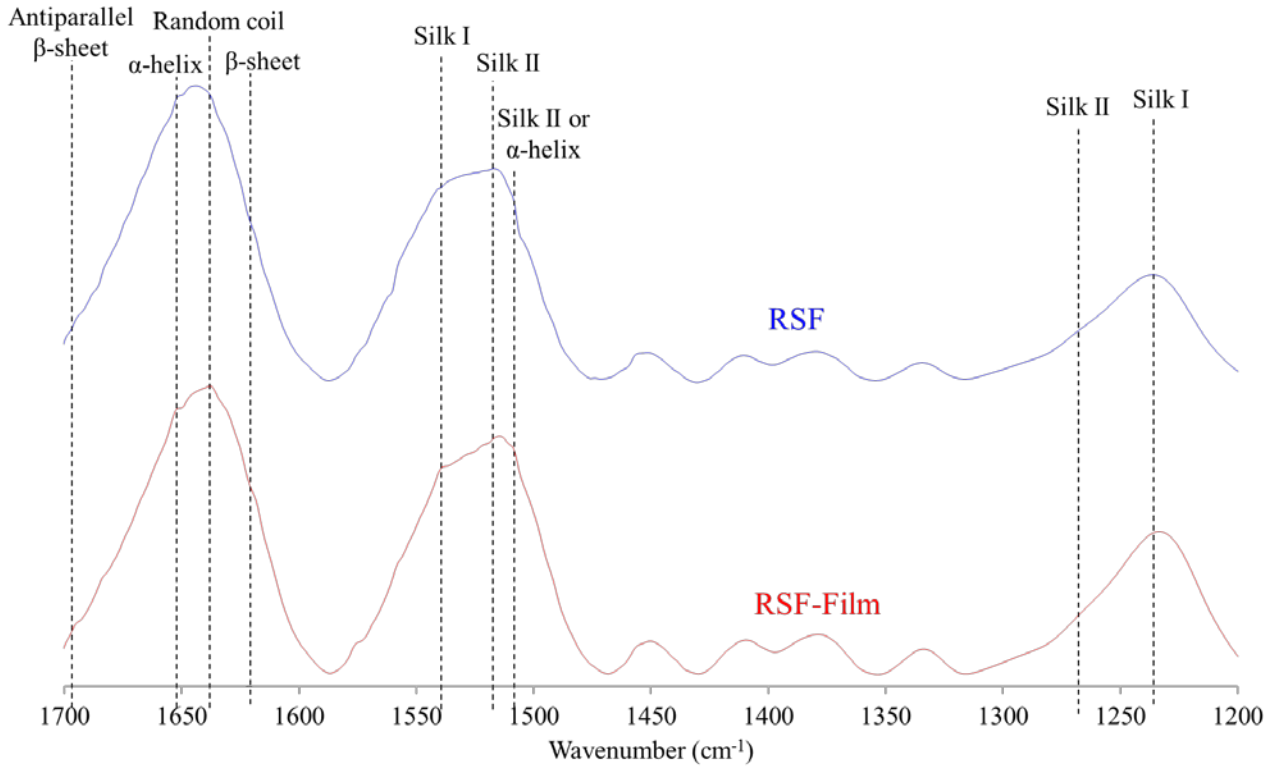


**FIGURE 3-7.** Scope of the FTIR spectrum within the region for amide I, II, and III, for the Electrospun RSF (RSF) and RSF in film (RSF-Film).

The main peaks in the amide I region for the RSF film occurred in the vibration frequency of randomly coiled structures near 1645 $cm^{-1}$. Whereas, for the electrospun RSF, the main peak shifted leftwards to a position between the vibrational frequency for α-helices and random coils.

The low or negligible intensity of the peak corresponding to β-sheet between 1630-1620 $cm^{-1}$, along with the absence of the peak from antiparallel β-sheet, demonstrated that both samples exhibited a predominantly silk I form, rather than water insoluble structure. Likewise, in both samples, the occurrence of a strong peak attributed to α-helices, confirmed that their crystalline structure was mainly composed on this type of structures, and not on β-sheets.

In the amide II band, in both samples, the peak assigned to silk I and silk II presented similar intensities, where the intensity of the peak from silk II was slightly higher. According to this analysis, both samples exhibited silk II structures that were not easily observed in the amine I band, however, the quantification of these structures along this band is not recommended and usually leads to biased results [208].

In contrast with the results from amide II, amide III showed that the peak assigned to silk II, localized at about 1260 $cm^{-1}$, had a very small or almost negligible intensity compared to the peak of silk I structures, positioned close to 1230 $cm^{-1}$. The analysis of this band served for the identification of the main type of structures in both samples, that showed a favorable silk I form. Additionally, it is believed that the lower intensity of the peak circa 1230 $cm^{-1}$, in the electrospun sample compared to the film, may be an indication of a higher crystallinity in the electrospun sample, in agreement with the higher stretching and shear forces experienced by the polymer during electrospinning, which might have led to more ordered structures [18], [41], [72], [81], [58]–[60].

Consequently, the evaluation of the amide I and amide III bands indicated that silk I or water soluble silk was the main type of structure in both samples. Such result, may be a consequence of the regeneration process of silk fibroin, performed to yield water soluble silk [3], [21], [2], [20], [25], [104]. In both cases, the processing technique did not result in notorious changes on the structure of RSF, as it could be expected.

Likewise, the effects from the addition of CNC in different loadings, on the chemical structure of electrospun nonwovens of RSF were evaluated. Figure 3-8 displays the infrared spectra for the electrospun nanocomposites of RSF/CNC and for oven-dried cellulose nanocrystals. Like in Figure 3-6, in this figure the bands corresponding to the main functional groups in RSF and CNC were highlighted.

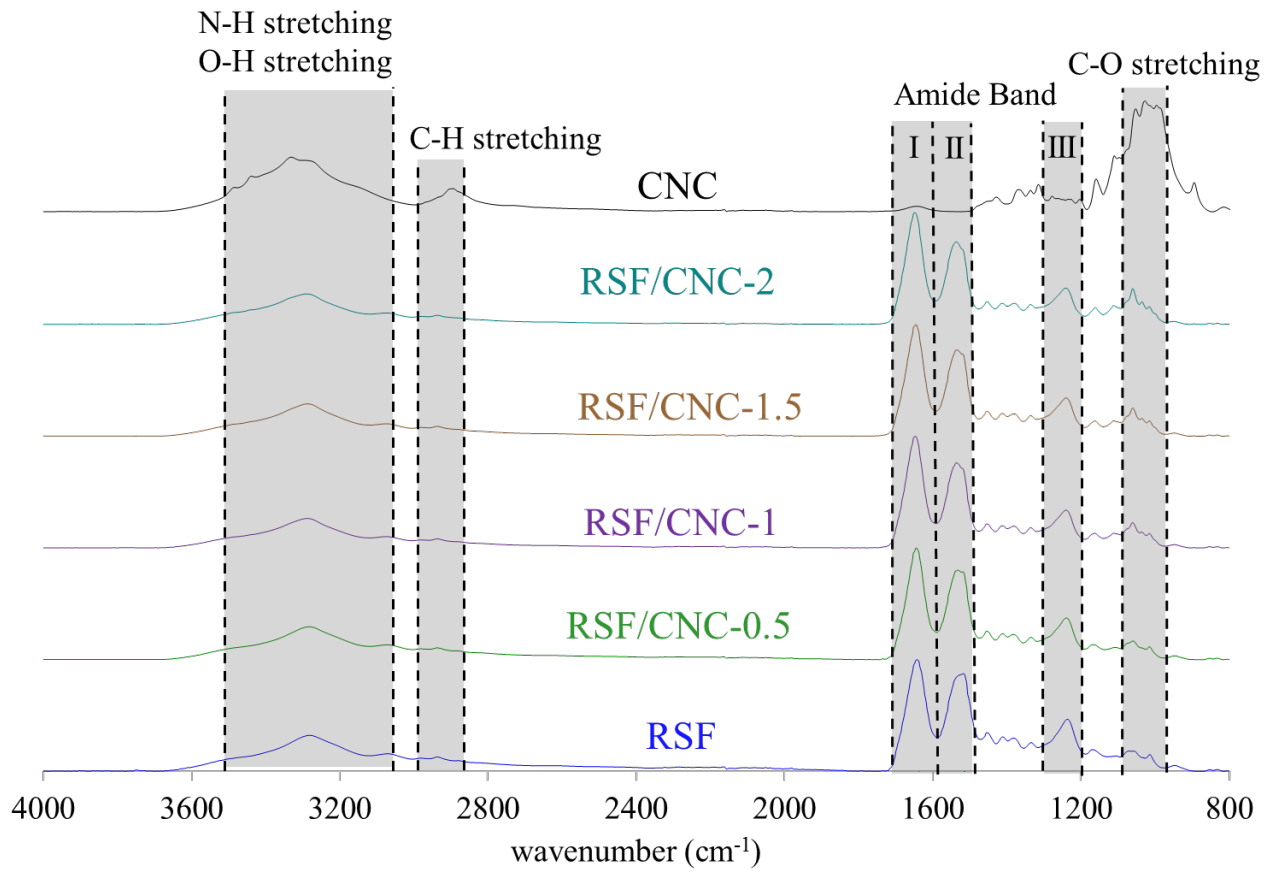


**FIGURE 3-8.** FTIR spectra for cellulose nanocrystals (CNC), the electrospun nonwoven of RSF (RSF), and the electrospun nanocomposites of RSF/CNC.

In the IR spectrum of CNC, characteristic vibrational modes for O-H stretching, C-H stretching, O-H bending, and C-O stretching, were resolved. The band for O-H stretching from the hydroxyl groups was identified as a medium intensity broad peak, centered circa 3410 $cm^{-1}$. The peak from the symmetric C-H stretching could be observed as low intensity peaks at around 2900 $cm^{-1}$. A peak close to 1640 $cm^{-1}$ was attributed to moisture absorbed by the sample, where the low intensity of this peak served as an indication of the low moisture content. A low intensity peak with a vibrational frequency near 1300 $cm^{-1}$ was assigned to the contributions from O-H bending. Finally, a strong intensity and broadly scattered peak between 1160-1030 $cm^{-1}$, resulted from the stretching of C-O bond [216]–[221].

For the spectra of the RSF/CNC electrospun nanocomposites, the low quantity of CNC and the superposition of the characteristic bands or peaks for RSF and CNC made the contributions of CNC almost negligible throughout most of the vibration modes, with the exception of the peak

from C-O stretching, which became more prominent in accordance with the increase in CNC content. The former could be observed in more detail in Figure 3-9, which shows the scope of the IR spectra in Figure 3-8 in the region between 1700 $cm^{-1}$ and 900 $cm^{-1}$.

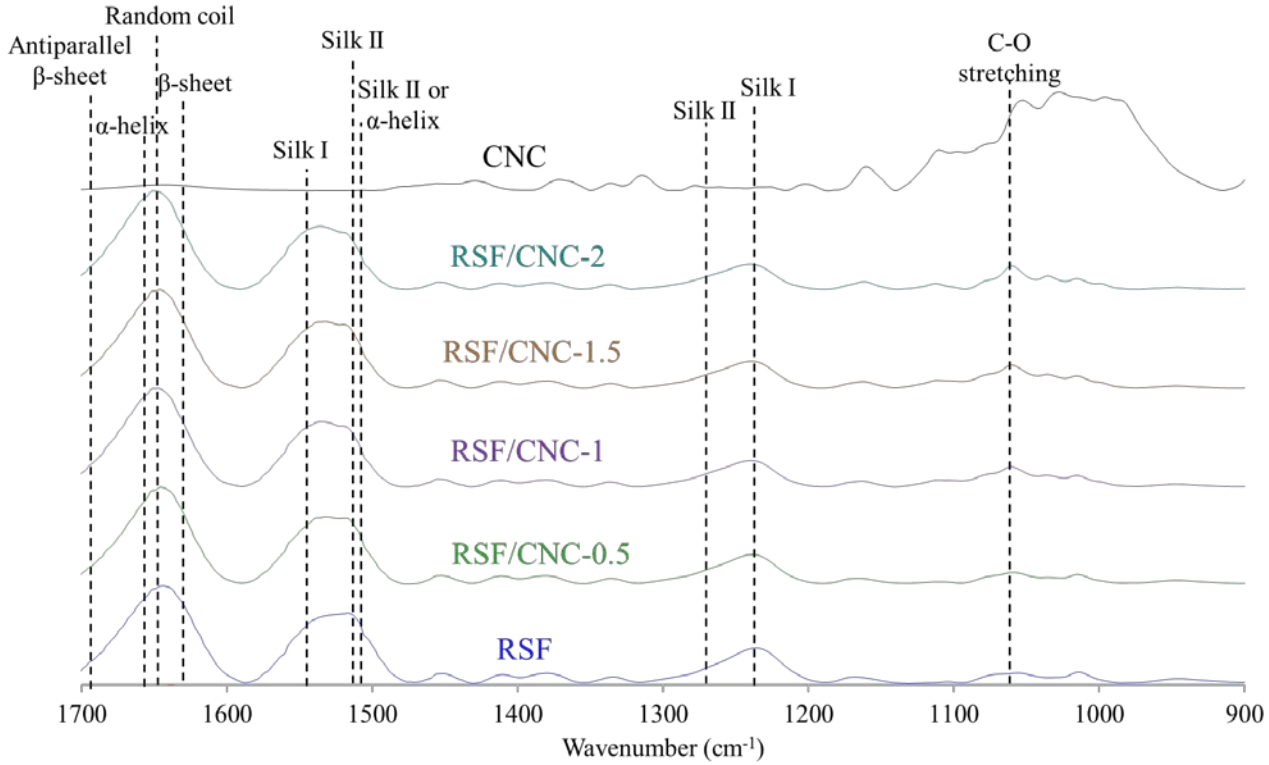


**FIGURE 3-9.** Scope of the IR spectra between 1700-900 $cm^{-1}$, for cellulose nanocrystals (CNC), the electrospun nonwoven of RSF (RSF), and the electrospun nanocomposites of RSF/CNC.

In the region of the amide band corresponding to amide I, II and III, no vibrational modes from the spectrum of CNC overlapped with the vibrations of the main functional groups from RSF, therefore, the analysis of the structure of RSF along this region was accurately performed for the RSF/CNC electrospun nanocomposites without the risk of biased results. By exploring these regions to find potential variations in the type of structure in RSF in response to the increasing loading of CNC, no relevant changes in the intensity of the peaks, nor in their position could be identified. Apparently, this initial glance indicated that the addition of CNC did not generate changes in RSF structure. However, the occurrence of a peak close to 1060 $cm^{-1}$, whose intensity increased in accordance with the higher amount of CNC in the nanocomposite, evidenced the raise

in C-O groups in the electrospun materials. Interestingly, the location of this vibrational mode shifted leftwards in the electrospun nanocomposites with respect to CNC. It might be caused due to some interactions between both components.

#### 3.4.2.3. Crystallinity

Similar as for the chemical characterization, the evaluation of crystallinity was carried out to elaborate on the effects from the process and from the addition of CNC. For both cases, X-ray diffraction was employed to establish the crystalline structure of the samples.

For the first analysis intended to explore the effects of the process, X-ray diffraction patterns for electrospun nonwovens of RSF and RSF in film were recorded and compared to evaluate differences in the crystallinity of the samples. Figure 3-10 shows the diffraction spectra for both samples, where the diffraction angles that resulted in maximum constructive interference were highlighted. It is important to note that the location of the peaks in this pattern is a function of the wavelength from the X-ray source, such that if the source of light is changed, the position of this peak will vary as well. Hence, the d-spacing provides a more accurate insight on the distances between crystalline planes and the type of structures in the sample, in comparison with the angle. This parameter was calculated using the Bragg's law, corresponding to the equation 3-1.

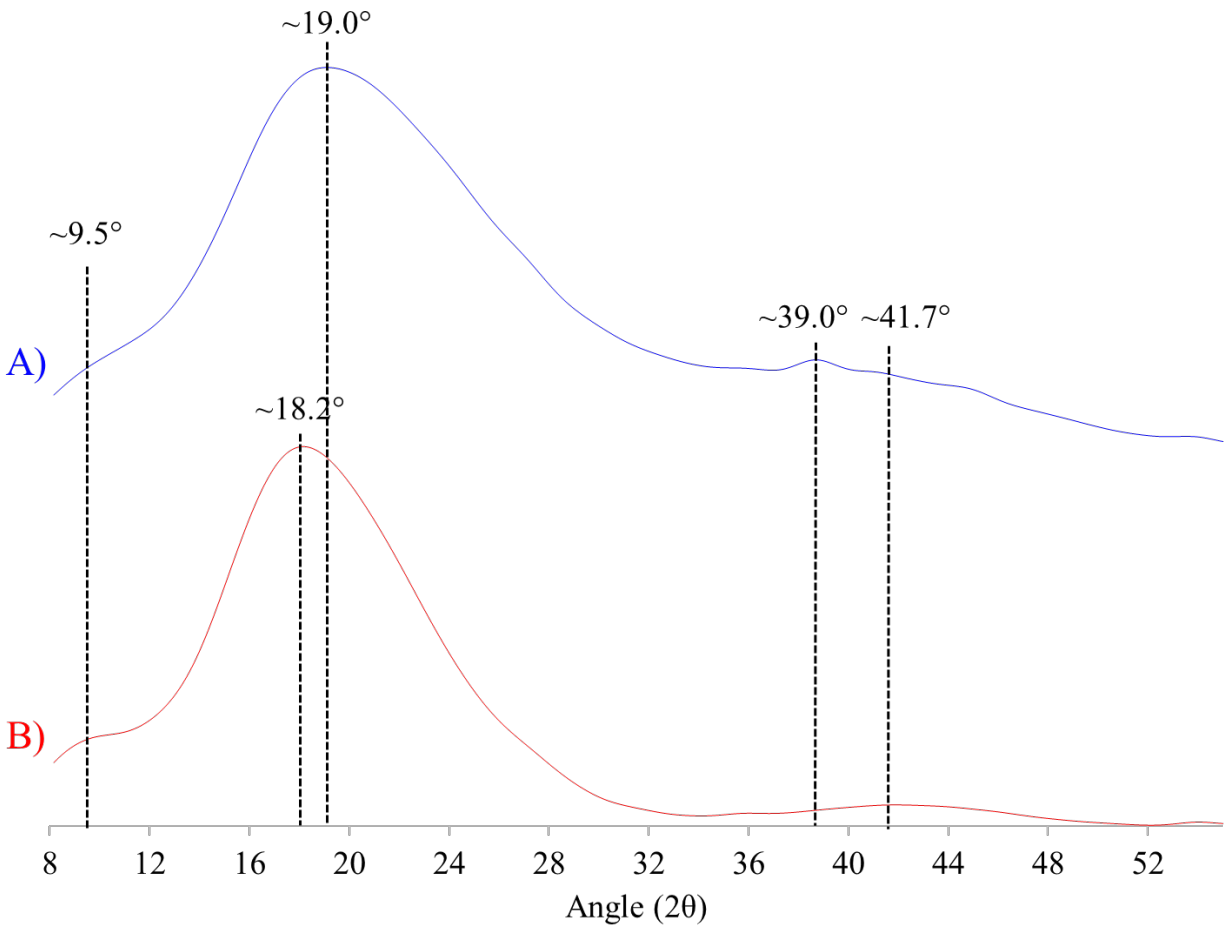


**FIGURE 3-10.** XRD pattern of A) electrospun RSF; and B) RSF film.

Therefore, by converting the main diffraction angles of the RSF film to d-spacing, using the equation 3-2, the corresponding distances between crystalline planes were found to be 0.901nm, 0.489 nm, and 0.216 nm, which were associated with the peaks at 9.8°, 18.1°, and 41.7°, respectively. Likewise, the three associated d-spacing for the electrospun RSF were 0.929 nm, 0.464 nm, and 0.233 nm, resulting in peaks located at 9.5°, 19.1°, and 38.7°. The monoclinic unit cell of antiparallel β-sheets of silk fibroin shows crystalline planes with d-spacing close to 0.92 nm, 0.69 nm, and 0.47 nm. The first plane corresponds to the distance between stacked β-sheets, whereas the other two are related to the distances between interacting alanine-alanine and glycine-glycine residues in neighboring chains, which are the intermolecular distances between residues in polypeptides strands [180], [12], [130], [222].

Both samples exhibited two out of three similar d-spacing characteristics for SF β-sheets while the additional d-spacing circa 0.22 nm has been associated with the reflection of the meridian of the forth layer of the sheets on the crystalline plane (004) or with disturbance in the main backbone of the protein created by periodic substitutions of alanine or glycine by serine. The last results are in accord with previous reports for the crystalline structure of precipitated crystals from a RSF dissolved in LiBr [223].

Interestingly, the lower value of the first reflection at 0.92 nm is associated with the formation of parallel β-sheets, whereas the increase in this value is clear evidence of antiparallel β-sheets or water-insoluble silk [12]. Despite that the shorter distance between sheets may be interpreted as an indication of a more closely stacked structure, the direction of the pendant groups in the parallel arrangement leads to a lower level of intermolecular interactions, which ultimately makes this type of structure weaker in terms of mechanical strength, as well as in thermal and chemical resistance. In contrast, reductions in the intramolecular distances (d-spacing near 0.69 nm and 0.47 nm) indicate a more tightly packed and stable arrangement of the polypeptide chains in strands, as the electrospun sample exhibited. It is important to mention that this fact applies to parallel and antiparallel β-sheets, as well as to α-helices; thus, this condition did not help to discern the presence of silk I or silk II [12], [117]. Figure 3-11 sketches the differences between the bonding patterns from antiparallel and parallel arrangements for a protein built up on polyglycine-Alanine peptides.

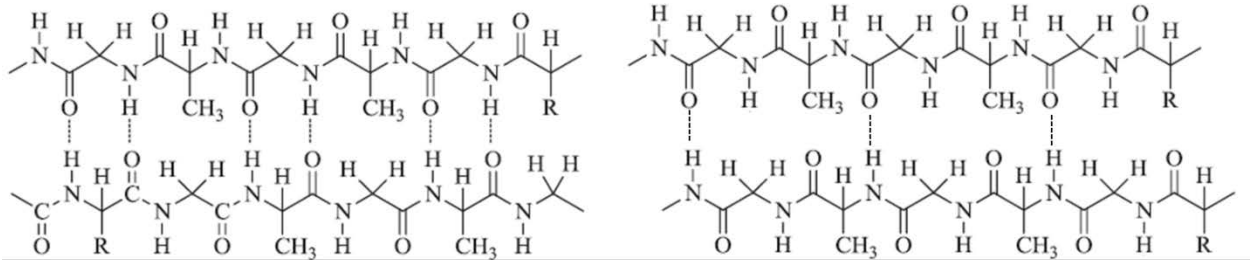


**FIGURE 3- 11.** Intermolecular bonding patterns for antiparallel and parallel arrangements of silk fibroin. The dashed lines indicate O-H bonds between chains. Adapted from [28]. Copyright Elsevier Ltda. 2013.

Additionally, in order to determine the crystallinity of the sample, calculated as the relationship between the sum of the peak area(s) associated with silk type II, divided by the total area of the spectrum, deconvolution of the diffraction patterns was performed. Accordingly, Figure 3-11 shows the peaks obtained from the deconvolution for the diffraction pattern of the electrospun RSF and RSF film. From this procedure, four characteristic peaks in spectrum of both samples were resolved, rather than just three peaks as shown in Figure 3-10. For the electrospun RSF, the main reflection event was separated into two peaks located at 17.63° and 22.25°, instead of a single peak at 19.10°. Whereas, for the RSF film, the principal peak in the spectra was divided in two peaks at 17.55° and 21.05°, rather than a peak at 18.1°. In this order, the new corresponding d-spacing and area of the peaks from the deconvolution are shown in Table 3-4.

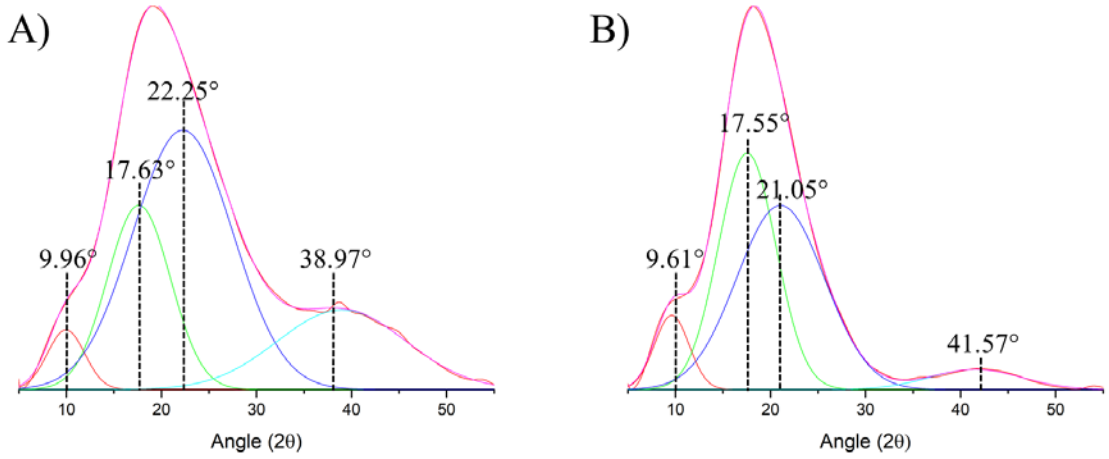


**FIGURE 3-12.** Deconvolution of the diffraction pattern for: A) Electrospun RSF and B) RSF film.

**TABLE 3-4.** Diffraction angle, standard deviation of the diffraction angle, associated d-spacing, peak area, and type of silk structure, resulting from the deconvolution of the diffraction pattern.

| Sample | Angle (2θ) | Standard deviation of Angle (2θ) | d-Spacing (nm) | Area | Type of silk |
|---|---|---|---|---|---|
| **RSF film** | 9.61 | 0.02 | 0.92 | 0.89 | II |
| | 17.55 | 0.02 | 0.50 | 4.70 | I |
| | 21.06 | 0.41 | 0.42 | 5.56 | II |
| | 41.57 | 0.05 | 0.22 | 0.65 | I |
| **Electrospun RSF** | 9.96 | 0.01 | 0.89 | 0.77 | II |
| | 17.63 | 0.01 | 0.50 | 3.99 | I |
| | 22.25 | 0.20 | 0.40 | 8.92 | II |
| | 38.97 | 0.05 | 0.23 | 3.54 | I |

In contrast to the former results, after deconvolution, the space between sheets decreased in the case of the electrospun RSF and slightly increased for the RSF film, which might be an indication of a favorable parallel arrangement for the electrospun sample. Notwithstanding, a reduction in the d-spacing, assigned to the breadth of glycine-glycine residues between chains, denotes the formation of more compact crystals. Furthermore, the new peak position at about 17.4° with a corresponding d-spacing of ~0.51 nm has been attributed to the inter-strand spacing produced by alanine-alanine interactions in water-soluble silk (silk I) [12], [212], [222]. Also, the reflections at 41.57° and 38.97° in the RSF film and electrospun RSF, respectively, are clear evidence of dislocations along the protein backbone caused by the replacement of glycine or alanine by a serine, which induces the formation of amorphous domains or water-soluble silk (silk I) [206], [12], [212].

Consequently, after assigning each peak to silk type I or II, the crystallinity for the RSF film and for the electrospun RSF were 54.70% and 56.25%, respectively. The small difference between the percentage of water-insoluble structures for both samples reflects that the electrospinning process by itself could not induce the formation of silk II or overcome the changes in the secondary structure of SF after the regeneration process. The low crystallinity of the electrospun sample could be explained by the weak stretching forces experienced by RSF during electrospinning, which could have prevented the orientational effects and alignment of polymer chains, in addition to a poor exclusion of the solvent in between the protein molecules, which ultimately hindered the formation of silk II structures. Likewise, the poor solvent evaporation,

along with the favorable occurrence of water soluble silk, may have led to higher mobility of the protein molecules in contact with the remaining solvent, which could have increased the time for the relaxation of the polymer and limited the formation of ordered structures [185], [192]–[194], [204], [186], [21], [201], [26].

Consequently, post treatment strategies to induce the crystallization are required to produce more stable and stronger RSF electrospun materials [29], [21], [20], [130], [117], [17], [26], [131]. Accordingly, as a second approach, the influence of CNC in the crystallinity of the electrospun nanocomposites was evaluated using the same methodology employed to evaluate the consequences of the electrospinning process on the crystallinity. Figure 3-12 displays the diffraction patters for the RSF/CNC electrospun composites, as well as the diffraction spectrum of CNC. Additionally, Table 3-5 presents the respective main diffraction peaks and their appointed d-spacing for the RSF/CNC electrospun nanocomposites and pure CNC.

The main diffraction peak for CNC occurred at 22.7°, which is related to the crystalline plane (200) from monoclinic unit cell of cellulose Iβ, with a corresponding d-spacing of 0.39 nm. Whereas, two other diffraction peaks were detected at 14.8° and 11.4°; the former has been appointed as the crystalline plane (110) from monoclinic unit cell of cellulose Iβ, whose d-spacing is 0.60 nm, and the latter has been appointed as a typical peak for cellulose type II with a d-spacing of 0.77 nm [29], [216], [224]–[226].

**TABLE 3-5.** Main diffraction peaks and their corresponding d-spacing for the RSF/CNC electrospun nanocomposites, and for CNC.

| Sample | RSF/CNC 20/0 (A) | RSF/CNC 19.5/0.5 (B) | RSF/CNC 19/1 (C) | RSF/CNC 18.5/1.5 (D) | RSF/CNC 18/2 (E) | CNC (F) |
|---|---|---|---|---|---|---|
| **Angle (2θ)** | 9.5 | 9.3 | 9.5 | 16.0 | 16.0 | 11.4 |
| | 18.2 | - | 20.0 | 20.0 | 20.0 | 14.8 |
| | - | 21.9 | 21.5 | 22.0 | 22.0 | 22.7 |
| | 38.7 | 39.0 | 39.0 | 39.0 | 39.0 | - |
| **d-Spacing (nm)** | 0.93 | 0.95 | 0.93 | 0.55 | 0.55 | 0.77 |
| | 0.46 | - | 0.44 | 0.44 | 0.44 | 0.60 |
| | - | 0.40 | 0.41 | 0.40 | 0.40 | 0.39 |
| | 0.23 | 0.23 | 0.23 | 0.23 | 0.23 | - |

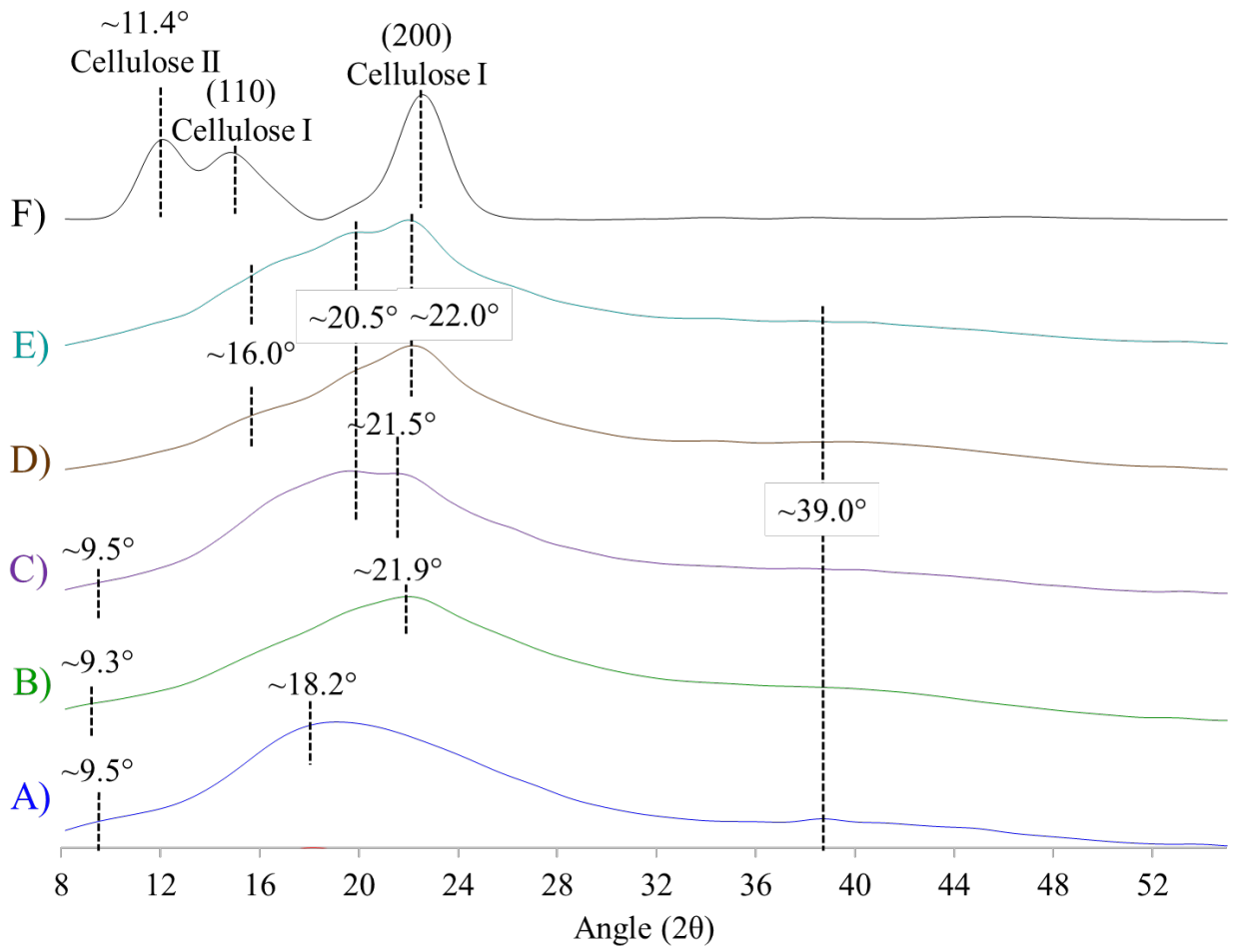


**FIGURE 3-13.** XRD diffraction pattern for the electrospun nanocomposites with RSF/CNC weight percentages in solution of: A) 20/0; B) 19.5/0.5; C) 19/1; D) 18.5/1.5; E) 18/2. And F) for pure CNC.

For the RSF/CNC electrospun nanocomposites, the addition of CNC produced a shift of the main diffraction peak from 18.2° for the nonwoven without CNC to almost 22° in the RSF/CNC nanocomposites. This variation in silk structure has been related to a transition from silk II to silk I [147], [222]. Nevertheless, the proximity of this peak to the main one from CNC results in some uncertainties about this transition, as it could have resulted from the presence of cellulose I in the composites. Additionally, when the CNC loading was above 1.5% w/w in solution (corresponding to a 7.5% in the solid), the peak at around 9.5° completely disappeared; instead, a peak at about 16.0° was resolved. In this case, the peak at 9.5° is a characteristic peak of silk II, and the one at 16.0° has been allocated to silk I. Thus, this might support the assumption

that the addition of CNC leads to a reduction in the amount of water insoluble form of the protein. Finally, when the amount of CNC was above the experimental percolation threshold, a new peak appeared close to 20.5°, assigned to the presence of silk type II [180], [147], [222].

In order to get an accurate assessment of the crystallinity for the nanocomposites, a similar analysis to the one carried out to compare this property in the electrospun RSF and RSF film was conducted for the electrospun nonwovens. Figure 3-13 shows the deconvolution of the diffraction spectrum for these samples, and Table 3-6 displays the location of the main diffraction peaks after deconvolution, with their respective standard error, d-spacing, peak area, and type of silk structure.

The crystallinity of each sample was calculated as the ratio between the sum of the peak area related to silk type II and CNC, divided by the total area of the diffraction spectrum [36], [104]. The crystallinity of the samples was 56.25%, 57.52%, 68.05%, 69.91%, and 77.84%, respectively, for the electrospun nanocomposites with a RSF/CNC weight percentage in the solution of 20/0, 19.5/0.5, 19/1, 18.5/1.5, and 18/2. It was observed that the percentage of crystallinity increased with the amount of CNC added to the RSF. This variation, was attributed to increased amount of silk II structures, and to the formation of a crystalline networks of CNC in silk. Interestingly, for the materials with CNC concentrations above the experimental percolation threshold, the crystallinity of the samples sharply increased about 10% when the CNC loading was increased from 0.5% to 1% w/w. This result could have been generated by the formation of a mechanical percolation network of CNCs in the polymer matrix that enlarged the amount of ordered or crystalline structures in the material.

The rise in crystallinity and/or the proportion of silk II structures is in accordance with previous investigations where silk fibroin matrixes were reinforced or mixed with other types of cellulosic materials such as regenerated cellulose pulp, bacterial cellulose nanocrystals, mulberry CNC, carboxymethyl cellulose, and microcrystalline cellulose [36], [214], [20], [104], [5], [9], [22], [35], [135], [227].

**TABLE 3-6.** Diffraction angle, standard deviation of the diffraction angle (Std of angle), associated d-spacing, peak area, and type of silk structure, resulting from the deconvolution of the diffraction pattern for the electrospun nanocomposites.

| Sample | Angle (2θ) | Std of Angle (2θ) | d-Spacing (nm) | Area | Type of structure |
|---|---|---|---|---|---|
| RSF/CNC 20/0 | 9.96 | 0.01 | 0.89 | 0.77 | Silk II |
| | 17.63 | 0.01 | 0.50 | 3.99 | Silk I |
| | 22.25 | 0.20 | 0.40 | 8.92 | Silk II |
| | 38.97 | 0.05 | 0.23 | 3.54 | Silk I |
| RSF/CNC 19.5/0.5 | 9.65 | 0.02 | 0.92 | 0.33 | Silk II |
| | 16.88 | 0.18 | 0.52 | 2.82 | Silk I |
| | 21.89 | 0.02 | 0.41 | 1.00 | Silk II |
| | 22.99 | 0.28 | 0.39 | 8.89 | CNC |
| | 38.03 | 0.06 | 0.24 | 4.73 | Silk I |
| RSF/CNC 19/1 | 10.94 | 0.12 | 0.81 | 0.30 | Silk II |
| | 15.53 | 0.87 | 0.57 | 1.57 | Silk I |
| | 19.46 | 0.79 | 0.46 | 4.67 | Silk II |
| | 22.22 | 0.03 | 0.40 | 0.11 | CNC |
| | 23.95 | 3.08 | 0.37 | 4.91 | Silk II |
| | 34.84 | 1.38 | 0.26 | 2.28 | Silk I |
| | 43.14 | 1.51 | 0.21 | 0.84 | Silk I |
| RSF/CNC 18.5/1.5 | 15.97 | 0.04 | 0.55 | 0.96 | Silk I |
| | 21.05 | 0.02 | 0.41 | 1.78 | Silk II |
| | 22.56 | 0.04 | 0.39 | 8.00 | CNC |
| | 33.98 | 0.04 | 0.26 | 0.10 | Silk I |
| | 39.84 | 0.03 | 0.23 | 3.15 | Silk I |
| RSF/CNC 18/2 | 17.90 | 0.24 | 0.49 | 4.05 | Silk II |
| | 21.41 | 0.04 | 0.41 | 0.64 | Silk II |
| | 22.51 | 0.70 | 0.40 | 6.14 | CNC |
| | 37.81 | 0.08 | 0.24 | 3.08 | Silk I |

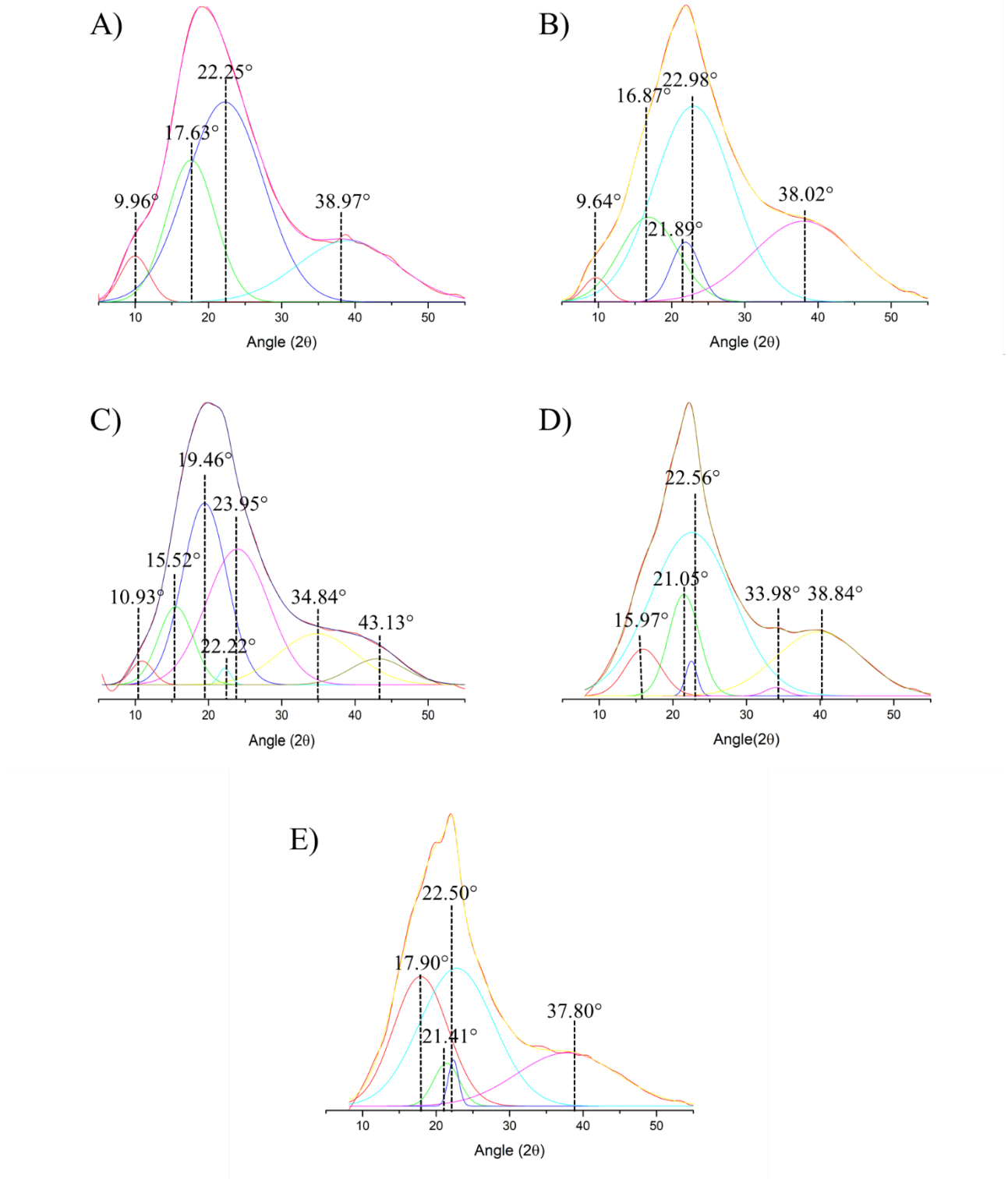


**FIGURE 3-14.** Deconvolution of the diffraction pattern for the electrospun nanocomposites with RSF/CNC weight percentages of: A) 20/0; B) 19.5/0.5; C) 19/1; D) 18.5/1.5; E) 18/2.

### 3.4.2.4. Thermal stability

The analysis of the thermal stability was performed by analyzing the effects of the process and the addition of CNC over this property for the produced materials made up of RSF. This property was evaluated through thermogravimetric analysis (TGA).

For the evaluation of the effects from the process, the thermal decomposition of RSF in film and electrospun nonwovens of RSF were recorded and plotted in Figure 3-14. Additionally, the first derivatives of these results are shown in Figure 3-15, and the summary of the thermal properties are displayed in Table 3-7, where the values for the temperature for the onset of degradation ($T_{onset}$) and the temperature of maximum decomposition rate ($T_{max}$) can be observed.

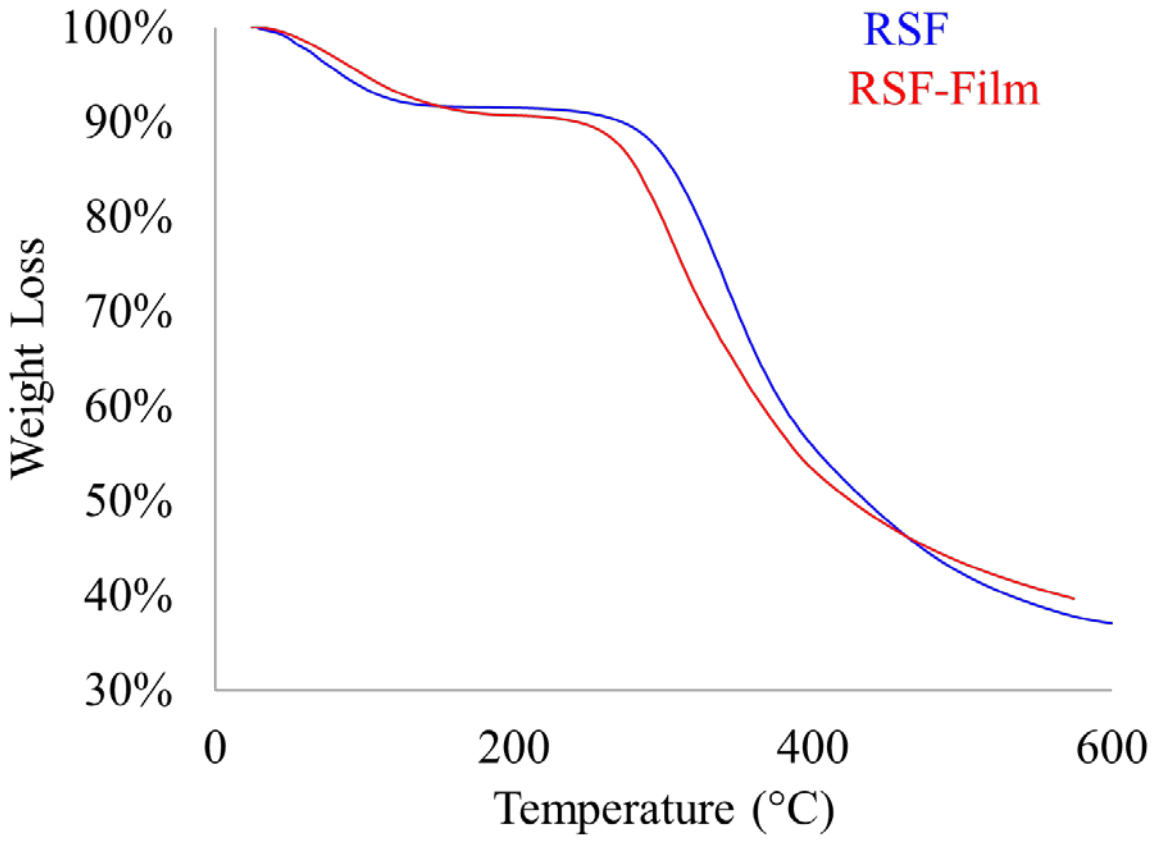


**FIGURE 3-15.** Thermogravimetric analysis for the electrospun nonwoven of RSF (RSF) and RSF in film (RSF-Film).

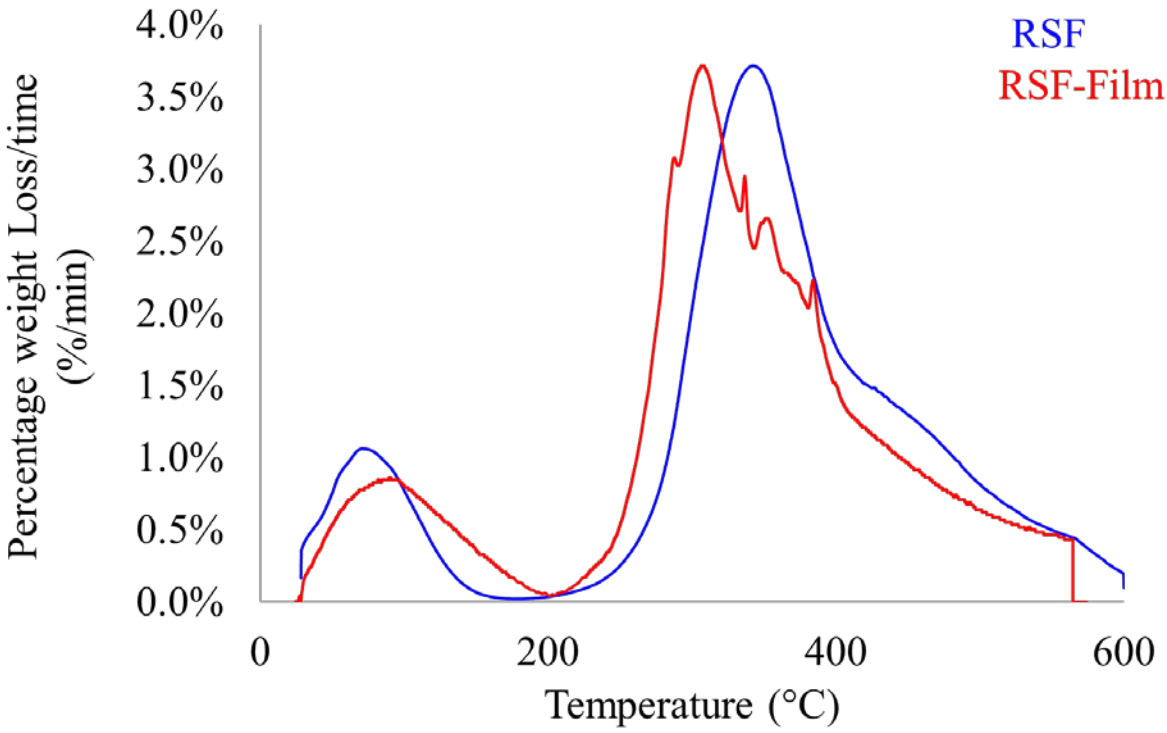


**FIGURE 3-16.** First derivate of the thermogravimetric analysis for the electrospun nonwoven of RSF (RSF) and RSF in film (RSF-Film).

**TABLE 3-7.** Values of the temperature for the onset of degradation ($T_{onset}$) and temperature of maximum degradation rate ($T_{max}$) for electrospun nonwovens of RSF (RSF) and RSF in film (RSF-Film).

| Sample | $T_{max}$ (°C) | $T_{onset}$ (°C) |
|---|---|---|
| RSF | 342.39 | 295.64 |
| RSF-Film | 306.58 | 271.80 |

According to the results from Figure 3-14, the thermal stability of the regenerated silk fibroin increased when the polymer was electrospun. From Table 3-7, it could be observed that the differences in $T_{max}$ and $T_{onset}$ for between both samples were 35.81 °C and 23.84 °C, respectively. This improvement in the thermal resistance might be attributed to the alignment effects of the electrospinning process, which may have led to better distribution of the crystalline portion along

the fiber [18], [41], [26]. In addition, the analysis of crystallinity showed that the electrospun sample presented more tightly packed crystals that could resist higher thermal stresses.

Given that, both samples were kept under the same conditions before testing, the lower mass loss at the end of the first thermal event, related to the evaporation of water, could be evidence of a higher retention of water in the electrospun material at higher temperatures. The latter was probably produced by the highly porous structure, in the electrospun sample, which may have allowed a higher water retention inside the porous structure, and consequently, to reduced mass loss during this event. Finally, the water retained inside the pores could have contributed to delay the onset of thermal degradation for RSF.

Finally, the high $T_{max}$ for the electrospun sample may be an advantage in potential applications for this material in fields like catalysis, biomedicine, food packing, and immobilization of compounds [18], [41], [52], [57], [102], [103]. The enhancement of this property was indicative that other characteristics of the material could be potentially affected by the process, but they were not properly identified through the characterization techniques employed in this work.

Once the effects from the process on the thermal stability of RSF were identified, an analysis of the effect of adding CNC to the polymer matrix was carried out. At first, the $T_{onset}$ and $T_{max}$ for pure CNC, and for the electrospun nanocomposites of RSF/CNC were measured. These results are shown in Figure 3-16, whereas, the first derivative for these thermograms are displayed in Figure 3-17. Also, Table 3-8 summarizes the values for the $T_{onset}$ and $T_{max}$ for each sample.

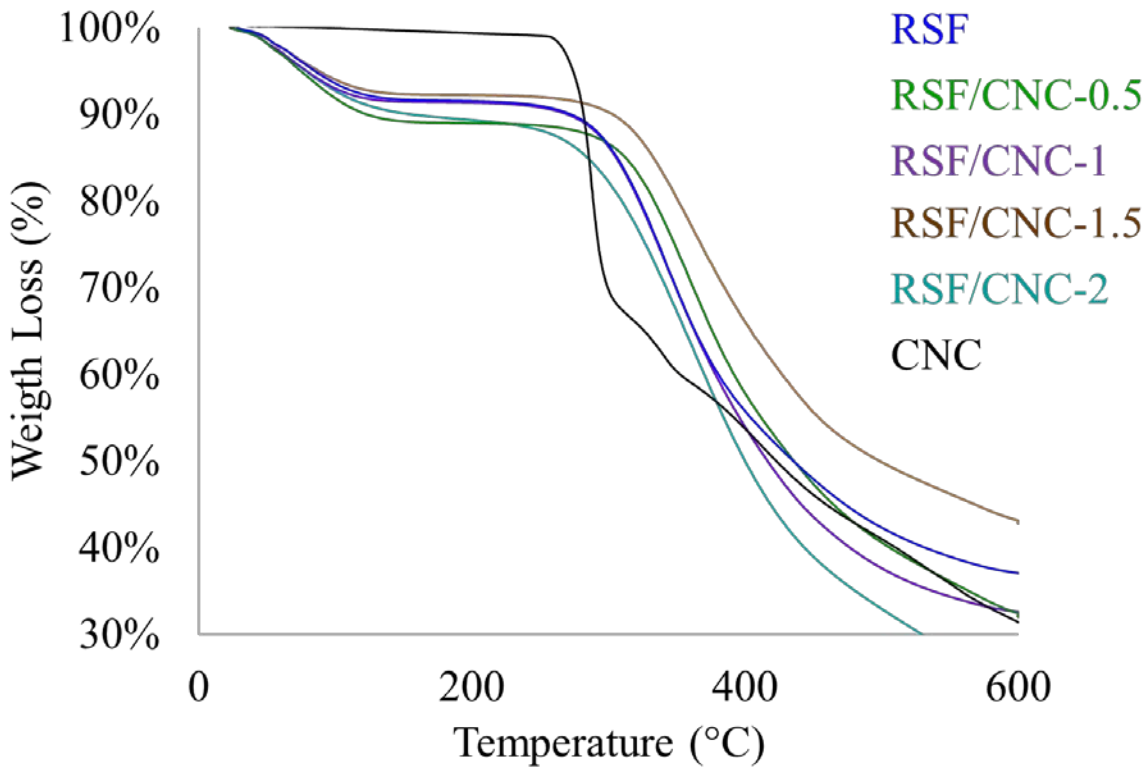


**FIGURE 3-17.** Thermogravimetric analysis for pure cellulose nanocrystals (CNC), electrospun nonwoven of RSF, and the electrospun nanocomposites of RSF/CNC.

**TABLE 3-8**.Values of the temperature for the onset of degradation ($T_{onset}$) and temperature of maximum degradation rate ($T_{max}$) for pure cellulose nanocrystals (CNC), the electrospun nonwoven of RSF, and the electrospun nanocomposites of RSF/CNC.

| Sample | $T_{max}$ (°C) | $T_{onset}$ (°C) |
|---|---|---|
| RSF/CNC 20/0 | 342.4 | 295.6 |
| RSF/CNC 19.5/0.5 | 360.5 | 304.3 |
| RSF/CNC 19/1 | 358.3 | 299.4 |
| RSF/CNC 18.5/1.5 | 360.2 | 303.8 |
| RSF/CNC 18/2 | 353.1 | 292.8 |
| CNC | 288.0 | 274.5 |

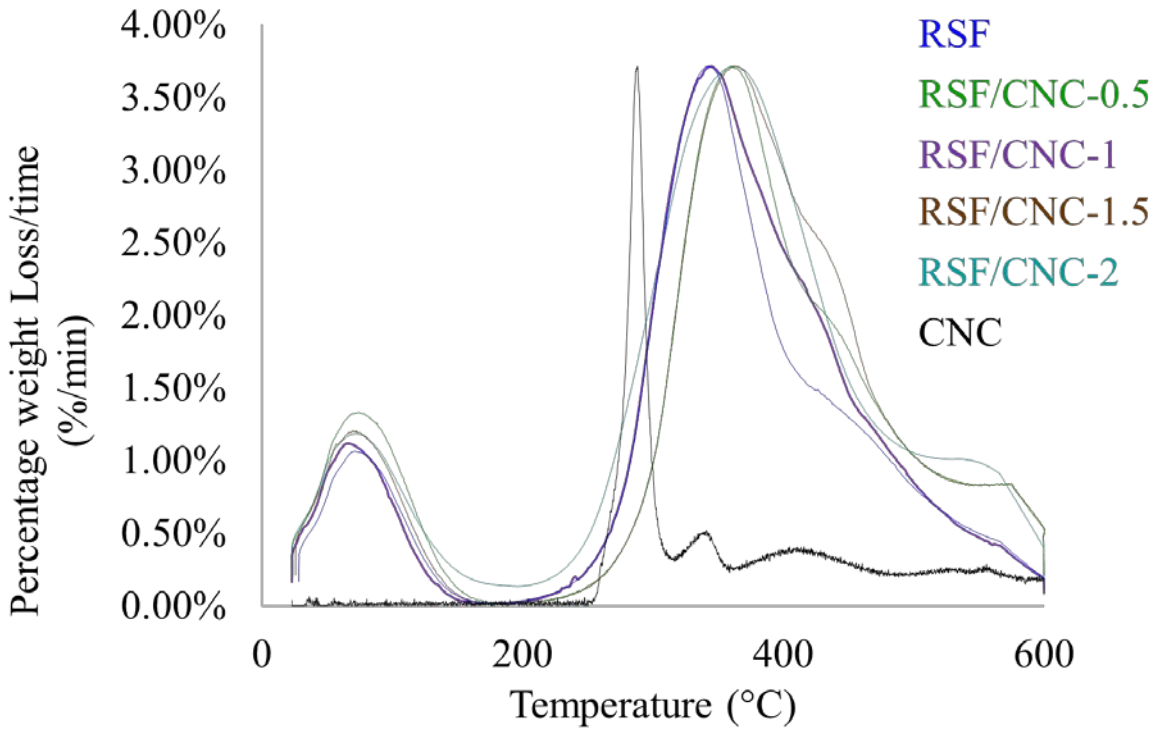


**FIGURE 3- 18.** First derivative of the thermogravimetric analysis for pure cellulose nanocrystals (CNC), electrospun nonwoven of RSF (RSF), and the electrospun nanocomposites of RSF/CNC.

From Table 3-8, it could be observed that the thermal degradation of the electrospun nanocomposites was enhanced when CNC was added to the polymer matrix, up to a CNC concentration of 1.5% w/w. Addition of CNC above this value of concentration produced a reduction in $T_{max}$. The best thermal performance was obtained when only 0.5% w/w of CNC was added, however, the thermal stability of this composite was not much different than those of the nanocomposites produced using CNC loadings of 1% and 1.5%. Also, all the electrospun nanocomposites regardless the concentration of CNC, exhibited more elevated $T_{max}$ than the electrospun nonwoven of RSF, but, the latter presented a superior $T_{onset}$ compared to the electrospun nanocomposite with a concentration of CNC of 2% w/w.

In contrast to the effects in crystallinity, when the amount of CNC was above the experimental percolation threshold, it seemed that the excess of CNC decreased the thermal stability of the electrospun nanocomposites. This phenomenon probably occurred due to a better thermal conductivity for the electrospun nanocomposites with concentrations of filler above the percolation threshold, which promoted the formation of a continuous and more complex network

of crystals, that enabled a faster heat transference inside the polymer matrix, and reduced the temperature needed to degrade RSF.

On the other hand, CNC by itself showed a lower thermal stability compared to the RSF. Nevertheless, when both components were blended, a raise in the thermal properties was observed. Ideally, it could be the result of some type of interaction between CNC and RSF that enlarged the thermal stability of RSF. This statement is supported by the occurrence of a new peak in the electrospun nanocomposites when compared to the electrospun nonwoven of RSF.

Finally, there is a direct relationship between fiber diameter and the enhancement of thermal stability; the smaller the size, the higher the thermal resistance of the electrospun nonwoven. This result was in contrast to some investigations that report a detriment in thermal properties of polymers upon reduction in diameter, as consequence of the higher in surface area [228]. However, smaller diameters could drive to more intricate structures that enabled a higher water and gas adsorption, which could restrain the thermal degradation.

#### 3.4.2.5. Mechanical properties

The analysis of the mechanical properties for the RSF/CNC composites was performed in films instead of in electrospun materials due to the brittleness and softness of the nonwovens, which made complicated the process of removing the fibers form the collected without affecting their integrity. Such that, films of RSF/CNC were produced following the protocol reported by Asakura, *et al*. [206], and using similar solutions as those employed for electrospinning. Figure 3-18, shows the stress-strain curves for each film by duplicate.

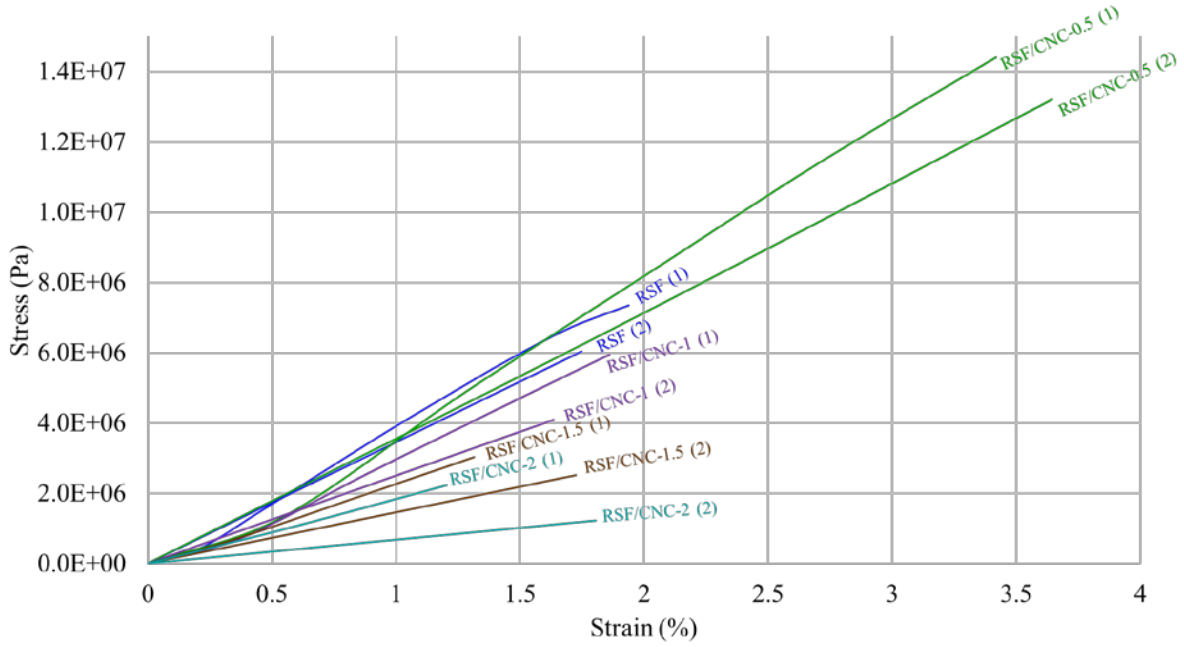


**FIGURE 3- 19.** Stress strain curves for the film of regenerated silk fibroin with loadings of cellulose nanocrystals of: RSF) 0% w/w, RSF/CNC-0.5) 0.5% w/w, RSF/CNC-1) 1% w/w, RSF/CNC-1.5) 1.5% w/w, RSF/CNC-2) 2% w/w.

As it could be observed, the matrix of regenerated silk fibroin (RSF) experienced a material failure at very low strain, characteristic of brittle materials [201]. According to the data, it suggested that the material became more fragile in response to the increase in CNC content for concentrations from 1% to 2% w/w. Under this conditions, apparently, RSF was less stretchable, yielding strains at break in orders of less than 2%, which has been previously reported in other polymeric matrices such as atactic polystyrene, polycaprolactone, and polyurethane [27], [229], [175], [230]. It is believed that the detrimental in this property could be caused by the formations of a rigid continuous network of filler, in concentrations above the percolation threshold, which reduce the capacity of the material to be elongated without break, leading to higher stiffness [167]. This behavior has been observed for other composites of silk fibroin blended with cellulose nanocrystals. Lui and Yao [4], fabricated wet-spun fibers of silk fibroin reinforced with CNC by adding the filler to aqueous solutions of the protein, and then concentrating the solution via reverse dialysis. For these materials, the best strain at breaking was obtained for the composites with lower content of CNC; but, in contrast with the current work, the yield stress was enhanced with the

addition of the filler. Similar properties were observed in the work developed by Rongji, Yanhong and Zhu [135], where films of silk fibroin were reinforced with cellulose nanocrystals, and polyethylene glycol was employed as plasticizer; and in the research carried out by Huang, Liu, and Yao [20], for electrospun nonwovens of silk fibroin/cellulose nanocrystals made up by dissolving SF in formic acid, and then, dispersing CNC in the solutions.

Table 3-9 presents the values of the average Young's modulus, yield stress, and strain at break for the films of RSF/CNC prepared with different concentrations of CNC. It was perceived that the composite film of RSF/CNC with concentration of filler of 0.5% w/w, corresponding to a concentration of CNC below the percolation threshold, exhibited the highest Young's modulus, elongation at break, and yield stress among the samples. Moreover, for the composites with concentration of CNC above the experimental percolation threshold, it was not evidence of the variation of the mechanical properties among them.

**TABLE 3- 9.** Young's modulus, yield stress, and strain at break for the composites of RSF/CNC in film

| sample | Young's modulus ($1x10^7$ Pa) | yield stress ($1x10^5$ Pa) | strain at break (%) |
|---|---|---|---|
| RSF | 37.0 ± 2.4 | 66.9 ± 6.5 | 1.8 ± 0.1 |
| RSF/CNC-0.5 | 39.2 ± 2.9 | 138.1 ± 6.1 | 3.5 ± 0.1 |
| RSF/CNC-1 | 28.5 ± 3.5 | 50.3 ± 9.2 | 1.7 ± 0.1 |
| RSF/CNC-1.5 | 18.8 ± 4.2 | 27.7 ± 2.5 | 1.5 ± 0.2 |
| RSF/CNC-2 | 12.6 ± 5.8 | 17.3 ± 4.9 | 1.5 ± 0.3 |

The work of fracture or toughness, measured as the area under of the curve corresponding to each sample in the strain-stress plot [65], as it occurred with the thermal stability, the better performance for the samples was obtained for the composite with lower concentration of CNC. It is believed that this condition occurred due to the low concentration of filler in the polymer which led to reduced interactions filler-filler. Therefore, as less fillers are in contact, the interactions polymer-filler may be enhanced, yielding better dissipation of the mechanical and thermal stresses by CNC [172]. However, additional measurements must be performed for this to be proved.

It has been reported that the addition of crystalline fillers like cellulose nanocrystals to polymeric matrices with high crystallinity does not help to improve much the toughness of the polymer, as they probably lead to higher yield strength, but, do not contribute to the elongation, then, causing a catastrophic failure at lower deformations [201]. Likewise, it has been observed that the addition of CNC to other polymeric matrices working at temperatures below their glass transition temperature ($T_g$) has not produced changes in their mechanical performance [109], [27], [230], [231]. It is assumed that the fracture of the materials at this temperature occurs due to the breaking up of the amorphous regions due to their low mobility and mechanical resistance, which is not enhanced by the introduction of a highly crystalline filler.

In silk fibroin/cellulose nanocrystals composites, working below 178-200 °C which is assigned as the threshold when the glass transition temperature for SF occurs [16], [232], [233], the minimal or negligible enhancement of the mechanical properties when crystalline fillers are introduced may result in reduced the mobility of the amorphous portions of silk fibroin though stiffening the matrix and by the formation of interactions [36], [135].

## 3.5. Conclusions

For the different combinations of parameters tested, the best conditions to produce electrospun nonwovens of RSF were found to be at 20 cm, 20 kV, 0.1 ml/h, and a concentration of polymer of 20% w/w in solids. Lower distances or voltages led to defective fibrous structures that exhibited irregular fiber size, beads, and coalescence of fibers.

The electrospun nanocomposites of RSF/CNC showed thinner fiber diameter and more homogeneous shapes and morphologies, compared to the electrospun nonwoven of RSF. It may have occurred in response to a higher conductivity in the polymer solution imparted by the addition of CNC, which helped to the stretching of the fibers. But, interestingly when only the nanocomposites were compared, an increase in fiber diameter happened in response to higher loadings of CNC, which could have arisen from the raise in viscosity caused by CNC.

The electrospinning process by itself did not generate any perceivable change in the chemical or secondary structure, nor in the crystallinity of RSF. However, an improvement on the thermal resistance of regenerated silk fibroin was observed for the electrospun material compared to the RSF film.

The analysis of crystallinity and IR spectrum of the electrospun nonwoven of RSF and RSF in film, revealed that a large portion of the protein exhibited a silk I structure, referred as water soluble form of silk. It may be due to the regeneration process carried out to facilitate the dissolution of the protein in water.

The infrared spectra of the electrospun nanocomposites of RSF/CNC indicated that the secondary structure of the protein was unaffected by the addition of the filler. However, the occurrence of a new peak in the electrospun nanocomposites of RSF/CNC corresponding to the stretching of the C-O bond, whose intensity increased along with a higher amount of CNC, and whose position shifted leftwards respect to the position in the spectrum of pure CNC, may be an indication of interactions between both components.

The crystallinity of the electrospun nanocomposites greatly increased with the addition of CNC. This may be due to a nucleation effect of CNC over RSF, or by the formation of continuous network of cellulose nanocrystals in the polymer matrix, when the concentration of the filler was above its percolation threshold.

The thermal stability and resistance of RSF was improved by only adding a small amount of CNC until loadings up to 1.5% w/w. Above this concentration, the improvement was not representative. Interestingly, the enhancement in thermal stability went in accordance with the decrease in fiber diameter for the electrospun materials, so, the smaller the fibers, the higher the thermal resistance. Additionally, it is believed that the formation of a continuous network of filler in the polymer matrix could have increased the thermal conductivity of the samples and promoted a faster degradation.

Apparently, the mechanical properties of RSF referred to Young's modulus, yield stress, strain at break, and toughness were enhanced when cellulose nanocrystals were added up to a concentration of 0.5% w/w in the solution, probably in response to better interactions between polymer-filler. Above this loading, a detrimental in the mechanical properties could be presumably attributed to a higher stiffness and rigidity of RSF, as the formation of a network of filler could have reduced the mobility of the amorphous segments of the polymer, leading to materials failure at very low strain. Likewise, working at temperatures below the glass transition temperature could have contributed to the lower mobility as well.

## 3.6. References


[1] Y. Cao and B. Wang, “Biodegradation of silk biomaterials,” *Int. J. Mol. Sci.*, vol. 10, no. 4, pp. 1514–1524, 2009.

[2] D. N. Rockwood, R. C. Preda, T. Yücel, X. Wang, M. L. Lovett, and D. L. Kaplan, “Materials fabrication from Bombyx mori silk fibroin,” *Nat. Protoc.*, vol. 6, no. 10, pp. 1612–1631, 2011.

[3] M. P. Ho, H. Wang, and K. T. Lau, “Effect of degumming time on silkworm silk fibre for biodegradable polymer composites,” *Appl. Surf. Sci.*, vol. 258, no. 8, pp. 3948–3955, 2012.

[4] L. S. Wray *et al.*, “Effect of processing on silk-based biomaterials: Reproducibility and biocompatibility,” *J. Biomed. Mater. Res. - Part B Appl. Biomater.*, vol. 99 B, no. 1, pp. 89–101, 2011.

[5] T. Yongzhen, X. Weilin, Y. Yun, and Y. Cao, “Preparation and Characterization of Silk fibroin nanocrystals.” .

[6] S. D. Aznar-Cervantes, D. Vicente-Cervantes, L. Meseguer-Olmo, J. L. Cenis, and A. A. Lozano-Pérez, “Influence of the protocol used for fibroin extraction on the mechanical properties and fiber sizes of electrospun silk mats,” *Mater. Sci. Eng. C*, vol. 33, no. 4, pp. 1945–1950, 2013.

[7] T. Hodgkinson, Y. Chen, A. Bayat, and X.-F. Yuan, “Rheology and Electrospinning of Regenerated *Bombyx mori* Silk Fibroin Aqueous Solutions,” *Biomacromolecules*, vol. 15, no. 4, pp. 1288–1298, 2014.

[8] X. Zhang, M. R. Reagan, and D. L. Kaplan, “Electrospun silk biomaterial scaffolds for regenerative medicine,” *Adv. Drug Deliv. Rev.*, vol. 61, no. 12, pp. 988–1006, 2009.

[9] H. Wang, Y. Zhang, H. Shao, and X. Hu, “Electrospun ultra-fine silk fibroin fibers from aqueous solutions,” *J. Mater. Sci.*, vol. 40, no. 20, pp. 5359–5363, 2005.

[10] C. Chen, C. Chuanbao, M. Xilan, T. Yin, and Z. Hesun, “Preparation of non-woven mats from all-aqueous silk fibroin solution with electrospinning method,” *Polymer (Guildf).*, vol.

47, no. 18, pp. 6322–6327, 2006.

[11] H. Wang, H. Shao, and X. Hu, “Structure of silk fibroin fibers made by an electrospinning process from a silk fibroin aqueous solution,” *J. Appl. Polym. Sci.*, vol. 101, no. 2, pp. 961–968, 2006.

[12] J. Zhu, H. Shao, and X. Hu, “Morphology and structure of electrospun mats from regenerated silk fibroin aqueous solutions with adjusting pH,” *Int. J. Biol. Macromol.*, vol. 41, no. 4, pp. 469–474, 2007.

[13] J. Zhu, Y. Zhang, H. Shao, and X. Hu, “Electrospinning and rheology of regenerated Bombyx mori silk fibroin aqueous solutions: The effects of pH and concentration,” *Polymer (Guildf).*, vol. 49, no. 12, pp. 2880–2885, 2008.

[14] C. Solanas *et al.*, “Insights into the production and characterization of electrospun fibers from regenerated silk fibroin,” *Eur. Polym. J.*, vol. 60, pp. 123–134, 2014.

[15] B. N. Singh, N. N. Panda, and K. Pramanik, “A novel electrospinning approach to fabricate high strength aqueous silk fibroin nanofibers,” *Int. J. Biol. Macromol.*, vol. 87, pp. 201–207, 2016.

[16] N. Bhardwaj and S. C. Kundu, “Electrospinning: A fascinating fiber fabrication technique,” *Biotechnol. Adv.*, vol. 28, no. 3, pp. 325–347, 2010.

[17] J. Stranger, N. Tucker, and M. Staiger, “Electrospinnin.” pp. 1–218, 2005.

[18] T. Asakura, A. Kuzuhara, R. Tabeta, and H. Saito, “Conformation Characterization of Bombyx mori Silk Fibroin in the Solid State by High-Frequency13C Cross Polarization-Magic Angle Spinning NMR, X-ray Diffraction, and Infrared Spectroscopy,” *Macromolecules*, vol. 18, no. 10, pp. 1841–1845, 1985.

[19] L. Liu, X. Yang, H. Yu, C. Ma, and J. Yao, “Biomimicking the structure of silk fibers via cellulose nanocrystal as β-sheet crystallite,” *R. Soc. Chem. Adv.*, vol. 4, no. 27, p. 14304, 2014.

[20] L. M. Duque Sánchez, L. Rodriguez, and M. López, “Electrospinning: The Nanofibers Age,” *Rev. Iberoam. Polímeros Vol. Iber. Polímeros*, vol. 14, no. 141, pp. 10–27, 2014.

[21] L. Larrondo and R. St. John Manley, “Electrostatic fiber spinning from polymer melts. I. Experimental observations on fiber formation and properties,” *J. Polym. Sci. Polym. Phys. Ed.*, vol. 19, no. 6, pp. 909–920, Jun. 1981.

[22] V. Sencadas *et al.*, “Determination of the parameters affecting electrospun chitosan fiber size distribution and morphology,” *Carbohydr. Polym.*, vol. 87, no. 2, pp. 1295–1301, Jan. 2012.

[23] C. S. Ki, D. H. Baek, K. D. Gang, K. H. Lee, I. C. Um, and Y. H. Park, “Characterization of gelatin nanofiber prepared from gelatin–formic acid solution,” *Polymer (Guildf).*, vol. 46, no. 14, pp. 5094–5102, Jun. 2005.

[24] J. S. Lee *et al.*, “Role of molecular weight of atactic poly(vinyl alcohol) (PVA) in the structure and properties of PVA nanofabric prepared by electrospinning,” *J. Appl. Polym. Sci.*, vol. 93, no. 4, pp. 1638–1646, Aug. 2004.

[25] R. J. Moon, A. Martini, J. Nairn, J. Simonsen, and J. Youngblood, *Cellulose nanomaterials review: structure, properties and nanocomposites*, vol. 40, no. 7. 2011.

[26] F. Du, R. C. Scogna, W. Zhou, S. Brand, J. E. Fischer, and K. I. Winey, “Nanotube networks in polymer nanocomposites: Rheology and electrical conductivity,” *Macromolecules*, vol. 37, no. 24, pp. 9048–9055, 2004.

[27] Y. Habibi, L. A. Lucia, and O. J. Rojas, “Cellulose Nanocrystals : Chemistry , Self-Assembly , and Applications,” *Chem. Rev.*, vol. 110, no. 6, pp. 3479–3500, 2010.

[28] I. Hayati, A. . Bailey, and T. . Tadros, “Investigations into the mechanisms of electrohydrodynamic spraying of liquids: I. Effect of electric field and the environment on pendant drops and factors affecting the formation of stable jets and atomization,” *J. Colloid Interface Sci.*, vol. 117, no. 1, pp. 205–221, May 1987.

[29] N. A. M. Barakat, M. A. Kanjwal, F. A. Sheikh, and H. Y. Kim, “Spider-net within the N6, PVA and PU electrospun nanofiber mats using salt addition: Novel strategy in the electrospinning process,” *Polymer (Guildf).*, vol. 50, no. 18, pp. 4389–4396, Aug. 2009.

[30] M. S. Peresin, Y. Habibi, J. O. Zoppe, J. J. Pawlak, and O. J. Rojas, “Nanofiber Composites

of Polyvinyl Alcohol and Cellulose Nanocrystals: Manufacture and Characterization," *Biomacromolecules*, vol. 11, no. 3, pp. 674–681, Mar. 2010.

[31] R. B. Bird, W. E. Stewart, and E. N. Lightfoot, *Trnasport Phenomena*. New York: John Willey & Sons Inc., 2007.

[32] S. Shin and D.-Y. Keum, "Continuous Viscosity Measurement of Non-Newtonian Fluids over a Range of Shear Rates Using a Mass-Detecting Capillary Viscometer," 2002.

[33] J. . Deitzel, W. Kosik, S. . McKnight, N. . Beck Tan, J. . DeSimone, and S. Crette, "Electrospinning of polymer nanofibers with specific surface chemistry," *Polymer (Guildf).*, vol. 43, no. 3, pp. 1025–1029, Feb. 2002.

[34] J. T. Pelton and L. R. McLean, "Spectroscopy Methods for Analysis of Protein Secondary Structure," *Anal. Biochem.*, vol. 277, pp. 167–176, 2000.

[35] B. Lotz and F. Colonna Cesari, "The chemical structure and the crystalline structures of Bombyx mori silk fibroin," *Biochimie*, vol. 61, no. 2, pp. 205–214, 1979.

[36] C. Z. Zhou, F. Confalonieri, M. Jacquet, R. Perasso, Z. G. Li, and J. Janin, "Silk fibroin: structural implications of a remarkable amino acid sequence.," *Proteins*, vol. 44, no. 2, pp. 119–22, Aug. 2001.

[37] L. P. Gage and R. F. Manning, "Internal structure of the silk fibroin gene of Bombyx mori. I The fibroin gene consists of a homogeneous alternating array of repetitious crystalline and amorphous coding sequences.," *J. Biol. Chem.*, vol. 255, no. 19, pp. 9444–50, Oct. 1980.

[38] X. Li, J. Qin, and J. Ma, "Silk fibroin/poly (vinyl alcohol) blend scaffolds for controlled delivery of curcumin," *Regen. Biomater.*, vol. 2, no. 2, pp. 97–105, Jun. 2015.

[39] H. Zhang *et al.*, "Preparation and characterization of silk fibroin as a biomaterial with potential for drug delivery," *J. Transl. Med.*, vol. 10, no. 1, p. 117, 2012.

[40] S.-W. Ha, A. E. Tonelli, and S. M. Hudson, "Structural Studies of Bombyx mori Silk Fibroin during Regeneration from Solutions and Wet Fiber Spinning," 2005.

[41] T. Miyazawa and E. R. Blout, "The Infrared Spectra of Polypeptides in Various Conformations: Amide I and II Bands," *J. Am. Chem. Soc.*, vol. 83, no. 3, pp. 712–719,

1961.

[42] X. Wu, X. Wu, B. Yang, M. Shao, and G. Feng, “Methanol–Water-Dependent Structural Changes of Regenerated Silk Fibroin Probed Using Terahertz Spectroscopy,” *Appl. Spectrosc.*, vol. 71, no. 8, pp. 1785–1794, 2017.

[43] W. Zhou, J. He, S. Du, S. Cui, and W. Gao, “Electrospun silk fibroin/cellulose acetate blend nanofibres: structure and properties,” *Iran. Polym. J.*, vol. 20, no. 5, pp. 389–397, 2011.

[44] S. Shang, L. Zhu, and J. Fan, “Intermolecular interactions between natural polysaccharides and silk fibroin protein,” *Carbohydr. Polym.*, vol. 93, no. 2, pp. 561–573, 2013.

[45] S. Ling, Z. Qi, D. P. Knight, Z. Shao, and X. Chen, “Synchrotron FTIR microspectroscopy of single natural silk fibers,” *Biomacromolecules*, vol. 12, no. 9, pp. 3344–3349, 2011.

[46] G. Freddi, M. Romano, M. R. Massafra, and M. Tsukada, “Silk Fibroin / Cellulose Blend Films : Preparation , Structure , and Physical Properties,” pp. 1537–1545, 1995.

[47] H. Yang, S. Yang, J. Kong, A. Dong, and S. Yu, “Obtaining information about protein secondary structures in aqueous solution using Fourier transform IR spectroscopy.,” *Nat. Protoc.*, vol. 10, no. 3, pp. 382–96, 2015.

[48] M. M. Hohman, M. Shin, G. Rutledge, and M. P. Brenner, “Electrospinning and electrically forced jets. I. Stability theory,” *Phys. Fluids*, vol. 13, no. 8, pp. 2201–2220, 2001.

[49] D. H. Reneker, A. L. Yarin, H. Fong, S. Koombhongse, and D. H. Reneker, “Bending instability of electrically charged liquid jets of polymer solutions in electrospinning,” *J. Appl. Phys.*, vol. 87, no. 9, pp. 4531–4548, 2000.

[50] Y. M. Shin, M. M. Hohman, M. P. Brenner, and G. C. Rutledge, “Experimental characterization of electrospinning: the electrically forced jet and instabilities,” *Polymer (Guildf).*, vol. 42, no. 25, pp. 9955–9967, 2001.

[51] C. Vepari and D. L. Kaplan, “Silk as a biomaterial,” *Prog. Polym. Sci.*, vol. 32, no. 8–9, pp. 991–1007, 2007.

[52] J. Huang, L. Liu, and J. Yao, “Electrospinning of Bombyx mori silk fibroin nanofiber mats reinforced by cellulose nanowhiskers,” *Fibers Polym.*, vol. 12, no. 8, pp. 1002–1006, 2011.

[53] U. J. Kim, J. Park, C. Li, H. J. Jin, R. Valluzzi, and D. L. Kaplan, “Structure and properties of silk hydrogels,” *Biomacromolecules*, vol. 5, no. 3, pp. 786–792, 2004.

[54] E. Marsano, P. Corsini, M. Canetti, and G. Freddi, “Regenerated cellulose-silk fibroin blends fibers,” *Int. J. Biol. Macromol.*, vol. 43, no. 2, pp. 106–114, 2008.

[55] N. Lin, C. Bruzzese, and A. Dufresne, “TEMPO-oxidized nanocellulose participating as crosslinking aid for alginate-based sponges,” *ACS Appl. Mater. Interfaces*, vol. 4, no. 9, pp. 4948–4959, 2012.

[56] B. Sun, Q. Hou, Z. Liu, and Y. Ni, “Sodium periodate oxidation of cellulose nanocrystal and its application as a paper wet strength additive,” *Cellulose*, vol. 22, no. 2, pp. 1135–1146, 2015.

[57] M. Zaman, H. Xiao, F. Chibante, and Y. Ni, “Synthesis and characterization of cationically modified nanocrystalline cellulose,” *Carbohydr. Polym.*, vol. 89, no. 1, pp. 163–170, Jun. 2012.

[58] S. M. A. S. Keshk, “Homogenous reactions of cellulose from different natural sources,” *Carbohydr. Polym.*, vol. 74, no. 4, pp. 942–945, Nov. 2008.

[59] M. S. Jahan, A. Saeed, Z. He, and Y. Ni, “Jute as raw material for the preparation of microcrystalline cellulose,” *Cellulose*, vol. 18, no. 2, pp. 451–459, Apr. 2011.

[60] R. Sun, X. Sun, G. Liu, P. Fowler, and J. Tomkinson, “Structural and physicochemical characterization of hemicelluloses isolated by alkaline peroxide from barley straw,” *Polym. Int.*, vol. 51, no. 2, pp. 117–124, Feb. 2002.

[61] H.-J. Jin and D. L. Kaplan, “Mechanism of silk processing in insects and spiders,” *Nature*, vol. 424, no. 6952, pp. 1057–1061, Aug. 2003.

[62] Q. Lu *et al.*, “Water-insoluble silk films with silk I structure,” *Acta Biomater.*, vol. 6, no. 4, pp. 1380–1387, 2010.

[63] R. Fraser, *Conformation in Fibrous Proteins and Related synthetic Polypeptides*. Elsevier Science, 1973.

[64] Y. X. He *et al.*, “N-terminal domain of Bombyx mori fibroin mediates the assembly of silk

in response to pH decrease," *J. Mol. Biol.*, vol. 418, no. 3–4, pp. 197–207, 2012.

[65] L. H. Sperling, *Introduction to Physical Polymer Science*, Fourth Edi. New Jersey: John Wiley & Sons Ltd, 2006.

[66] A. Baji, Y. W. Mai, S. C. Wong, M. Abtahi, and P. Chen, "Electrospinning of polymer nanofibers: Effects on oriented morphology, structures and tensile properties," *Compos. Sci. Technol.*, vol. 70, no. 5, pp. 703–718, 2010.

[67] J. G. Hardy and T. R. Scheibel, "Composite materials based on silk proteins," *Prog. Polym. Sci.*, vol. 35, no. 9, pp. 1093–1115, 2010.

[68] S. Rammensee, U. Slotta, T. Scheibel, and A. R. Bausch, "Assembly mechanism of recombinant spider silk proteins," *Proc. Natl. Acad. Sci.*, vol. 105, no. 18, pp. 6590–6595, May 2008.

[69] W. Gindl and J. Keckes, "All-cellulose nanocomposite," *Polymer (Guildf).*, vol. 46, no. 23, pp. 10221–10225, Nov. 2005.

[70] Z. Liu *et al.*, "Characterization of the regenerated cellulose films in ionic liquids and rheological properties of the solutions," *Mater. Chem. Phys.*, vol. 128, no. 1–2, pp. 220–227, Jul. 2011.

[71] P. Mansikkamäki, M. Lahtinen, and K. Rissanen, "Structural Changes of Cellulose Crystallites Induced by Mercerisation in Different Solvent Systems; Determined by Powder X-ray Diffraction Method," *Cellulose*, vol. 12, no. 3, pp. 233–242, Jun. 2005.

[72] Y. Yao *et al.*, "Morphology and properties of cellulose/silk fibroin blend fiber prepared with 1-butyl-3-methylimidazolium chloride as solvent," *Cellulose*, vol. 22, no. 1, pp. 625–635, 2015.

[73] E. Marsano, M. Canetti, G. Conio, P. Corsini, and G. Freddi, "Fibers based on cellulose-silk fibroin blend," *J. Appl. Polym. Sci.*, vol. 104, no. 4, pp. 2187–2196, 2007.

[74] B. N. Singh, N. N. Panda, R. Mund, and K. Pramanik, "Carboxymethyl cellulose enables silk fibroin nanofibrous scaffold with enhanced biomimetic potential for bone tissue engineering application," *Carbohydr. Polym.*, vol. 151, pp. 335–347, 2016.

[75] J. Y. Rongji Li, Yanhong Zhang, Liangjun Zhu, “Fabrication and Characterization of Silk Fibroin/Poly(ethylene glycol)/Cellulose Nanowhisker Composite Films,” *J. Appl. Polym. Sci.*, vol. 124, pp. 2080–2086, 2012.

[76] D. J. Park, Y. Choi, S. Heo, S. Y. Cho, and H.-J. Jin, “Bacterial Cellulose Nanocrystals-Embedded Silk Nanofibers,” *J. Nanosci. Nanotechnol.*, vol. 12, no. 7, pp. 6139–6144, 2012.

[77] Y. Noishiki, Y. Nishiyama, M. Wada, S. Kuga, and J. Magoshi, “Mechanical properties of silk fibroin-microcrystalline cellulose composite films,” *J. Appl. Polym. Sci.*, vol. 86, no. 13, pp. 3425–3429, 2002.

[78] M. Mirjalili and S. Zohoori, “Review for application of electrospinning and electrospun nanofibers technology in textile industry,” *J. Nanostructure Chem.*, vol. 6, no. 3, pp. 207–213, 2016.

[79] Z.-M. Huang, Y.-Z. Zhang, M. Kotaki, and S. Ramakrishna, “A review on polymer nanofibers by electrospinning and their applications in nanocomposites,” *Compos. Sci. Technol.*, vol. 63, no. 15, pp. 2223–2253, 2003.

[80] C. Burger, B. S. Hsiao, and B. Chu, “NANOFIBROUS MATERIALS AND THEIR APPLICATIONS,” *Annu. Rev. Mater. Res.*, vol. 36, no. 1, pp. 333–368, Aug. 2006.

[81] S. Ramakrishna *et al.*, “Science and engineering of electrospun nanofibers for advances in clean energy, water filtration, and regenerative medicine,” *J. Mater. Sci.*, vol. 45, no. 23, pp. 6283–6312, Dec. 2010.

[82] S. Curgul, K. J. Van Vliet, and G. C. Rutledge, “Molecular Dynamics Simulation of Size-Dependent Structural and Thermal Properties of Polymer Nanofibers,” 2007.

[83] S. Fujisawa, T. Ikeuchi, M. Takeuchi, T. Saito, and A. Isogai, “Superior reinforcement effect of TEMPO-oxidized cellulose nanofibrils in polystyrene matrix: optical, thermal, and mechanical studies.,” *Biomacromolecules*, vol. 13, no. 7, pp. 2188–2194, 2012.

[84] A. Boujemaoui *et al.*, “Polycaprolactone Nanocomposites Reinforced with Cellulose Nanocrystals Surface-Modified via Covalent Grafting or Physisorption: A Comparative Study,” 2017.

[85] N. E. Marcovich, M. L. Auad, N. E. Bellesi, S. R. Nutt, and M. I. Aranguren, “Cellulose micro/nanocrystals reinforced polyurethane,” *J. Mater. Res.*, vol. 21, no. 4, pp. 870–881, 2006.

[86] A. Pei, J.-M. Malho, J. Ruokolainen, Q. Zhou, and L. A. Berglund, “Strong Nanocomposite Reinforcement Effects in Polyurethane Elastomer with Low Volume Fraction of Cellulose Nanocrystals,” *Macromolecules*, vol. 44, pp. 4422–4427, 2011.

[87] J. Bras, D. Viet, C. Bruzzese, and A. Dufresne, “Correlation between stiffness of sheets prepared from cellulose whiskers and nanoparticles dimensions,” *Carbohydr. Polym.*, vol. 84, no. 1, pp. 211–215, 2011.

[88] L. Liu and J. M. Yao, “Wet-spinning of reinforced artificial silk hybrid fibres by cellulose whiskers,” *Adv. Mater. Res.*, vol. 175–176, pp. 272–275, 2011.

[89] E. Guth, “Theory of filler reinforcement,” *J. Appl. Phys.*, vol. 16, no. 1, pp. 20–25, 1945.

[90] M. Grunert and W. T. Winter, “Nanocomposites of Cellulose Acetate Butyrate Reinforced with Cellulose Nanocrystals,” *J. Polym. Environ.*, vol. 10, no. 2, pp. 27–30, 2002.

[91] X. Hu, Q. Lu, D. L. Kaplan, and P. Cebe, “Microphase Separation Controlled β-Sheet Crystallization Kinetics in Fibrous Proteins,” *Macromolecules*, vol. 42, no. 6, pp. 2079–2087, Mar. 2009.

[92] X. Hu, D. Kaplan, and P. Cebe, “Determining Beta-Sheet Crystallinity in Fibrous Proteins by Thermal Analysis and Infrared Spectroscopy,” *Macromolecules*, vol. 39, no. 18, pp. 6161–6170, 2006.

## References for used on this work


[1] Y. Gong, L. Li, D. Gong, H. Yin, and J. Zhang, "Biomolecular Evidence of Silk from 8 , 500 Years Ago," *PLoS One*, vol. 11, no. 12, pp. 1–9, 2016.

[2] C. Vepari and D. L. Kaplan, "Silk as a biomaterial," *Prog. Polym. Sci.*, vol. 32, no. 8–9, pp. 991–1007, 2007.

[3] M. Elices, J. Perez Rigueiro, G. R. Plaza, and G. V. Guinea, "Usos médicos de la seda," *Investig. Cienc.*, pp. 28–35, 2011.

[4] L. Liu and J. M. Yao, "Wet-spinning of reinforced artificial silk hybrid fibres by cellulose whiskers," *Adv. Mater. Res.*, vol. 175–176, pp. 272–275, 2011.

[5] D. J. Park, Y. Choi, S. Heo, S. Y. Cho, and H.-J. Jin, "Bacterial Cellulose Nanocrystals-Embedded Silk Nanofibers," *J. Nanosci. Nanotechnol.*, vol. 12, no. 7, pp. 6139–6144, 2012.

[6] G. Shelach-Lavi, *The Archaeology of Early China, from prehistory to the Han dynasty*. 2015.

[7] D. L. Dunn, "Wound closure manual." Ethicon Products, Minnesota, pp. 1–127, 2005.

[8] Y. Cao and B. Wang, "Biodegradation of silk biomaterials," *Int. J. Mol. Sci.*, vol. 10, no. 4, pp. 1514–1524, 2009.

[9] B. N. Singh, N. N. Panda, R. Mund, and K. Pramanik, "Carboxymethyl cellulose enables silk fibroin nanofibrous scaffold with enhanced biomimetic potential for bone tissue engineering application," *Carbohydr. Polym.*, vol. 151, pp. 335–347, 2016.

[10] J. Pérez-Rigueiro, C. Viney, J. Llorca, and M. Elices, "Mechanical properties of silkworm silk in liquid media," *J. Appl. Polym. Sci.*, vol. 75, no. 10, pp. 1270–1277, 2000.

[11] H. P. Zhao, X. Q. Feng, S. W. Yu, W. Z. Cui, and F. Z. Zou, "Mechanical properties of silkworm cocoons," *Polymer (Guildf).*, vol. 46, no. 21, pp. 9192–9201, 2005.

[12] B. Lotz and F. Colonna Cesari, "The chemical structure and the crystalline structures of Bombyx mori silk fibroin," *Biochimie*, vol. 61, no. 2, pp. 205–214, 1979.

[13] Q. Zhang, S. Yan, and M. Li, “Silk fibroin based porous materials,” *Materials (Basel).*, vol. 2, no. 4, pp. 2276–2295, 2009.

[14] G. H. Altman *et al.*, “Silk-based biomaterials,” *Biomaterials*, vol. 24, no. 3, pp. 401–416, 2003.

[15] R. I. Kunz, R. M. C. Brancalhao, L. D. F. C. Ribeiro, and M. R. M. Natali, “Silkworm Sericin: Properties and Biomedical Applications,” *Biomed Res. Int.*, vol. 2016, 2016.

[16] D. N. Rockwood, R. C. Preda, T. Yücel, X. Wang, M. L. Lovett, and D. L. Kaplan, “Materials fabrication from Bombyx mori silk fibroin,” *Nat. Protoc.*, vol. 6, no. 10, pp. 1612–1631, 2011.

[17] J. G. Hardy and T. R. Scheibel, “Composite materials based on silk proteins,” *Prog. Polym. Sci.*, vol. 35, no. 9, pp. 1093–1115, 2010.

[18] N. Bhardwaj and S. C. Kundu, “Electrospinning: A fascinating fiber fabrication technique,” *Biotechnol. Adv.*, vol. 28, no. 3, pp. 325–347, 2010.

[19] X. Zhang, M. R. Reagan, and D. L. Kaplan, “Electrospun silk biomaterial scaffolds for regenerative medicine,” *Adv. Drug Deliv. Rev.*, vol. 61, no. 12, pp. 988–1006, 2009.

[20] J. Huang, L. Liu, and J. Yao, “Electrospinning of Bombyx mori silk fibroin nanofiber mats reinforced by cellulose nanowhiskers,” *Fibers Polym.*, vol. 12, no. 8, pp. 1002–1006, 2011.

[21] W. Zhou, J. He, S. Du, S. Cui, and W. Gao, “Electrospun silk fibroin/cellulose acetate blend nanofibres: structure and properties,” *Iran. Polym. J.*, vol. 20, no. 5, pp. 389–397, 2011.

[22] E. Marsano, M. Canetti, G. Conio, P. Corsini, and G. Freddi, “Fibers based on cellulose-silk fibroin blend,” *J. Appl. Polym. Sci.*, vol. 104, no. 4, pp. 2187–2196, 2007.

[23] T. Kitagawa and K. Yabuki, “Physical properties of silk fibroin/chitosan blend films,” *J. Appl. Polym. Sci.*, vol. 80, no. 7, pp. 928–934, 2001.

[24] L.-D. Koh *et al.*, “Structures, mechanical properties and applications of silk fibroin materials,” *Prog. Polym. Sci.*, vol. 46, pp. 86–110, 2015.

[25] U. J. Kim, J. Park, C. Li, H. J. Jin, R. Valluzzi, and D. L. Kaplan, “Structure and properties of silk hydrogels,” *Biomacromolecules*, vol. 5, no. 3, pp. 786–792, 2004.

[26] A. Baji, Y. W. Mai, S. C. Wong, M. Abtahi, and P. Chen, “Electrospinning of polymer nanofibers: Effects on oriented morphology, structures and tensile properties,” *Compos. Sci. Technol.*, vol. 70, no. 5, pp. 703–718, 2010.

[27] S. Fujisawa, T. Ikeuchi, M. Takeuchi, T. Saito, and A. Isogai, “Superior reinforcement effect of TEMPO-oxidized cellulose nanofibrils in polystyrene matrix: optical, thermal, and mechanical studies.,” *Biomacromolecules*, vol. 13, no. 7, pp. 2188–2194, 2012.

[28] S. Shang, L. Zhu, and J. Fan, “Intermolecular interactions between natural polysaccharides and silk fibroin protein,” *Carbohydr. Polym.*, vol. 93, no. 2, pp. 561–573, 2013.

[29] R. J. Moon, A. Martini, J. Nairn, J. Simonsen, and J. Youngblood, *Cellulose nanomaterials review: structure, properties and nanocomposites*, vol. 40, no. 7. 2011.

[30] J. G. Hardy, L. M. Romer, and T. R. Scheibel, “Polymeric materials based on silk proteins,” *Polymer (Guildf).*, vol. 49, no. 20, pp. 4309–4327, 2008.

[31] M. Mariano, N. El Kissi, and A. Dufresne, “Cellulose nanocrystals and related nanocomposites: Review of some properties and challenges,” *J. Polym. Sci. Part B Polym. Phys.*, vol. 52, no. 12, pp. 791–806, 2014.

[32] Y. Habibi, L. A. Lucia, and O. J. Rojas, “Cellulose Nanocrystals : Chemistry , Self-Assembly , and Applications,” *Chem. Rev.*, vol. 110, no. 6, pp. 3479–3500, 2010.

[33] A. Isogai, T. Saito, and H. Fukuzumi, “TEMPO-oxidized cellulose nanofibers,” *Nanoscale*, vol. 3, no. 1, pp. 71–85, 2011.

[34] J. H. Lee, C. H. Bae, B.-D. Park, and I. C. Um, “Preparation of Cellulose Nanofibril/Regenerated Silk Fibroin Composite Fibers,” *Int. J. Ind. Entomol.*, vol. 26, no. 2, pp. 81–88, 2013.

[35] Y. Yao *et al.*, “Morphology and properties of cellulose/silk fibroin blend fiber prepared with 1-butyl-3-methylimidazolium chloride as solvent,” *Cellulose*, vol. 22, no. 1, pp. 625–

635, 2015.

[36] L. Liu, X. Yang, H. Yu, C. Ma, and J. Yao, “Biomimicking the structure of silk fibers via cellulose nanocrystal as β-sheet crystallite,” *R. Soc. Chem. Adv.*, vol. 4, no. 27, p. 14304, 2014.

[37] A. A. Shefa *et al.*, “In vitro and in vivo evaluation of effectiveness of a novel TEMPO-oxidized cellulose nanofiber-silk fibroin scaffold in wound healing,” *Carbohydr. Polym.*, vol. 177, no. April, pp. 284–296, 2017.

[38] L. L. Guo, Y. B. Liu, and J. B. Yao, “A Review on Existing Tecgnology of Electrospinning at Large Scale,” *Proc. 2010 Int. Conf. Inf. Technol. Sci. Manag. Vols 1-2*, pp. 279–282, 2010.

[39] L. M. Duque Sánchez, L. Rodriguez, and M. López, “Electrospinning: The Nanofibers Age,” *Rev. Iberoam. Polímeros Vol. Iber. Polímeros*, vol. 14, no. 141, pp. 10–27, 2014.

[40] J. F. Cooley, “Apparatus for electrically dispersing fluids,” US Patent 692,631, 1902.

[41] J. Stranger, N. Tucker, and M. Staiger, “Electrospinnin.” pp. 1–218, 2005.

[42] W. J. Morton, “Method of dispersing fluids,” US Patent705,691, 1902.

[43] J. Zeleny, “The electrical discharge from liquid points, and a hydrostatic method of measuring the electrical intensity at their surfaces,” *Physycal Rev.*, vol. 3, no. 2, pp. 69–91, 1914.

[44] A. Formhals, “Process and apparatus for preparing artificial threads,” US Patent 1,975,504, 1934.

[45] anton Formhals, “Artificial Fiber Construction,” US Patent 2,109,333, 1938.

[46] A. Formhals, “Method of Producing Artificial Fibers,” US Patent 2,158,415, 1939.

[47] A. Formhals, “Method and apparatus for spinning,” US Patent 2,160,962, 1939.

[48] A. Formhals, “Artificial thread and method of producing same,” US Patent2,187,306, 1940.

[49] A. Formhals, “Production of artificial fibers from fiber forming liquids,” 2,323,025, 1943.

[50] A. Formhals, “Method and apparatus for spinning,” US Patent 2,349,950, 1944.

[51] T. Subbiah, G. S. Bhat, R. W. Tock, S. Parameswaran, and S. S. Ramkumar, "Electrospinning of nanofibers," *J. Appl. Polym. Sci.*, vol. 96, no. 2, pp. 557–569, 2005.

[52] M. Mirjalili and S. Zohoori, "Review for application of electrospinning and electrospun nanofibers technology in textile industry," *J. Nanostructure Chem.*, vol. 6, no. 3, pp. 207–213, 2016.

[53] G. Taylor, "Disintegration of water drops in an electric field," *Proc. R. Soc. London A*, vol. 280, no. 22, pp. 383–397, 1964.

[54] G. Taylor and M. D. Van Dyke, "Electrically driven jets," *Proc. R. Soc. London A.*, vol. 313, pp. 453–475, 1969.

[55] J. Doshi and D. H. Reneker, "Electrospinning process and applications of electrospun fibers," *Conf. Rec. 1993 IEEE Ind. Appl. Conf. Twenty-Eighth IAS Annu. Meet.*, vol. 35, pp. 151–160, 1993.

[56] S. Y. Chew, Y. Wen, Y. Dzenis, and K. W. Leong, "The role of electrospinning in the emerging field of nanomedicine.," *Curr. Pharm. Des.*, vol. 12, no. 36, pp. 4751–70, 2006.

[57] Z.-M. Huang, Y.-Z. Zhang, M. Kotaki, and S. Ramakrishna, "A review on polymer nanofibers by electrospinning and their applications in nanocomposites," *Compos. Sci. Technol.*, vol. 63, no. 15, pp. 2223–2253, 2003.

[58] M. M. Hohman, M. Shin, G. Rutledge, and M. P. Brenner, "Electrospinning and electrically forced jets. I. Stability theory," *Phys. Fluids*, vol. 13, no. 8, pp. 2201–2220, 2001.

[59] D. H. Reneker, A. L. Yarin, H. Fong, S. Koombhongse, and D. H. Reneker, "Bending instability of electrically charged liquid jets of polymer solutions in electrospinning," *J. Appl. Phys.*, vol. 87, no. 9, pp. 4531–4548, 2000.

[60] Y. M. Shin, M. M. Hohman, M. P. Brenner, and G. C. Rutledge, "Experimental characterization of electrospinning: the electrically forced jet and instabilities," *Polymer (Guildf).*, vol. 42, no. 25, pp. 9955–9967, 2001.

[61] A. Greiner and J. H. Wendorff, "Electrospinning: A fascinating method for the preparation

of ultrathin fibers," *Angew. Chemie - Int. Ed.*, vol. 46, no. 30, pp. 5670–5703, 2007.

[62] A. J. Dekker, *Electrical engineering materials*, Prentice-Hall. Minnesota: Prentice-Hall INC., 1959.

[63] S. Kidoaki, I. K. Kwon, and T. Matsuda, "Mesoscopic spatial designs of nano- and microfiber meshes for tissue-engineering matrix and scaffold based on newly devised multilayering and mixing electrospinning techniques," *Biomaterials*, vol. 26, no. 1, pp. 37–46, Jan. 2005.

[64] J. J. Stankus, J. Guan, K. Fujimoto, and W. R. Wagner, "Microintegrating smooth muscle cells into a biodegradable, elastomeric fiber matrix," *Biomaterials*, vol. 27, no. 5, pp. 735–744, Feb. 2006.

[65] S. Agarwal, J. H. Wendorff, and A. Greiner, "Use of electrospinning technique for biomedical applications," *Polymer (Guildf).*, vol. 49, no. 26, pp. 5603–5621, 2008.

[66] R. Sahay, V. Thavasi, and S. Ramakrishna, "Design modifications in electrospinning setup for advanced applications," *J. Nanomater.*, vol. 2011, 2011.

[67] F. E. Ahmed, B. S. Lalia, and R. Hashaikeh, "A review on electrospinning for membrane fabrication: Challenges and applications," *Desalination*, vol. 356, pp. 15–30, 2015.

[68] W. E. Teo and S. Ramakrishna, "A review on electrospinning design and nanofibre assemblies," *Nanotechnology*, vol. 17, no. 14, pp. R89–R106, Jul. 2006.

[69] P. Gupta, C. Elkins, T. E. Long, and G. L. Wilkes, "Electrospinning of linear homopolymers of poly(methyl methacrylate): exploring relationships between fiber formation, viscosity, molecular weight and concentration in a good solvent," *Polymer (Guildf).*, vol. 46, no. 13, pp. 4799–4810, Jun. 2005.

[70] E. P. S. Tan, S. Y. Ng, and C. T. Lim, "Tensile testing of a single ultrafine polymeric fiber," *Biomaterials*, vol. 26, no. 13, pp. 1453–1456, May 2005.

[71] J. . Deitzel, W. Kosik, S. . McKnight, N. . Beck Tan, J. . DeSimone, and S. Crette, "Electrospinning of polymer nanofibers with specific surface chemistry," *Polymer (Guildf).*, vol. 43, no. 3, pp. 1025–1029, Feb. 2002.

[72] L. Larrondo and R. St. John Manley, “Electrostatic fiber spinning from polymer melts. I. Experimental observations on fiber formation and properties,” *J. Polym. Sci. Polym. Phys. Ed.*, vol. 19, no. 6, pp. 909–920, Jun. 1981.

[73] A. K. Haghi and M. Akbari, “Trends in electrospinning of natural nanofibers,” *Phys. status solidi*, vol. 204, no. 6, pp. 1830–1834, Jun. 2007.

[74] H. Fong, I. Chun, and D. . Reneker, “Beaded nanofibers formed during electrospinning,” *Polymer (Guildf).*, vol. 40, no. 16, pp. 4585–4592, Jul. 1999.

[75] I. Hayati, A. . Bailey, and T. . Tadros, “Investigations into the mechanisms of electrohydrodynamic spraying of liquids: I. Effect of electric field and the environment on pendant drops and factors affecting the formation of stable jets and atomization,” *J. Colloid Interface Sci.*, vol. 117, no. 1, pp. 205–221, May 1987.

[76] N. A. M. Barakat, M. A. Kanjwal, F. A. Sheikh, and H. Y. Kim, “Spider-net within the N6, PVA and PU electrospun nanofiber mats using salt addition: Novel strategy in the electrospinning process,” *Polymer (Guildf).*, vol. 50, no. 18, pp. 4389–4396, Aug. 2009.

[77] R. Jalili, S. A. Hosseini, and M. Morshed, “The Effects of Operating Parameters on the morphology of electrospun polyacrilonitile nanofibres,” *Iran. Polym. J.*, vol. 14, no. 12, pp. 1074–1081, 2005.

[78] K. H. Lee, H. Y. Kim, M. S. Khil, Y. M. Ra, and D. R. Lee, “Characterization of nano-structured poly(ε-caprolactone) nonwoven mats via electrospinning,” *Polymer (Guildf).*, vol. 44, no. 4, pp. 1287–1294, Feb. 2003.

[79] Y. Zhang, H. Ouyang, C. T. Lim, S. Ramakrishna, and Z.-M. Huang, “Electrospinning of gelatin fibers and gelatin/PCL composite fibrous scaffolds,” *J. Biomed. Mater. Res.*, vol. 72B, no. 1, pp. 156–165, Jan. 2005.

[80] M. . Demir, I. Yilgor, E. Yilgor, and B. Erman, “Electrospinning of polyurethane fibers,” *Polymer (Guildf).*, vol. 43, no. 11, pp. 3303–3309, May 2002.

[81] V. Sencadas *et al.*, “Determination of the parameters affecting electrospun chitosan fiber size distribution and morphology,” *Carbohydr. Polym.*, vol. 87, no. 2, pp. 1295–1301, Jan.

2012.

[82] K.-H. Kim *et al.*, “Biological efficacy of silk fibroin nanofiber membranes for guided bone regeneration,” *J. Biotechnol.*, vol. 120, no. 3, pp. 327–339, Nov. 2005.

[83] X. Zong, K. Kim, D. Fang, S. Ran, B. S. Hsiao, and B. Chu, “Structure and process relationship of electrospun bioabsorbable nanofiber membranes,” *Polymer (Guildf).*, vol. 43, no. 16, pp. 4403–4412, Jul. 2002.

[84] C. S. Ki, D. H. Baek, K. D. Gang, K. H. Lee, I. C. Um, and Y. H. Park, “Characterization of gelatin nanofiber prepared from gelatin–formic acid solution,” *Polymer (Guildf).*, vol. 46, no. 14, pp. 5094–5102, Jun. 2005.

[85] J. S. Lee *et al.*, “Role of molecular weight of atactic poly(vinyl alcohol) (PVA) in the structure and properties of PVA nanofabric prepared by electrospinning,” *J. Appl. Polym. Sci.*, vol. 93, no. 4, pp. 1638–1646, Aug. 2004.

[86] X. Wang, I. C. Um, D. Fang, A. Okamoto, B. S. Hsiao, and B. Chu, “Formation of water-resistant hyaluronic acid nanofibers by blowing-assisted electro-spinning and non-toxic post treatments,” *Polymer (Guildf).*, vol. 46, no. 13, pp. 4853–4867, Jun. 2005.

[87] J. Doshi and D. H. Reneker, “Electrospinning process and applications of electrospun fibers,” *J. Electrostat.*, vol. 35, no. 2–3, pp. 151–160, Aug. 1995.

[88] J. . Deitzel, J. Kleinmeyer, D. Harris, and N. . Beck Tan, “The effect of processing variables on the morphology of electrospun nanofibers and textiles,” *Polymer (Guildf).*, vol. 42, no. 1, pp. 261–272, Jan. 2001.

[89] K. W. Kim, K. H. Lee, M. S. Khil, Y. S. Ho, and H. Y. Kim, “The effect of molecular weight and the linear velocity of drum surface on the properties of electrospun poly(ethylene terephthalate) nonwovens,” *Fibers Polym.*, vol. 5, no. 2, pp. 122–127, Jun. 2004.

[90] C. S. Ki *et al.*, “Electrospun three-dimensional silk fibroin nanofibrous scaffold,” *J. Appl. Polym. Sci.*, vol. 106, no. 6, pp. 3922–3928, Dec. 2007.

[91] C. J. Thompson, G. G. Chase, A. L. Yarin, and D. H. Reneker, “Effects of parameters on

nanofiber diameter determined from electrospinning model," *Polymer (Guildf).*, vol. 48, no. 23, pp. 6913–6922, Nov. 2007.

[92] S. Zhao, X. Wu, L. Wang, and Y. Huang, "Electrospinning of ethyl-cyanoethyl cellulose/tetrahydrofuran solutions," *J. Appl. Polym. Sci.*, vol. 91, no. 1, pp. 242–246, Jan. 2004.

[93] G. L. Wilkes, "An Overview of the Basic Rheological Behavior of Polymer Fluids with an Emphasis on Polymer Melts," *J. Chem. Educ.*, vol. 58, no. 11, p. 880-, 1981.

[94] L. C. Cheryl, J. S. Stephens, G. Tassi, Nancy, D. B. Chase, and J. F. Rabolt, "Controlling Surface Morphology of Electrospun Polystyrene Fibers: Effect of Humidity and Molecular Weight in the Electrospinning Process," *Macromolecules*, vol. 37, no. 2, pp. 573–578, 2003.

[95] P. K. Baumgarten, "Electrostatic spinning of acrylic microfibers," *J. Colloid Interface Sci.*, vol. 36, no. 1, pp. 71–79, May 1971.

[96] S. A. Theron, A. L. Yarin, E. Zussman, and E. Kroll, "Multiple jets in electrospinning: experiment and modeling," *Polymer (Guildf).*, vol. 46, no. 9, pp. 2889–2899, Apr. 2005.

[97] D. Li and Y. Xia, "Electrospinning of Nanofibers: Reinventing the Wheel?," *Adv. Mater.*, vol. 16, no. 14, pp. 1151–1170, Jul. 2004.

[98] M. Li, M. J. Mondrinos, M. R. Gandhi, F. K. Ko, A. S. Weiss, and P. I. Lelkes, "Electrospun protein fibers as matrices for tissue engineering," *Biomaterials*, vol. 26, no. 30, pp. 5999–6008, Oct. 2005.

[99] J. Pelipenko, J. Kristl, B. Janković, S. Baumgartner, and P. Kocbek, "The impact of relative humidity during electrospinning on the morphology and mechanical properties of nanofibers," *Int. J. Pharm.*, vol. 456, no. 1, pp. 125–134, Nov. 2013.

[100] E. S. Medeiros *et al.*, "Electrospun Nanofibers of Poly(vinyl alcohol) Reinforced with Cellulose Nanofibrils," *J. Biobased Mater. Bioenergy*, vol. 2, no. 3, pp. 231–242, Sep. 2008.

[101] C. Mit-uppatham, M. Nithitanakul, and P. Supaphol, "Ultrafine Electrospun Polyamide-6

Fibers: Effect of Solution Conditions on Morphology and Average Fiber Diameter," *Macromol. Chem. Phys.*, vol. 205, no. 17, pp. 2327–2338, Nov. 2004.

[102] C. Burger, B. S. Hsiao, and B. Chu, "NANOFIBROUS MATERIALS AND THEIR APPLICATIONS," *Annu. Rev. Mater. Res.*, vol. 36, no. 1, pp. 333–368, Aug. 2006.

[103] S. Ramakrishna *et al.*, "Science and engineering of electrospun nanofibers for advances in clean energy, water filtration, and regenerative medicine," *J. Mater. Sci.*, vol. 45, no. 23, pp. 6283–6312, Dec. 2010.

[104] E. Marsano, P. Corsini, M. Canetti, and G. Freddi, "Regenerated cellulose-silk fibroin blends fibers," *Int. J. Biol. Macromol.*, vol. 43, no. 2, pp. 106–114, 2008.

[105] H. Hou and D. H. Reneker, "Carbon Nanotubes on Carbon Nanofibers: A Novel Structure Based on Electrospun Polymer Nanofibers," *Adv. Mater.*, vol. 16, no. 1, pp. 69–73, Jan. 2004.

[106] H. Ma, J. Zeng, M. L. Realff, S. Kumar, and D. A. Schiraldi, "Processing, structure, and properties of fibers from polyester/carbon nanofiber composites," *Compos. Sci. Technol.*, vol. 63, no. 11, pp. 1617–1628, Aug. 2003.

[107] Y. Liu, S. Sagi, R. Chandrasekar, L. Zhang, N. E. Hedin, and H. Fong, "Preparation and Characterization of Electrospun SiO2 Nanofibers," *J. Nanosci. Nanotechnol.*, vol. 8, no. 3, pp. 1528–1536, Mar. 2008.

[108] W. Shi, W. Lu, and L. Jiang, "The fabrication of photosensitive self-assembly Au nanoparticles embedded in silica nanofibers by electrospinning," *J. Colloid Interface Sci.*, vol. 340, no. 2, pp. 291–297, Dec. 2009.

[109] M. S. Peresin, Y. Habibi, J. O. Zoppe, J. J. Pawlak, and O. J. Rojas, "Nanofiber Composites of Polyvinyl Alcohol and Cellulose Nanocrystals: Manufacture and Characterization," *Biomacromolecules*, vol. 11, no. 3, pp. 674–681, Mar. 2010.

[110] P. Bhattarai, K. B. Thapa, R. B. Basnet, and S. Sharma, "Electrospinning: How to Produce Nanofibers Using Most Inexpensive Technique? An Insight into the Real Challenges of Electrospinning Such Nanofibers and Its Application Areas," *Int. J. Biomed. Adv. Res.*,

vol. 5, no. 09, pp. 401–405, 2014.

[111] X. Shi *et al.*, “Electrospinning of Nanofibers and Their Applications for Energy Devices,” *J. Nanomater.*, vol. 2015, pp. 1–20, May 2015.

[112] V. Kumar and A. Rawal, “Elastic moduli of electrospun mats: Importance of fiber curvature and specimen dimensions,” *J. Mech. Behav. Biomed. Mater.*, vol. 72, no. February, pp. 6–13, 2017.

[113] L. Y. Wan, H. Wang, W. Gao, and F. Ko, “An analysis of the tensile properties of nanofiber mats,” *Polym. (United Kingdom)*, vol. 73, pp. 62–67, 2015.

[114] A. C. Fischer-Cripps, *Nanoindentation*, Third edit. Springer US, 2011.

[115] S. Ghosh, S. T. Parker, X. Wang, D. L. Kaplan, and J. A. Lewis, “Direct-Write Assembly of Microperiodic Silk Fibroin Scaffolds for Tissue Engineering Applications,” *Adv. Funct. Mater.*, vol. 18, no. 13, pp. 1883–1889, Jul. 2008.

[116] M. Wang, H.-J. Jin, D. L. Kaplan, and G. C. Rutledge, “Mechanical Properties of Electrospun Silk Fibers,” *Macromolecules*, vol. 37, no. 18, pp. 6856–6864, Sep. 2004.

[117] Y. X. He *et al.*, “N-terminal domain of Bombyx mori fibroin mediates the assembly of silk in response to pH decrease,” *J. Mol. Biol.*, vol. 418, no. 3–4, pp. 197–207, 2012.

[118] Q. Xia *et al.*, “Complete resequencing of 40 genomes reveals domestication events and genes in silkworm (Bombyx).,” *Science*, vol. 326, no. 5951, pp. 433–6, Oct. 2009.

[119] D. Christian, “Silk Roads or Steppe Roads? The Silk Road in World History,” *J. world Hist.*, vol. 11, no. 1, pp. 1–26, 2000.

[120] D. D. N. Rockwood, R. R. C. Preda, T. Yücel, X. Wang, M. L. Lovett, and D. L. Kaplan, “Materials fabrication from Bombyx mori silk fibroin,” *Nat. Protoc.*, vol. 6, no. 10, pp. 1–43, 2011.

[121] S. Hirano, N. Tamayo, M. Zhang, M. Nakagawa, M. Yoshikawa, and T. Midorikawa, “Wet-spun blend biofibers of cellulose-silk fibroin and cellulose-chitin-silk fibroin,” *Carbohydr. Polym.*, vol. 47, no. 2, pp. 121–124, 2002.

[122] S. Inoue, K. Tanaka, F. Arisaka, S. Kimura, K. Ohtomo, and S. Mizuno, “Silk Fibroin of

Bombyx mori is Secreted, Assembling a High Molecular Mass Elementary Unit Consisting of H-chain, L-chain, and P25, with a 6:6:1 Molar Ratio," *J. Biol. Chem.*, vol. 275, no. 51, pp. 40517–40528, Dec. 2000.

[123] K. Tanaka *et al.*, "Determination of the site of disulfide linkage between heavy and light chains of silk fibroin produced by Bombyx mori," *Biochim. Biophys. Acta - Protein Struct. Mol. Enzymol.*, vol. 1432, no. 1, pp. 92–103, Jun. 1999.

[124] M. Chevillard, P. Couble, and J. C. Prudhomme, "Complete nucleotide sequence of the gene encoding the Bombyx mori silk protein P25 and predicted amino acid sequence of the protein.," *Nucleic Acids Res.*, vol. 14, no. 15, pp. 6341–2, Aug. 1986.

[125] C. Z. Zhou, F. Confalonieri, M. Jacquet, R. Perasso, Z. G. Li, and J. Janin, "Silk fibroin: structural implications of a remarkable amino acid sequence.," *Proteins*, vol. 44, no. 2, pp. 119–22, Aug. 2001.

[126] L. P. Gage and R. F. Manning, "Internal structure of the silk fibroin gene of Bombyx mori. I The fibroin gene consists of a homogeneous alternating array of repetitious crystalline and amorphous coding sequences.," *J. Biol. Chem.*, vol. 255, no. 19, pp. 9444–50, Oct. 1980.

[127] S. K. Rajput and M. Kumar Singh, "Sericin - A Unique Biomaterial," *J. Polym. Text. Eng.*, vol. 2, no. 3, pp. 29–35, 2015.

[128] Y.-Q. Zhang, "Applications of natural silk protein sericin in biomaterials," *Biotechnol. Adv.*, vol. 20, no. 2, pp. 91–100, 2002.

[129] S. He, R. Valluzzi, and S. P. Gido, "Silk I structure in bomyx mori silk foams," *Int. J. Biol. Macromol.*, vol. 24, pp. 187–195, 1999.

[130] H.-J. Jin and D. L. Kaplan, "Mechanism of silk processing in insects and spiders," *Nature*, vol. 424, no. 6952, pp. 1057–1061, Aug. 2003.

[131] S. Rammensee, U. Slotta, T. Scheibel, and A. R. Bausch, "Assembly mechanism of recombinant spider silk proteins," *Proc. Natl. Acad. Sci.*, vol. 105, no. 18, pp. 6590–6595, May 2008.

[132] A. Motta, L. Fambri, and C. Migliaresi, “Regenerated silk fibroin films: Thermal and dynamic mechanical analysis,” *Macromol. Chem. Phys.*, vol. 203, no. 10–11, pp. 1658–1665, Jul. 2002.

[133] P. Cebe *et al.*, “Beating the heat-fast scanning melts silk beta sheet crystals,” *Sci. Rep.*, vol. 3, pp. 1–7, 2013.

[134] G. Salvi, P. De Los Rios, and M. Vendruscolo, “Effective interactions between chaotropic agents and proteins,” *Proteins Struct. Funct. Genet.*, vol. 61, no. 3, pp. 492–499, Sep. 2005.

[135] J. Y. Rongji Li, Yanhong Zhang, Liangjun Zhu, “Fabrication and Characterization of Silk Fibroin/Poly(ethylene glycol)/Cellulose Nanowhisker Composite Films,” *J. Appl. Polym. Sci.*, vol. 124, pp. 2080–2086, 2012.

[136] L. S. Wray *et al.*, “Effect of processing on silk-based biomaterials: Reproducibility and biocompatibility,” *J. Biomed. Mater. Res. - Part B Appl. Biomater.*, vol. 99 B, no. 1, pp. 89–101, 2011.

[137] I. C. Um, H. Y. Kweon, K. G. Lee, D. W. Ihm, J. H. Lee, and Y. H. Park, “Wet spinning of silk polymer: I. Effect of coagulation conditions on the morphological feature of filament,” *Int. J. Biol. Macromol.*, vol. 34, no. 1–2, pp. 89–105, 2004.

[138] H. J. Cho, Y. J. Yoo, J. W. Kim, Y. H. Park, D. G. Bae, and I. C. Um, “Effect of molecular weight and storage time on the wet- and electro-spinning of regenerated silk fibroin,” *Polym. Degrad. Stab.*, vol. 97, no. 6, pp. 1060–1066, 2012.

[139] B. Kundu, R. Rajkhowa, S. C. Kundu, and X. Wang, “Silk fibroin biomaterials for tissue regenerations,” *Adv. Drug Deliv. Rev.*, vol. 65, no. 4, pp. 457–470, 2013.

[140] P. Wongpanit, O. Pornsunthorntawee, and R. Rujiravanit, *Chapter 11: Silk Fibre Composites*, vol. 1, no. 1. The royal Society of Chemistry, 2012.

[141] L. Grasset, D. Cordier, and A. Ville, “Woven Silk as a Carrier for the Immobilization of Enzymes,” *J. Biotecnol. Bioeng.*, vol. 19, pp. 611–618, 1977.

[142] Y. Q. Zhang, “Natural silk fibroin as a support for enzyme immobilization,” *Biotechnol.*

*Adv.*, vol. 16, no. 5–6, pp. 961–971, 1998.

[143] H. Yoshimizu and T. Asakura, “Preparation and Characterization of Silk Fibroin Powder andApplication to Enzyme Immobilization,” *J. Appl. Polym. Sci.*, vol. 40, no. 1–2, pp. 127–134, 1990.

[144] Kuzuhara A, Asakura T, Tomoda R, and Matsunaga T, “Use of silk fibroin for enzyme membrane,” *J. Biotechnol.*, vol. 5, no. 3, pp. 199–207, May 1987.

[145] M. Demura and T. Asakura, “Porous membrane of Bombyx mori silk fibroin: structure characterization, physical properties and application to glucose oxidase immobilization,” *J. Memb. Sci.*, vol. 59, no. 1, pp. 39–52, 1991.

[146] Y. Q. Zhang, J. Zhu, and R. a Gu, “Improved biosensor for glucose based on glucose oxidase-immobilized silk fibroin membrane.,” *Appl. Biochem. Biotechnol.*, vol. 75, pp. 215–233, 1999.

[147] H. Zhang *et al.*, “Preparation and characterization of silk fibroin as a biomaterial with potential for drug delivery,” *J. Transl. Med.*, vol. 10, no. 1, p. 117, 2012.

[148] M. P. Ho, H. Wang, and K. T. Lau, “Effect of degumming time on silkworm silk fibre for biodegradable polymer composites,” *Appl. Surf. Sci.*, vol. 258, no. 8, pp. 3948–3955, 2012.

[149] R. M. Brown, “The biosynthesis of cellulose,” *J. Macromolecurar Sci. Part A*, vol. 33, no. 10, pp. 345–351, Oct. 1996.

[150] I. M. Saxena and R. M. Brown, “Cellulose Biosynthesis: Current Views and Evolving Concepts,” *Ann. Bot.*, vol. 96, no. 1, pp. 9–21, Jul. 2005.

[151] L. Liu and J. M. Yao, “Wet-Spinning of Reinforced Artificial Silk Hybrid Fibres by Cellulose Whiskers,” *Adv. Mater. Res.*, vol. 175–176, pp. 272–275, 2011.

[152] A. Dufresne, *Nanocellulose: From natural to high performance tailored materials*. Berlin: De Gruyter, 2012.

[153] R. Pelton, “Bioactive paper provides a low-cost platform for diagnostics,” *TrAC - Trends Anal. Chem.*, vol. 28, no. 8, pp. 925–942, 2009.

[154] A. H. Free, E. C. Adams, M. L. Kercher, H. M. Free, and M. H. Cook, “Simple specific test for urine glucose.,” *Clin. Chem.*, vol. 3, no. 3, pp. 163–168, 1957.

[155] H. Orelma, *Cellulose based bio- interfaces for immunodiagnostic applications*. 2012.

[156] K. Abe, K. Suzuki, and D. Citterio, “Inkjet-printed microfluidic multianalyte chemical sensing paper,” *Anal. Chem.*, vol. 80, no. 18, pp. 6928–6934, 2008.

[157] E. M. Fenton, M. R. Mascarenas, G. P. López, and S. S. Sibbett, “Multiplex lateral-flow test strips fabricated by two-dimensional shaping,” *ACS Appl. Mater. Interfaces*, vol. 1, no. 1, pp. 124–129, 2009.

[158] A. W. Martinez, S. T. Phillips, G. M. Whitesides, and E. Carrilho, “Diagnostics for the developing world: Microfluidic paper-based analytical devices,” *Anal. Chem.*, vol. 82, no. 1, pp. 3–10, 2010.

[159] R. F. ZuI *et al.*, “Enzyme Immunochromatography-AQuantitativeImmunoassayRequinng No Instrumentation,” *Clin. Chem.*, vol. 3117, no. 7, pp. 1144–1150, 1985.

[160] R. Krska and A. Molinelli, “Rapid test strips for analysis of mycotoxins in food and feed,” *Anal. Bioanal. Chem.*, vol. 393, no. 1, pp. 67–71, 2009.

[161] C. M. Cheng *et al.*, “Paper-based elisa,” *Angew. Chemie - Int. Ed.*, vol. 49, no. 28, pp. 4771–4774, 2010.

[162] J. M. Hammersley, “Percolation processes,” *Math. Proc. Cambridge Philos. Soc.*, vol. 53, no. 03, p. 642, Jul. 1957.

[163] S. R. Broadbent and J. M. Hammersley, “Percolation processes,” *Math. Proc. Cambridge Philos. Soc.*, vol. 53, no. 03, p. 629, Jul. 1957.

[164] I. Balberg, N. Binenbaum, and N. Wagner, “Percolation Thresholds in the Three-Dimensional Sticks System,” *Phys. Rev. Lett.*, vol. 52, no. 17, pp. 1465–1468, Apr. 1984.

[165] A. Dufresne, “Comparing the Mechanical Properties of High Performances Polymer Nanocomposites from Biological Sources,” *J. Nanosci. Nanotechnol.*, vol. 6, no. 2, pp. 322–330, 2006.

[166] M. A. S. Azizi Samir, F. Alloin, and A. Dufresne, “Review of recent research into

cellulosic whiskers, their properties and their application in nanocomposite field," *Biomacromolecules*, vol. 6, no. 2, pp. 612–626, 2005.

[167] J. Bras, D. Viet, C. Bruzzese, and A. Dufresne, "Correlation between stiffness of sheets prepared from cellulose whiskers and nanoparticles dimensions," *Carbohydr. Polym.*, vol. 84, no. 1, pp. 211–215, 2011.

[168] W. Helbert, J. Y. Cavaillé, and A. Dufresne, "Thermoplastic nanocomposites filled with wheat straw cellulose whiskers. Part I: Processing and mechanical behavior," *Polym. Compos.*, vol. 17, no. 4, pp. 604–611, Aug. 1996.

[169] V. Favier, R. Dendievel, G. Canova, J. Y. Cavaille, and P. Gilormini, "Simulation and modeling of three-dimensional percolating structures: Case of a latex matrix reinforced by a network of cellulose fibers," *Acta Mater.*, vol. 45, no. 4, pp. 1557–1565, Apr. 1997.

[170] L. Flandin, J. Y. Cavaillé, G. Bidan, and Y. Brechet, "New nanocomposite materials made of an insulating matrix and conducting fillers: Processing and properties," *Polym. Compos.*, vol. 21, no. 2, pp. 165–174, Apr. 2000.

[171] I. Balberg and N. Binenbaum, "Computer study of the percolation threshold in a two-dimensional anisotropic system of conducting sticks," *Phys. Rev. B*, vol. 28, no. 7, pp. 3799–3812, Oct. 1983.

[172] E. Guth, "Theory of filler reinforcement," *J. Appl. Phys.*, vol. 16, no. 1, pp. 20–25, 1945.

[173] M. Takayanagi, S. Uemura, and S. Minami, "Application of Equivalent Model Method to Dynamic Rheo-Optical Properties of Crystalline Polymers," *J. Polym. Sci. Part C*, vol. 5, pp. 113–122, 1964.

[174] F. Du, R. C. Scogna, W. Zhou, S. Brand, J. E. Fischer, and K. I. Winey, "Nanotube networks in polymer nanocomposites: Rheology and electrical conductivity," *Macromolecules*, vol. 37, no. 24, pp. 9048–9055, 2004.

[175] N. E. Marcovich, M. L. Auad, N. E. Bellesi, S. R. Nutt, and M. I. Aranguren, "Cellulose micro/nanocrystals reinforced polyurethane," *J. Mater. Res.*, vol. 21, no. 4, pp. 870–881, 2006.

[176] J. M. Benoit, B. Corraze, and O. Chauvet, “Localization, Coulomb interactions, and electrical heating in single-wall carbon nanotubes/polymer composites,” *Phys. Rev. B*, vol. 65, no. 24, p. 241405, Jun. 2002.

[177] C. Qiong, P. Tuzhi, and Y. Liju, “Silk fibroin/cellulose acetate membrane electrodes incorporating xanthine oxidase for the determination of fish freshness,” *Anal. Chim. Acta*, vol. 369, no. 3, pp. 245–251, 1998.

[178] Y. Q. Guan, J. M. Chen, Z. Bin Li, Q. L. Feng, and J. M. Liu, “Immobilisation of bifenthrin for termite control,” *Pest Manag. Sci.*, vol. 67, no. 2, pp. 244–251, 2011.

[179] I. Drachuk, S. Harbaugh, R. Geryak, D. L. Kaplan, V. V. Tsukruk, and N. Kelley-Loughnane, “Immobilization of Recombinant E. coli Cells in a Bacterial Cellulose-Silk Composite Matrix to Preserve Biological Function,” *ACS Biomater. Sci. Eng.*, vol. 3, no. 10, pp. 2278–2292, 2017.

[180] T. Yongzhen, X. Weilin, Y. Yun, and Y. Cao, “Preparation and Characterization of Silk fibroin nanocrystals.” .

[181] S. D. Aznar-Cervantes, D. Vicente-Cervantes, L. Meseguer-Olmo, J. L. Cenis, and A. A. Lozano-Pérez, “Influence of the protocol used for fibroin extraction on the mechanical properties and fiber sizes of electrospun silk mats,” *Mater. Sci. Eng. C*, vol. 33, no. 4, pp. 1945–1950, 2013.

[182] T. Hodgkinson, Y. Chen, A. Bayat, and X.-F. Yuan, “Rheology and Electrospinning of Regenerated *Bombyx mori* Silk Fibroin Aqueous Solutions,” *Biomacromolecules*, vol. 15, no. 4, pp. 1288–1298, 2014.

[183] H. J. Kim and I. C. Um, “Relationship between rheology and electro-spinning performance of regenerated silk fibroin prepared using different degumming methods,” *Korea Aust. Rheol. J.*, vol. 26, no. 2, pp. 119–125, 2014.

[184] A. E. Terry, D. P. Knight, D. Porter, and F. Vollrath, “pH Induced Changes in the Rheology of Silk Fibroin Solution from the Middle Division of Bombyx mori Silkworm,” 2004.

[185] J. Zhu, Y. Zhang, H. Shao, and X. Hu, “Electrospinning and rheology of regenerated Bombyx mori silk fibroin aqueous solutions: The effects of pH and concentration,” *Polymer (Guildf).*, vol. 49, no. 12, pp. 2880–2885, 2008.

[186] B. N. Singh, N. N. Panda, and K. Pramanik, “A novel electrospinning approach to fabricate high strength aqueous silk fibroin nanofibers,” *Int. J. Biol. Macromol.*, vol. 87, pp. 201–207, 2016.

[187] T. A. Witten and M. H. Cohen, “Crosslinking in shear-thickening ionomers,” *Macromolecules*, vol. 18, no. 10, pp. 1915–1918, Oct. 1985.

[188] G. Bokias, D. Hourdet, and I. Iliopoulos, “Positively Charged Amphiphilic Polymers Based on Poly(N-isopropylacrylamide): Phase Behavior and Shear-Induced Thickening in Aqueous Solution,” *Macromolecules*, vol. 33, no. 8, pp. 2929–2935, 2000.

[189] A. Ochi, K. Hossain, J. Magoshi, and N. Nemoto, “Rheology and Dynamic Light Scattering of Silk Fibroin Solution Extracted from the Middle Division of Bombyx mori Silkworm,” *Biomacromolecules*, vol. 3, no. 6, pp. 1187–1196, 2002.

[190] R. B. Bird, W. E. Stewart, and E. N. Lightfoot, *Trnasport Phenomena*. New York: John Willey & Sons Inc., 2007.

[191] T. Yamasaki and T. F. Irvine, “A comparative Capillary Tube Viscometer to Measure the Viscous Properties of Newtonian and Power-Law Fluids,” *Exp. Therm. Fluid Sci.*, vol. 3, pp. 458–462, 1990.

[192] H. Wang, H. Shao, and X. Hu, “Structure of silk fibroin fibers made by an electrospinning process from a silk fibroin aqueous solution,” *J. Appl. Polym. Sci.*, vol. 101, no. 2, pp. 961–968, 2006.

[193] H. Wang, Y. Zhang, H. Shao, and X. Hu, “Electrospun ultra-fine silk fibroin fibers from aqueous solutions,” *J. Mater. Sci.*, vol. 40, no. 20, pp. 5359–5363, 2005.

[194] J. Zhu, H. Shao, and X. Hu, “Morphology and structure of electrospun mats from regenerated silk fibroin aqueous solutions with adjusting pH,” *Int. J. Biol. Macromol.*, vol. 41, no. 4, pp. 469–474, 2007.

[195] M. A. S. Azizi Samir, F. Alloin, J.-Y. Sanchez, N. El Kissi, and A. Dufresne, “Preparation of Cellulose Whiskers Reinforced Nanocomposites from an Organic Medium Suspension,” *Macromolecules*, vol. 37, pp. 1386–1393, 2004.

[196] M. M. de Souza Lima and R. Borsali, “Rodlike Cellulose Microcrystals: Structure, Properties, and Applications,” *Macromol. Rapid Commun.*, vol. 25, no. 7, pp. 771–787, Apr. 2004.

[197] P. Pötschke, T. D. Fornes, and D. R. Paul, “Rheological behavior of multiwalled carbon nanotube/polycarbonate composites,” *Polymer (Guildf).*, vol. 43, no. 11, pp. 3247–3255, May 2002.

[198] L. A. Utracki, “Flow and flow orientation of composites containing anisometric particles,” *Polym. Compos.*, vol. 7, no. 5, pp. 274–282, Oct. 1986.

[199] J. M. Dealy and K. F. Wissbrun, “Rheology of Multiphase Systems,” in *Melt Rheology and Its Role in Plastics Processing*, Dordrecht: Springer Netherlands, 1999, pp. 390–409.

[200] D. Tian *et al.*, “Conformations and Intermolecular Interactions in Cellulose/Silk Fibroin Blend Films: A Solid-State NMR Perspective,” *J. Phys. Chem. B*, vol. 121, no. 25, pp. 6108–6116, 2017.

[201] L. H. Sperling, *Introduction to Physical Polymer Science*, Fourth Edi. New Jersey: John Wiley & Sons Ltd, 2006.

[202] M. I. Aranguren, E. Mora, J. V. DeGroot, and C. W. Macosko, “Effect of reinforcing fillers on the rheology of polymer melts,” *J. Rheol. (N. Y. N. Y).*, vol. 36, no. 6, pp. 1165–1182, Aug. 1992.

[203] M. Bercea and P. Navard, “Shear Dynamics of Aqueous Suspensions of Cellulose Whiskers,” *Macromolecules*, vol. 33, no. 16, pp. 6011–6016, 2000.

[204] C. Chen, C. Chuanbao, M. Xilan, T. Yin, and Z. Hesun, “Preparation of non-woven mats from all-aqueous silk fibroin solution with electrospinning method,” *Polymer (Guildf).*, vol. 47, no. 18, pp. 6322–6327, 2006.

[205] C. Solanas *et al.*, “Insights into the production and characterization of electrospun fibers

from regenerated silk fibroin," *Eur. Polym. J.*, vol. 60, pp. 123–134, 2014.

[206] T. Asakura, A. Kuzuhara, R. Tabeta, and H. Saito, "Conformation Characterization of Bombyx mori Silk Fibroin in the Solid State by High-Frequency13C Cross Polarization-Magic Angle Spinning NMR, X-ray Diffraction, and Infrared Spectroscopy," *Macromolecules*, vol. 18, no. 10, pp. 1841–1845, 1985.

[207] S. Shin and D.-Y. Keum, "Continuous Viscosity Measurement of Non-Newtonian Fluids over a Range of Shear Rates Using a Mass-Detecting Capillary Viscometer," 2002.

[208] J. T. Pelton and L. R. McLean, "Spectroscopy Methods for Analysis of Protein Secondary Structure," *Anal. Biochem.*, vol. 277, pp. 167–176, 2000.

[209] X. Li, J. Qin, and J. Ma, "Silk fibroin/poly (vinyl alcohol) blend scaffolds for controlled delivery of curcumin," *Regen. Biomater.*, vol. 2, no. 2, pp. 97–105, Jun. 2015.

[210] S.-W. Ha, A. E. Tonelli, and S. M. Hudson, "Structural Studies of Bombyx mori Silk Fibroin during Regeneration from Solutions and Wet Fiber Spinning," 2005.

[211] T. Miyazawa and E. R. Blout, "The Infrared Spectra of Polypeptides in Various Conformations: Amide I and II Bands," *J. Am. Chem. Soc.*, vol. 83, no. 3, pp. 712–719, 1961.

[212] X. Wu, X. Wu, B. Yang, M. Shao, and G. Feng, "Methanol–Water-Dependent Structural Changes of Regenerated Silk Fibroin Probed Using Terahertz Spectroscopy," *Appl. Spectrosc.*, vol. 71, no. 8, pp. 1785–1794, 2017.

[213] S. Ling, Z. Qi, D. P. Knight, Z. Shao, and X. Chen, "Synchrotron FTIR microspectroscopy of single natural silk fibers," *Biomacromolecules*, vol. 12, no. 9, pp. 3344–3349, 2011.

[214] G. Freddi, M. Romano, M. R. Massafra, and M. Tsukada, "Silk Fibroin / Cellulose Blend Films : Preparation , Structure , and Physical Properties," pp. 1537–1545, 1995.

[215] H. Yang, S. Yang, J. Kong, A. Dong, and S. Yu, "Obtaining information about protein secondary structures in aqueous solution using Fourier transform IR spectroscopy.," *Nat. Protoc.*, vol. 10, no. 3, pp. 382–96, 2015.

[216] N. Lin, C. Bruzzese, and A. Dufresne, “TEMPO-oxidized nanocellulose participating as crosslinking aid for alginate-based sponges,” *ACS Appl. Mater. Interfaces*, vol. 4, no. 9, pp. 4948–4959, 2012.

[217] B. Sun, Q. Hou, Z. Liu, and Y. Ni, “Sodium periodate oxidation of cellulose nanocrystal and its application as a paper wet strength additive,” *Cellulose*, vol. 22, no. 2, pp. 1135–1146, 2015.

[218] M. Zaman, H. Xiao, F. Chibante, and Y. Ni, “Synthesis and characterization of cationically modified nanocrystalline cellulose,” *Carbohydr. Polym.*, vol. 89, no. 1, pp. 163–170, Jun. 2012.

[219] S. M. A. S. Keshk, “Homogenous reactions of cellulose from different natural sources,” *Carbohydr. Polym.*, vol. 74, no. 4, pp. 942–945, Nov. 2008.

[220] M. S. Jahan, A. Saeed, Z. He, and Y. Ni, “Jute as raw material for the preparation of microcrystalline cellulose,” *Cellulose*, vol. 18, no. 2, pp. 451–459, Apr. 2011.

[221] R. Sun, X. Sun, G. Liu, P. Fowler, and J. Tomkinson, “Structural and physicochemical characterization of hemicelluloses isolated by alkaline peroxide from barley straw,” *Polym. Int.*, vol. 51, no. 2, pp. 117–124, Feb. 2002.

[222] Q. Lu *et al.*, “Water-insoluble silk films with silk I structure,” *Acta Biomater.*, vol. 6, no. 4, pp. 1380–1387, 2010.

[223] R. Fraser, *Conformation in Fibrous Proteins and Related synthetic Polypeptides.* Elsevier Science, 1973.

[224] W. Gindl and J. Keckes, “All-cellulose nanocomposite,” *Polymer (Guildf).*, vol. 46, no. 23, pp. 10221–10225, Nov. 2005.

[225] Z. Liu *et al.*, “Characterization of the regenerated cellulose films in ionic liquids and rheological properties of the solutions,” *Mater. Chem. Phys.*, vol. 128, no. 1–2, pp. 220–227, Jul. 2011.

[226] P. Mansikkamäki, M. Lahtinen, and K. Rissanen, “Structural Changes of Cellulose Crystallites Induced by Mercerisation in Different Solvent Systems; Determined by

Powder X-ray Diffraction Method," *Cellulose*, vol. 12, no. 3, pp. 233–242, Jun. 2005.

[227] Y. Noishiki, Y. Nishiyama, M. Wada, S. Kuga, and J. Magoshi, "Mechanical properties of silk fibroin-microcrystalline cellulose composite films," *J. Appl. Polym. Sci.*, vol. 86, no. 13, pp. 3425–3429, 2002.

[228] S. Curgul, K. J. Van Vliet, and G. C. Rutledge, "Molecular Dynamics Simulation of Size-Dependent Structural and Thermal Properties of Polymer Nanofibers," 2007.

[229] A. Boujemaoui *et al.*, "Polycaprolactone Nanocomposites Reinforced with Cellulose Nanocrystals Surface-Modified via Covalent Grafting or Physisorption: A Comparative Study," 2017.

[230] A. Pei, J.-M. Malho, J. Ruokolainen, Q. Zhou, and L. A. Berglund, "Strong Nanocomposite Reinforcement Effects in Polyurethane Elastomer with Low Volume Fraction of Cellulose Nanocrystals," *Macromolecules*, vol. 44, pp. 4422–4427, 2011.

[231] M. Grunert and W. T. Winter, "Nanocomposites of Cellulose Acetate Butyrate Reinforced with Cellulose Nanocrystals," *J. Polym. Environ.*, vol. 10, no. 2, pp. 27–30, 2002.

[232] X. Hu, Q. Lu, D. L. Kaplan, and P. Cebe, "Microphase Separation Controlled β-Sheet Crystallization Kinetics in Fibrous Proteins," *Macromolecules*, vol. 42, no. 6, pp. 2079–2087, Mar. 2009.

[233] X. Hu, D. Kaplan, and P. Cebe, "Determining Beta-Sheet Crystallinity in Fibrous Proteins by Thermal Analysis and Infrared Spectroscopy," *Macromolecules*, vol. 39, no. 18, pp. 6161–6170, 2006.